Aspects of Magnetohydrodynamic Duct Flow at High Magnetic Reynolds Number.

by

R.B. TURNER.

A Thesis submitted to the University of Warwick for the degree of Doctor of Philosophy

July 1973

ABSTRACT.

In this thesis we attempt to predict the performance of a device, known as a flow coupler, which consists of an M.H.D. generator coupled to an M.H.D. pump so that one stream of fluid is induced to move by the motion of another.

The change of magnetic field experienced by a moving conductor as it passes into an M.H.D. device can cause large eddy curents to circulate within the M.H.D. duct. We have used apparatus in which we represent the moving stream of liquid by an annular disc of aluminium, to investigate the perturbation of the applied magnetic field and of the electric potential distribution caused by these eddy currents. A two dimensional solution of the equation $\nabla^2 B = \frac{R_m}{a} \frac{\partial B}{\partial z}$, where B is the transverse magnetic field, a is a scale length of the system, R_m is the magnetic Reynolds number and z is measured in the flow direction, produces results which agree well with the experimentally measured fields. We use a solution of the equation $\nabla^2 U = \frac{R_m}{a} \frac{\partial U}{\partial z}$, where U is the electric potential, in a first order analysis of the velocity perturbation which occurs as a liquid flows through a magnetic field.

We then examine both experimentally and theoretically, devices in which large currents flow through a moving conductor and through an external circuit. These currents are injected into the moving conductor through electrodes which have a high resistance to currents in the direction of motion. We show that for compensated devices, that is,

devices in which the external conductors are arranged so that they produce no transverse magnetic field, the perturbed magnetic field does not depend upon the current through the external circuit and is the same field that would exist if there were no contact between the moving metal and the external cirucit.

We observe experimentally that when two conductors move side by side through the gap of a magnet the magnetic field in one moving conductor is little affected by the motion of the other.

We compare the measured performance of a simulated M.H.D. generator and of a real M.H.D. pump with their computed performances and we calculate the expected performance of a flow coupler.

We suggest that the presence of a slowly moving liquid in the boundary layers adjacent to the duct walls may adversely affect the performance of a flow coupler and we conclude that an efficient flow coupler would require non-conducting duct walls and a high magnetic field.

PREFACE

Since February 1970 I have been working as a research student in the Department of Engineering at the University of Warwick. When I came to Warwick I was registered as a candidate for the Master of Science degree. I was supported by a research scholarship financed under an Agreement with the United Kingdom Atomic Energy Authority, Risley. After a period of one year the U.K.A.E.A. extended the Agreement for a further year, and my registration was changed to that of a Ph.D. student. I would like to thank the Authority for their support during this time. For most of my third and final year my grant was kindly provided by the University of Warwick.

The aim of the Agreement, which stemmed from the Authority's interest in sodium-filled cooled loops in fast breeder reactors, was to investigate the performance of devices in which one stream of liquid metal is electromagnetically induced to move by the motion of another. Such devices have come to be known as "flow couplers". A serious problem in the design of flow couplers is the perturbation of the applied magnetic field by induced fields arising from eddy currents circulating in the liquid metal at the edges of the magnetic field. The problems are particularly severe if the velocity and conductivity of the liquid metal and the physical dimensions of the device are large. The major part of this thesis concerns theoretical and experimental work on M.H.D. devices in which these eddy currents significantly modify the applied field and also cause ohmic heating within the ducts. In chapter 7 we calculate the likely efficiency of a flow coupler suitable for the duty specified by the U.K.A.E.A.

During the course of our work we have built two experimental rigs.

The first was quickly constructed so that we could make experimental observations during the first year of my studies. The second and more complex rig was made partly in University workshops and partly at the U.K.A.E.A. establishment at Risley, it did not become operational until shortly before the Agreement with the Authority expired at the end of March 1972.

I would like to thank my supervisor Dr. C.J.N. Alty for his advice and criticism and for the time which he has devoted to reading the draft of this thesis. I would also like to express my gratitude to Professor J.A. Shercliff and to Dr. M.K. Bevir who have always taken an interest in this work. I also thank Messrs A.E. Webb, A.C. Ross and C. Major who constructed the apparatus and helped in many other practical ways. Finally I wish to acknowledge the help of my wife Sylvia who has supported me in every possible way and who in addition has typed this thesis.

Contents. Page

Nomenclature

a	semi-width of duct in the x-direction.
A	constant.
A_c	Fourier coefficient.
A_n	Fourier coefficient.
B	constant.
$\underline{B}$	magnetic flux density vector.
B_a	an applied magnetic flux (in the y-direction).
B_o	magnitude of an applied magnetic flux.
B_i	the induced magnetic flux.
$B_{i_{if}}$	the induced flux due to a small element of applied field.
B_n	Fourier coefficient.
B_R	the magnetic flux density in the right hand channel of a flow coupler.
B_L	the magnetic flux density in the left hand channel of a flow coupler.
c	constant.
C	constant.
C_n	Fourier coefficient.
d	a length associated with the electrodes of an M.H.D. device.
D_n	Fourier coefficient.
$\underline{E}$	the electric field vector.
E	arbitary constant.
E'	" " .
F	" " .
F'	" " .
G	" " .
G_n	Fourier coefficient.
H_n	" " .
H_c	" " .
H_c'	" " .
I_c	" " .
I_n	Fourier coefficient.
I_T	the total current through the electrode of an M.H.D. device.
I_w	a current in the duct wall.
$\underline{j}$	current density vector.
j_e	the current density in the electrode.
j_{xa}	x-component of the applied current density.
j_{xi}	the x-component of the induced current density.
j_z	the z-component of the current density.
J_n	Fourier coefficient.
K	$\alpha_1 - \alpha_2$
l	half length of the magnetic field in the z-direction.
L_n	Fourier coefficient.
M_n	" " .
N_n	" " .
N	$1/a$
n	an odd integer.
p	the number of elements of applied magnetic flux density.
Δp	pressure drop
P	power.
P_T	the power extracted from the generator channel of a flow coupler.
P_{L_w}	the power dissipated in the walls of the left hand duct (the generator channel) of a flow coupler.
P_{R_w}	the power dissipated in the walls of the right hand duct (the pump channel)of a flow coupler.
P_e	the power dissipated in an electrode.
R	the ordinary Reynolds number.

R_m the magnetic Reynolds number.
R_L the magnetic Reynolds number in the left hand channel of a flow coupler.
R_R the magnetic Reynolds number in the right hand channel of a flow coupler.
R_{app} the apparent resistance of the liquid in an M.H.D. duct between x=a andx=o.
R_d the ordinary resistance of the liquid in an M.H.D. duct between x=a and x=o.
R_e the resistance of an electrode.
R_p the apparent resistance of an M.H.D. pump.
S the interaction parameter.
t the thickness of a duct in the y-direction.
t_m the thickness of the conducting fluid in the y-direction.
t_e the thickness of the electrodes.
U the electric potential.
U_a the potential at x=a (a function of z)
U_{aL} the potential at x=a in the left hand duct of a flow coupler.
U_{aR} the potential at x=a in the right hand duct of a flow coupler.
$\underline{v}$ the velocity vector.
v_m a mean velocity.
v_z the z-component of the velocity.
v_x the x-component of the velocity.
V_o an applied electric potential.
ΔV_a the potential difference between the ducts of a flow coupler.
w the thickness of a duct wall, a small perturbation in the z-component of the velocity.
x position co-ordinate.
y " " .
z " " .
α_1 roots of an auxiliary equation.
α_2 " " " " " .
β_1 " " " " " .
β_2 " " " " " .
η viscosity of fluid.
λ separation constant.
μ permeability.
ρ density.
σ conductivity.
σ_e conductivity of electrode material.
σ_f conductivity of fluid in M.H.D. duct.
σ_w conductivity of duct wall material.
ϕ separation constant.
ψ perturbation stream function.
$\underline{\omega}$ vorticity.
ω angular frequency.
∇^2 $\frac{\partial^2}{\partial x^2} + \frac{\partial^2}{\partial y^2} + \frac{\partial^2}{\partial z^2}$.

Illustrations.

Chapter 1.

The Introduction.

1.1 Flow Couplers.

There are many M.H.D devices in which a fluid is made to flow in a duct through a region of space in which there is a magnetic field. The change of field experienced by the fluid as it enters or leaves such a device will cause induced eddy currents to circulate. In the presence of a magnetic field these currents produce a body force within the fluid and hence may modify the way in which it flows through the duct; whether this happens or not the currents cause a power loss which ultimately gives rise to a pressure drop along the duct. The circulating eddy currents also produce an induced magnetic field which modifies the original field. It is well known that, provided the product $\mu\sigma va$ is much less than unity, this induced field $\underline{B}_i$, is of order $\mu\sigma va\,\underline{B}_a$, where μ is the magnetic permeability of the fluid, σ is the conductivity of the fluid, v is the velocity of the fluid, a is a scale length of the device, and $\underline{B}_a$ is the original applied field. The dimensionless group $\mu\sigma va$ is often referred to as the Magnetic Reynolds number (R_m).

In most of the M.H.D. devices which are used industrially the magnetic Reynolds number is small, and the modifying effect of the induced magnetic field upon the initial transverse field may be ignored. The transverse component of $\underline{B}$ is then considered to be independent of the fluid velocity $\underline{v}$. Only when large devices are used with liquids which have high conductivities or permeabilities does R_m become large, ie not $\ll 1$, so that $\underline{B}$ is no longer independent of $\underline{v}$. In these circumstances the relationship

$\underline{B}_i = R_m \underline{B}_a$ is no longer true and the induced magnetic field may be of the same order as the applied magnetic

field. These conditions occur in the sodium-filled coolant loops of fast breeder reactors.

The prototype fast breeder reactor at present being constructed for the U.K.A.E.A. at Dounreay and future commercial reactors will employ two separate alkali metal circuits. In the primary circuit sodium is drawn from the reactor vessel and pumped through the reactor core; it leaves the core at a temperature of about 600°C and passes through a number of intermediate heat exchangers. The heat exchangers transfer the heat output of the core from the primary coolant circuit, which is completely enclosed by the biological shield, to the secondary sodium circuit which will carry the heat to steam generators outside the reactor.

All reactors at present being designed have mechanical pumps within the primary reactor vessel to pump the primary coolant. These pumps are shaft-driven from electric motors outside the reactor. It has been suggested that by placing an M.H.D. generator in the secondary sodium stream and connecting its electrical output to an M.H.D. pump in the primary stream, the mechanical pumps in the reactor vessel, together with their rotating shafts and externally mounted electric motors, could be eliminated. In this way the power necessary to circulate the sodium in both the primary and the secondary loops would be provided by installing extra pumps in the external circuit. This combination of pump and generator, which is sometimes called a flow coupler, is the subject of two patents[1].

The flow coupler as it is envisaged by Davidson and Thatcher (private communication) is shown in figure 1. In this diagram (a) is the magnet block providing a transverse magnetic field, (b) is a duct containing the primary sodium flow, (c) is a duct containing the mechanically pumped secondary flow.

field. These conditions occur in the sodium-filled coolant loops of fast breeder reactors.

The prototype fast breeder reactor at present being constructed for the U.K.A.E.A. at Dounreay and future commercial reactors will employ two separate alkali metal circuits. In the primary circuit sodium is drawn from the reactor vessel and pumped through the reactor core; it leaves the core at a temperature of about 600°C and passes through a number of intermediate heat exchangers. The heat exchangers transfer the heat output of the core from the primary coolant circuit, which is completely enclosed by the biological shield, to the secondary sodium circuit which will carry the heat to steam generators outside the reactor.

All reactors at present being designed have mechanical pumps within the primary reactor vessel to pump the primary coolant. These pumps are shaft-driven from electric motors outside the reactor. It has been suggested that by placing an M.H.D. generator in the secondary sodium stream and connecting its electrical output to an M.H.D. pump in the primary stream, the mechanical pumps in the reactor vessel, together with their rotating shafts and externally mounted electric motors, could be eliminated. In this way the power necessary to circulate the sodium in both the primary and the secondary loops would be provided by installing extra pumps in the external circuit. This combination of pump and generator, which is sometimes called a flow coupler, is the subject of two patents[1].

The flow coupler as it is envisaged by Davidson and Thatcher (private communication) is shown in figure 1. In this diagram (a) is the magnet block providing a transverse magnetic field, (b) is a duct containing the primary sodium flow, (c) is a duct containing the mechanically pumped secondary flow.

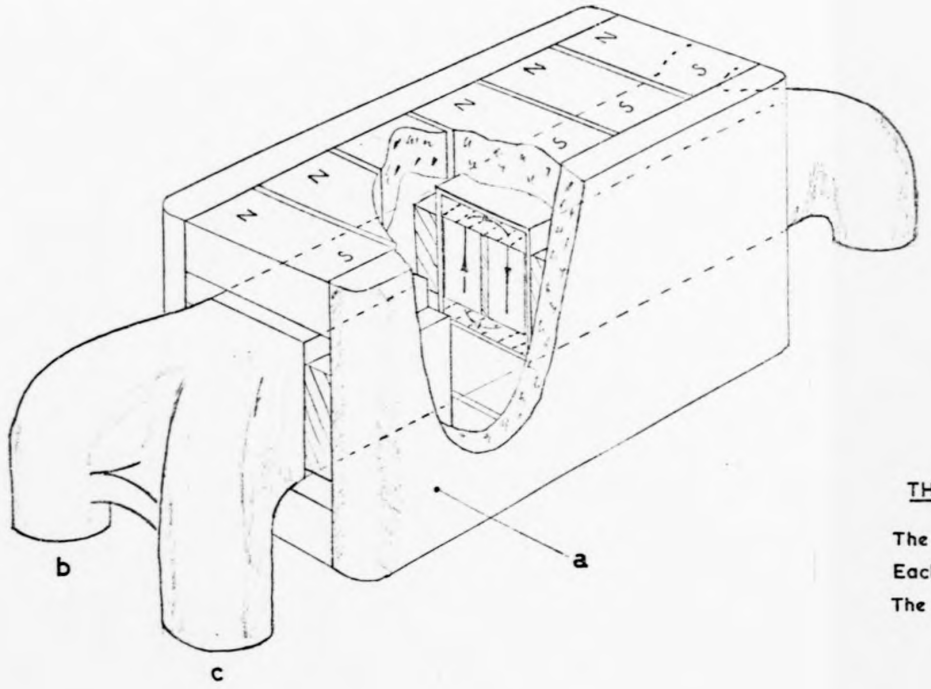

fig 1.

THE PROPOSED FLOW COUPLER

The length of the magnet is 200 cms.
Each duct is 40 cms. high X 20 cms wide.
The expected through-put is 20,000 gals./min.

The sodium flowing in the secondary stream is a conductor moving in a magnetic field and as such generates an E.M.F. between the upper and lower electrodes, these electrodes are coupled to the primary circuit so that a current flows through the sodium in the primary stream. The effect of this current in the presence of the tranverse magnetic field is to produce a force along the duct thus pumping the sodium through the primary circuit. This flow coupler is intended to have a throughput of 20,000 gallons per minute of liquid sodium in each stream, in ducts which are 0.4 metres in the direction perpendicular to the applied magnetic field and 0.2 metres in the direction parallel to the field. Using a, the half height of the duct in the direction perpendicular to the applied magnetic field, as a typical scale length of the system the magnetic Reynolds number for such a device is about 25. With such a high R_m the magnetic field will be severely altered and the circulating eddy currents will cause a significant power loss.

The U.K.A.E.A. at Risley agreed to finance work at the University of Warwick so that we could study the problems associated with a flow coupler and indicate what the efficiency of such a device is likely to be. The problem of eddy current loss and field convection, when the magnetic Reynolds number is high, occurs in many other M.H.D. devices, such as pumps and flow meters, and for this reason our work is not confined solely to the consideration of these problems as they affect flow couplers.

1.2 A Brief survey of Previous Work.

Davidson[2] made some approximate calculations of the pressure drop which occurs when sodium in a duct flows through a region of space in which there is a magnetic field perpendicular to the

direction of the flow. He assumed that the sodium flow was entirely along the duct and that the velocity of the flow was the same everywhere. The pressure drop was considered to be caused by the eddy currents which are induced as the sodium enters or leaves the magnetic field. He considered these currents as having circular paths with a maximum radius equal to the half height of the duct (fig. 2).

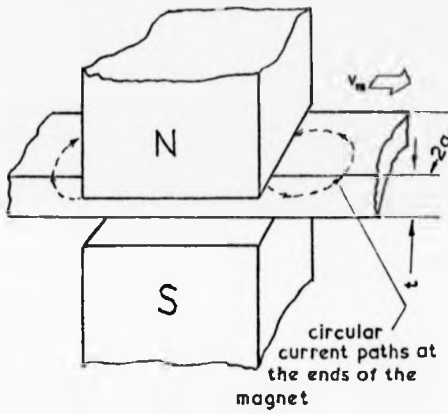

fig.2

He obtained an expression for the pressure drop at each end which is:-

$$\Delta p = 0.16\, \sigma B_o^2\, v_m\, a\,,$$

where v_m is the velocity of the sodium, σ is the conductivity of the sodium, a is the half height of the duct, and B_o is the abruptly ending applied magnetic field.

In a duct of thickness t this pressure drop would cause a power loss which is, $P = \dfrac{0.32\, B_o^2 R_m^2\, t}{\mu^2 \sigma}$, where $R_m = v_m \mu \sigma a$.

In these calculations Davidson assumed that the initial magnetic field would not be seriously modified by the induced field. His calculations are therefore only valid if the magnetic Reynolds number is small.

Shercliff[3] made a more realistic calculation for this case. He calculated the velocity perturbation in the fluid as it enters the magnetic field region and obtained an expression for the pressure drop associated with the change in the velocity profile. His equation is:-

$$\Delta p = 0.27\, \sigma B_o^2 v_m a,$$

In terms of power this is:-

$$P = \frac{0.54\, B_o^2 R_m^2\, t}{\mu^2 \sigma}\,.$$

The expressions obtained by Shercliff and Davidson are of the same form but differ by a numerical factor.

W.M. Wells[4] performed some experimental measurements using a low melting-point alloy in the solid and the liquid state for values of R_m of up to about 0.4. His apparatus consisted of a wheel carrying a hollow plastic tyre. This tyre was filled with a low melting point alloy. The torque necessary to rotate this wheel, so that its rim passed between the poles of a magnet, was measured.
These experiments were performed with the alloy in the rim in its solid and then in its liquid state. When the torque required to turn the wheel was converted into an equivalent pressure drop, Wells found that the pressure drop due to both the entry and exit loss was of the same form as that predicted by Shercliff but was numerically different.
He attributed this to the fact that his experiments were not conducted with an abruptly changing field and to the simplifications made in Shercliff's analysis. As Shercliff's analysis was for the case in which R_m is much less than unity whereas Well's experiments were conducted at magnetic Reynolds numbers of up to about 0.4, it is perhaps not surprising that the results are not in close agreement.
It is interesting to note that Wells' results for the solid and the liquid case were very similar.

Yu. M. Mikhailov[5] analysed the behaviour of an annular M.H.D. generator, fig.(3), in which a metal moves solely in the z-direction through a device in which there is a radial exciting magnetic field. He later examined the field for the case of a flow in a flat channel by considering it to be part of an annular device in which the radius of curvature is very large. He summarizes his results as follows:-

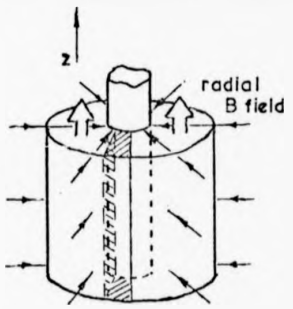

fig. 3

"1) In liquid M.H.D. generators there is a possibility of creating a magnetic field at the expense of currents in the metal itself by intensifying the exciting field. This intensification depends upon the geometry of the generator and at small R_m is proportional to the

magnetic Reynolds number.

2) At large R_m the depth of penetration of the magnetic field into the metal falls, which, in the general case, leads to a reduction in field intensification, the main field being carried beyond the limits of the working zone of the generator. This imposes certain limitations upon the length of the working section and the thickness of the metal layer."

We have observed some of these phenomena in the experimental work which we have performed and which will be described later in this thesis. Mikhailov's work also clearly indicates that it would be futile to make an M.H.D. device in which the duct was so large that the magnetic field could not penetrate the sodium.

Watt and others[6] built and tested a large electromagnetic pump for mercury at A.E.R.E. Harwell. The tests on these pumps are very well documented. Watt investigated the performance of these pumps at magnetic Reynolds numbers of up to 0.33, and observed that, because of end effect losses, their efficiency began to fall as the velocity of the mercury increased. He also noticed that the end losses were decreased if the magnetic field was made to change less abruptly at the ends of the device.

Watt believed that, as the velocity of the mercury increased, the current which would normally pass between the top and bottom electrodes of the duct, was swept downstream so that some of it passed through the duct in a region where there was no magnetic field: hence the pump became less efficient. Extending the magnetic field, by making the field gradient less at the ends of the pump, was thought to provide a field where this otherwise useless current would flow. In fact the end loss would still be present in a device in which no current was supplied from an external source, because the eddy currents which cause this loss are generated within the moving metal. Making the field gradient less at the ends of a pump decreases the loss due to these currents and hence increases the efficiency. In part III of this thesis we attempt to predict

the performance of Watt's pump and we compare our results with those of Watt.

Boucher and Ames[7] considered the fluid leaving an abruptly-ending region of magnetic field as being represented by a solid rectangular conductor passing between a pair of infinitely long pole pieces. These pole pieces had an infinite permeability so that the magnetic field had a component only in the transverse direction. Using Maxwell's equations and Ohm's law they deduced the equation:-

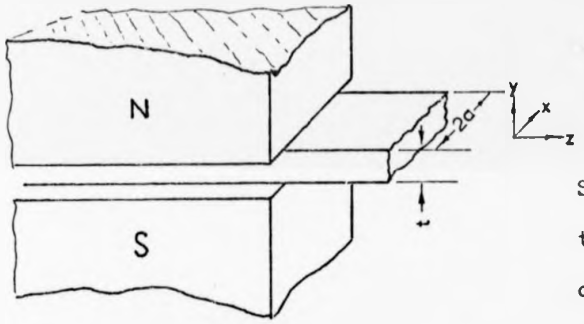

fig.4

$\frac{\partial^2 U}{\partial x^2} + \frac{\partial^2 U}{\partial z^2} = k\frac{\partial U}{\partial z}$, where U is the electric potential and $k = v\mu\sigma$.

Solving this equation for they calculated the components of the current density, j_x and j_z, and because the power dissipation is given by $\frac{1}{\sigma}\iiint \underline{j}\, dx\,dy\,dz$, they obtained an expression for the power dissipation which is:-

$P = \frac{4}{\pi^3} t E_o^2 \sigma$ for $ka \ll \pi$,

$P = \frac{8}{\pi^3} t E_o H$ for $ka \gg \pi$, where $E_o = 2vBa$.

Rewriting this in terms of the magnetic Reynolds number we have

$P = \frac{16}{\pi^3} \frac{t B_o^2 R_m^2}{\mu^2\sigma}$ when $R_m \ll \pi$.

$P = \frac{16}{\pi^4} \frac{t B_o^2 R_m}{\mu^2\sigma}$ when $R_m \gg \pi$.

Boucher and Ames work assumed slug flow through the magnet region and also assumed that the magnet is very long so that the currents which would be induced as the metal enters the field region would have no effect upon the exit end of the device. Unfortunately this work gives no information about the perturbation of the magnetic field caused by the eddy currents.

The results of Shercliff and Davidson are of the same form and the same approximate size as the expression derived by Boucher and Ames for $R_m \ll \pi$. A theory presented later in this thesis agrees well with the theory of Boucher and Ames, in the limits of high and low R_m, if the field region is long enough for the perturbation at the entry end not to affect the field at exit end of the magnet.

1.3 The Work at Warwick

The duct flow of a liquid through a region of magnetic field when the magnetic Reynolds number is high is imperfectly understood and requires further investigation. In the flow coupler design suggested by Davidson and Thatcher the ordinary Reynolds number is about 7×10^6 so that the flow of the liquid will be turbulent when it enters the field region. Shercliff[8] has pointed out that the gross field distortion and eddy current loss depend upon the mean velocity of the fluid and are unaffected by turbulence. The velocity profile in the fluid upstream of the flow coupler can be calculated from the universal velocity distribution. Figure 5 shows the calculated velocity profiles which correspond to magnetic Reynolds numbers of 5 and 20, in the proposed flow coupler.

The nature of these profiles suggests that an experiment using a solid conductor passing between the poles of a magnet might enable one to make a reasonable estimate of the field perturbation and power loss which would arise if a real liquid metal were to pass through the same magnetic field.

In Chapter 3 a theory has been developed for the electric potential distribution in a metal which moves with slug flow at high R_m through an abruptly ending transverse magnetic field. This theory is used, in Chapter 4, in a first order analysis of the velocity perturbation in a liquid as it passes through a magnetic field. This analysis is valid when the ratio of the $\underline{j} \times \underline{B}$ forces to the inertia force (the interaction

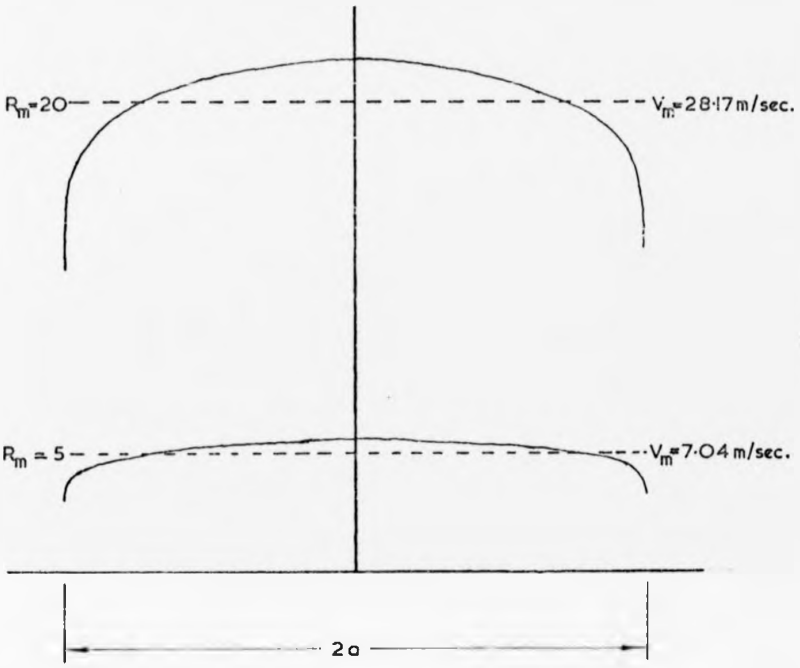

Velocity profiles, calculated from the universal velocity distribution, for mean velocities which correspond to R_m=5, and R_m=20.

fig. 5

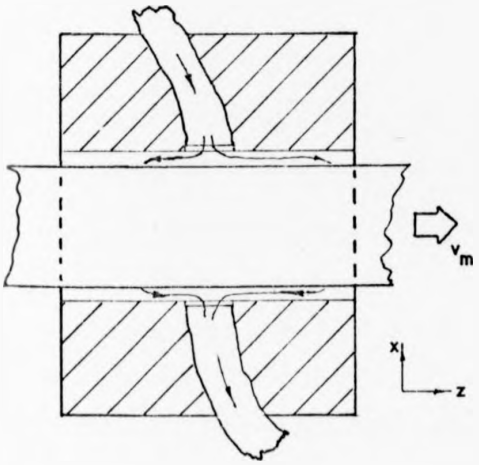

Continuous electrodes allow currents in the z-direction to flow within them.

fig. 6

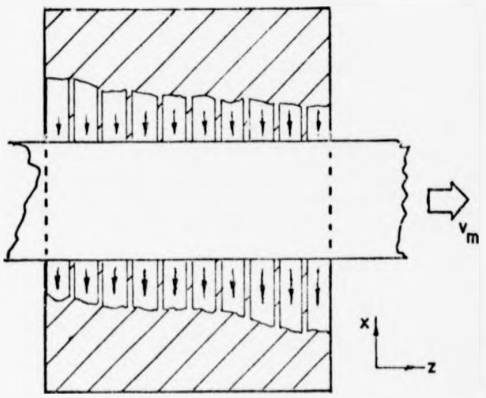

Segmented electrodes allow only currents in the x-direction to flow within them.

fig. 7

parameter) is less than 1 or 2. The theory indicates that the velocity of the liquid will be increased at the edges of the duct and decreased at the centre of the duct. This velocity perturbation could make the flow nearer to that of a slug flow case. At a magnetic Reynolds number of 20 and a magnetic field of 3000 gauss the interaction parameter for the flow coupler is about 0.3.

It is difficult and expensive to build a scale model of a flow coupler with which to investigate and optimize the performance of such a device, because the magnetic Reynolds number, and hence the field perturbation, depend upon a dimension of the duct as well as upon the conductivity of the fluid it contains. A one tenth scale model operating with sodium as the fluid, would have a velocity ten times that of the full size device in order that the ordinary Reynolds number and the magnetic Reynolds number were the same as those in the flow coupler. The high pressure needed to achieve this velocity would cause severe engineering problems. Other liquids could be used in place of sodium but it would not then be possible to match both the ordinary Reynolds number and the magnetic Reynolds number, and, because most liquid metals have a lower conductivity than sodium, an even higher velocity would be necessary to achieve the same R_m.

We are unable to perform experiments with liquid sodium at Warwick and therefore we have, in all our experiments, used moving solid conductors to simulate the flow of a liquid when the magnetic Reynolds number is high. In the work in Chaps.6&7 on the performance of M.H.D. devices, the field perturbation and the eddy current loss which would occur in a liquid metal are represented by the calculated field perturbation and eddy current loss for a solid moving conductor.

Electrodes fitted to large M.H.D. devices may consist of flat strips of metal attached to the top and bottom of the duct, as shown in figure 6,

or they may be segmented as shown in figure 7. Large devices used in liquid sodium circuits would normally have ducts constructed from stainless steel and electrodes made of copper. If long continuous electrodes were fixed to a stainless steel duct a change in temperature would cause very large stresses along the joints between the dissimilar metals due to their different thermal expansions. It would be difficult to ensure that long copper electrodes made contact with the steel over the whole of the top and bottom surfaces of the duct. For these practical reasons large devices used in liquid sodium circuits will probably have segmented electrodes.

In the absence of contact resistance the addition of a pair of highly conducting electrodes to an M.H.D. duct would allow streamwise currents to flow in the electrodes and thus ensure that the electric potential was nearly uniform along the top and bottom of the duct. Segmented electrodes would allow no current to flow in the streamwise direction. We therefore expect the field perturbation and potential distribution in devices which have continuous electrodes of low resistivity (compared to that of the liquid in the duct) to be different from those in devices which have segmented electrodes. Because practical M.H.D. devices in which R_m is high are not likely to have electrodes whose resistance is low compared to that of the liquid in the duct, and are likely to have segmented electrodes, we confine our attention to the segmented electrode case.

We have built two experimental rigs. The first enabled us to investigate the field perturbation and power loss which occurred when no external circuits were connected to the moving metal so that the only currents which could flow were eddy currents within the conductor. The second rig was designed as a solid analogue of a complete flow coupler. Using this apparatus we were able to investigate the more realistic

cases in which currents could be drawn from the moving conductor. We also investigated some cases in which two conductors moved, with different speeds, through a common magnetic field.

The chapters of this thesis are presented almost in the order in which the work was performed. The work falls naturally into three distinct parts. Part I presents those experiments and theories concerned with the case of a moving conductor which has no external circuit (the flowmeter case), whilst part II is concerned with cases in which current is fed into, or extracted from, the moving conductor, and cases where two metals move with different velocities through a magnetic field. In part III we discuss the way in which we expect the modification, due to eddy currents, of the magnetic field and the potential distribution to affect the performance of M.H.D. devices operating at high magnetic Reynolds number.

cases in which currents could be drawn from the moving conductor. We also investigated some cases in which two conductors moved, with different speeds, through a common magnetic field.

The chapters of this thesis are presented almost in the order in which the work was performed. The work falls naturally into three distinct parts. Part I presents those experiments and theories concerned with the case of a moving conductor which has no external circuit (the flowmeter case), whilst part II is concerned with cases in which current is fed into, or extracted from, the moving conductor, and cases where two metals move with different velocities through a magnetic field. In part III we discuss the way in which we expect the modification, due to eddy currents, of the magnetic field and the potential distribution to affect the performance of M.H.D. devices operating at high magnetic Reynolds number.

Part I

Chapter 2.

Experiments to investigate the field perturbation and power loss when the electric current is confined within the M.H.D. duct.

In these experiments the slug flow of the liquid metal through a duct situated in a transverse magnetic field, was represented by a solid moving conductor. This conductor was an annular aluminium rim, having an inside diameter of 0.82 metres and an outside diameter of 0.9 metres, fitted as a tyre onto a Tufnol wheel. This whole assembly was mounted on an axle which was rotated by a 3 phase variable speed motor so that its rim passed between the poles of an electromagnet. Apart from the curvature of the rim the arrangement was geometrically similar to one channel of the flow coupler and was one tenth of the full size. To achieve the same magnetic Reynolds numbers in these experiments as those which would occur in the flow coupler it was necessary to make the rim of the wheel from a good electrical conductor and to drive the wheel at speeds of up to about 1000 rpm. These high speeds gave rise to large centrifugal forces in the rotating parts of the apparatus. Aluminium was chosen as a suitable rim material because in addition to being a good conductor it has a high strength-to-weight ratio.

The watercooled electromagnet, which was powered by a 60 kW motor-generator set, had shaped pole pieces fixed inside the magnet gap. These pole pieces had grooves machined in them in the form of arcs of a circle so that a Hall probe (AEI type FB22), mounted on a trolley which ran in these slots, could be traversed around the rim of the wheel. This rim was made in two parts so that the sensitive plate of the Hall probe, which measured the transverse magnetic field, ran in a slot between the two halves. The shaft which supported the rotating wheel also drove an electric tachometer whose output was displayed upon an ultraviolet chart recorder. Figure 8 shows a schematic representation of the apparatus whilst figure 9 is a photograph of the actual rig.

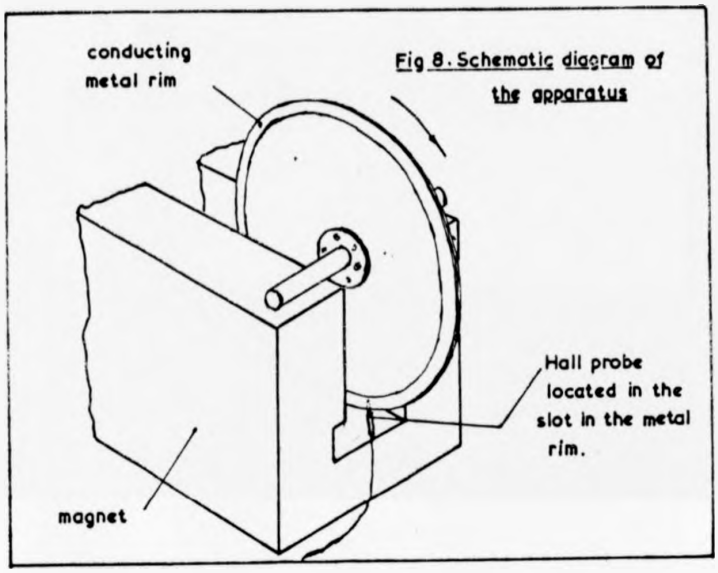

Fig 8. Schematic diagram of the apparatus

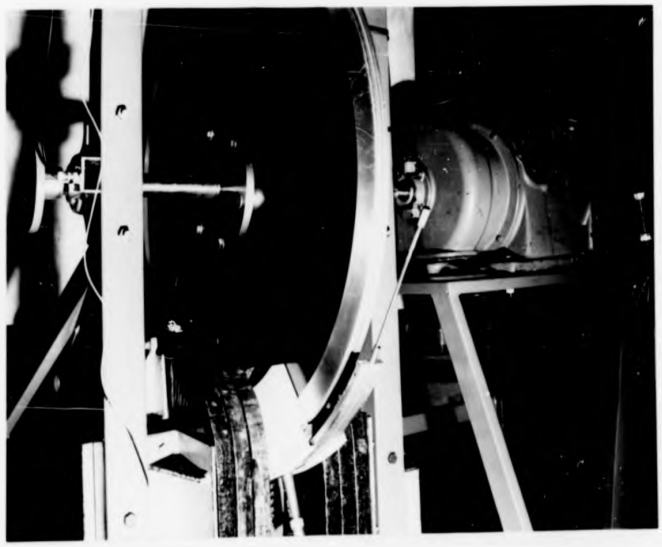

Fig. 9

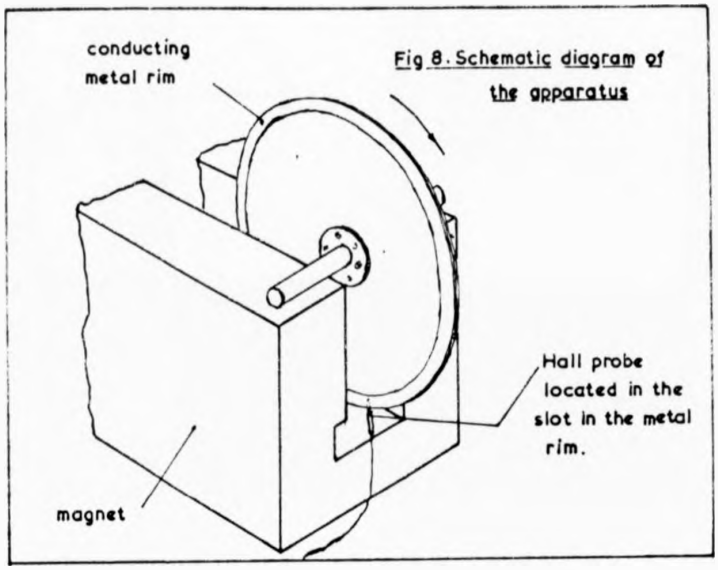

Fig 8. Schematic diagram of the apparatus

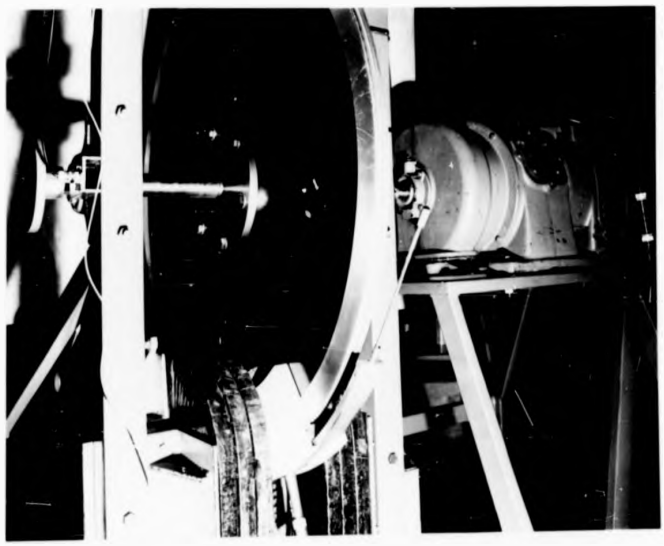

Fig. 9

The moment of inertia of the rotating parts of the apparatus, was measured by clamping a known mass to the rim of the wheel thereby converting it into a compound pendulum. From the period of oscillation the moment of inertia of the system was calculated.

Because the electric motor fitted to this apparatus produced insufficient torque to drive the rim of the wheel through the magnet gap at a steady speed the electromagnetic power loss was measured in the following way. The wheel was rotated at a high speed with no magnetic field. The motor was then switched off and the electromagnet switched on. As the wheel decelerated the ultraviolet chart recorder produced a graph showing speed of rotation of the wheel plotted against time. Part of the deceleration of the wheel was due to frictional losses and part due to eddy current losses in the rim.

Power (P) = torque (T) x angular velocity (ω) and torque (T) = moment of inertia (I) x angular acceleration ($\dot{\omega}$) so that $P = I\omega\dot{\omega}$

By measuring ω and $\dot{\omega}$ from the chart recorder graphs we were able to calculate the total power dissipation. The frictional losses were found by repeating the experiment with the electromagnet turned off. The electromagnetic loss in the rim was found by subtracting the frictional loss from the total power dissipation.

The Hall probe was connected to the chart recorder so that when the wheel decelerated graphs were obtained which showed the variation of magnetic field with time. Because simultaneous observations of speed were made, the magnetic field at this point in space could be found for any value of magnetic Reynolds number. By performing this experiment a number of times with the probe at a succession of points in the field region it was possible to build up field profiles for different magnetic Reynolds numbers.

Some principal parameters of the apparatus were measured and found to be:-

The aluminium rim: outside radius of curvature (R) = 0.45 metres,

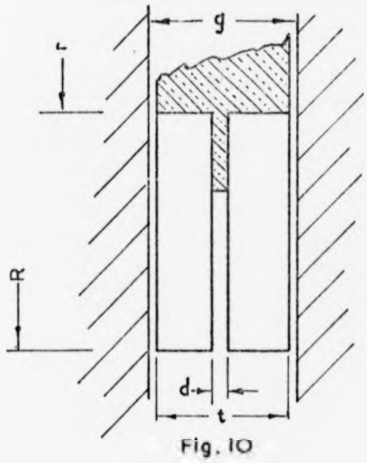

Fig. 10

inside radius of curvature (r) = 0.41 Metres,

thickness (t) = 0.022 metres,

width of slot (d) = 0.002 metres,

and electrical conductivity = 3.48×10^7 mhos/metre.

The magnet gap width (g) = 0.0252 metres and the moment of inertia of rotating parts = 3.406 kilogram metre^2.

Figure 10 shows a cross section of the wheel in the magnet gap.

The field in the magnet gap was measured, with the wheel removed, at a succession of different azimuthal positions firstly in the centre of the gap and then against one pole piece of the magnet. Figure 11 shows the magnetic field profiles obtained in this way. It can be seen that the corners of the pole pieces had the effect of locally increasing the magnetic field but that otherwise the two profiles are similar. When the Hall probe was traversed in a radial direction it was found that the magnetic field was constant over the region of interest.

Figure 12 shows the transverse magnetic field plotted against azimuthal position for several values of magnetic Reynolds number. These fields were measured in the slot between the two halves of the aluminium rim at a radius of 0.43 metres. It can be seen that the eddy currents produced an induced field which decreased the field at the entrance to the magnet and increased the field at the exit. At low magnetic Reynolds numbers, i.e. up about 5, the distortions of the field at the entry and the exit were separate from one another. At high R_m the effects blended together so that the enhancement of the field at the exit end was reduced. Similar observations of the tranverse magnetic

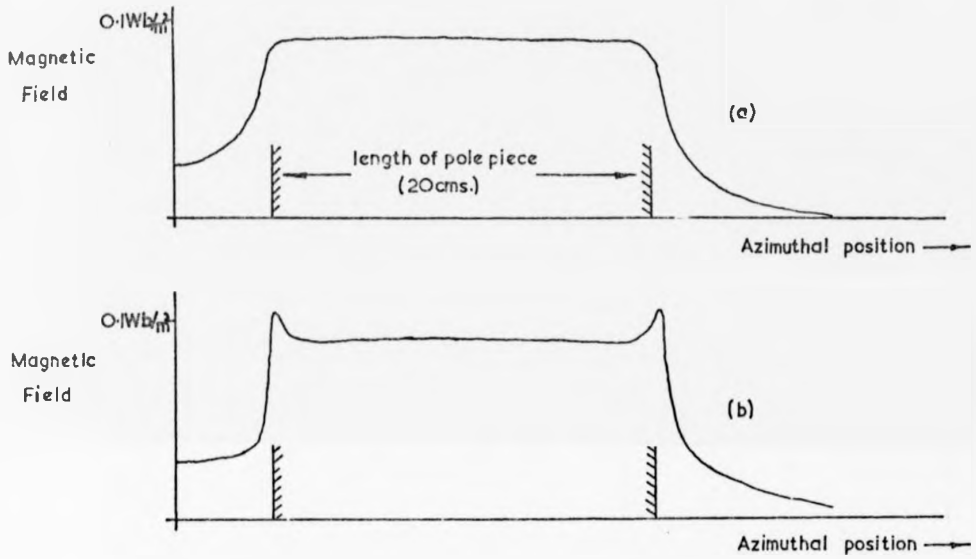

Transverse magnetic field plotted against azimuthal position, (a) at the centre of the magnet gap and (b) against the pole piece of the magnet.

fig. 11.

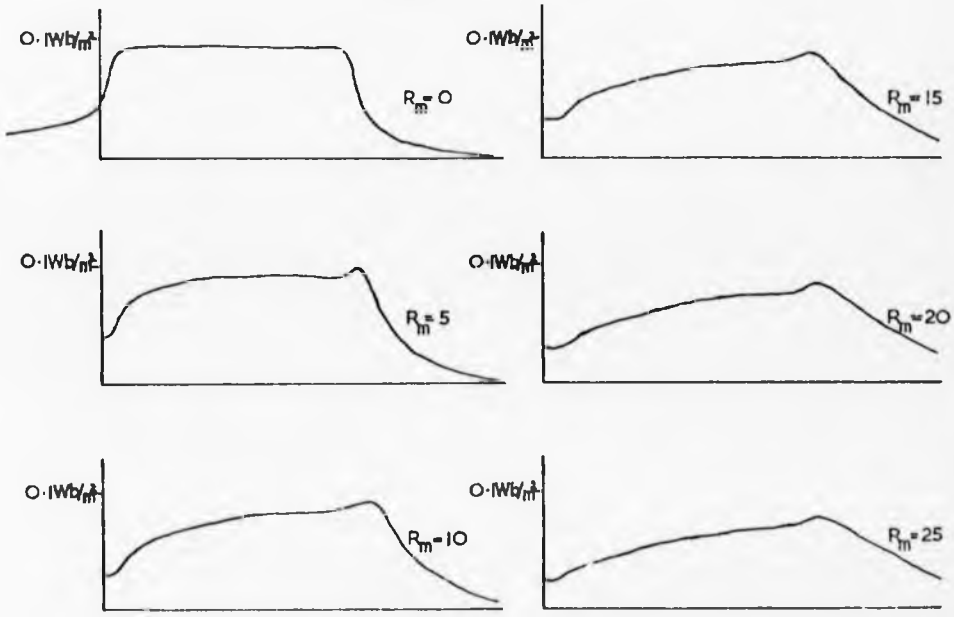

The transverse magnetic field at the centre of the magnet gap plotted against azimuthal position, for several values of Magnetic Reynolds No.

fig. 12.

field in the small gap between the iron pole piece and the moving aluminium rim were made for a number of values of R_m. Figure 13 contrasts the field profiles for $R_m = 5$ measured against a pole piece of the magnet and in the slot. It can be seen that the field in the gap is similar to the field at the surface of the pole piece.

Figure 14 shows profiles of the transverse magnetic field taken as the probe was traversed in a radial direction at the exit end of the magnet poles. Similar measurements were made at the entry end of the magnet, half way along the magnet and 0.107 metres outside the magnet at the exit end. These field measurements were made in the central slot where for mechanical reasons it was not possible to scan the probe across the whole of the rim. The dotted parts of the curves in this figure were obtained by assuming that, because the radius of curvature of the rim was large, the field distribution would be symmetrical about a line mid way between the upper and lower edges of the aluminium. All the field profiles obtained in this way showed that the field at the edge of the rim was always equal to the initial field provided by the electromagnet, that is, there was no induced field at the upper and lower edges of the aluminium.

Power measurements were made, using the previously-described deceleration methods, with several different values of magnetic field. Graphs were drawn upon which the logarithm of the power dissipation was plotted against the logarithm of the magnetic field for fixed values of magnetic Reynolds number. These graphs, which are shown in figure 15, indicate that the power dissipation was proportional to the square of the magnetic field.

Figure 16 shows how the eddy current loss in the rim of the wheel was found to depend upon the magnetic Reynolds number when the initial magnetic field was ·1050 and ·2060 Wb/m^2. It would appear that at high

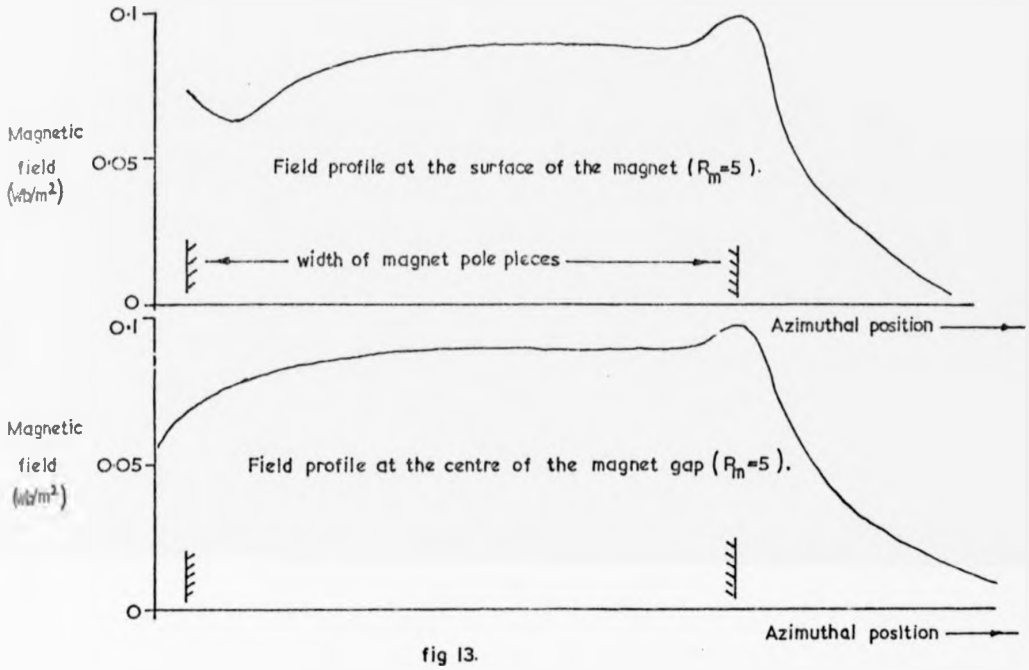

fig 13.

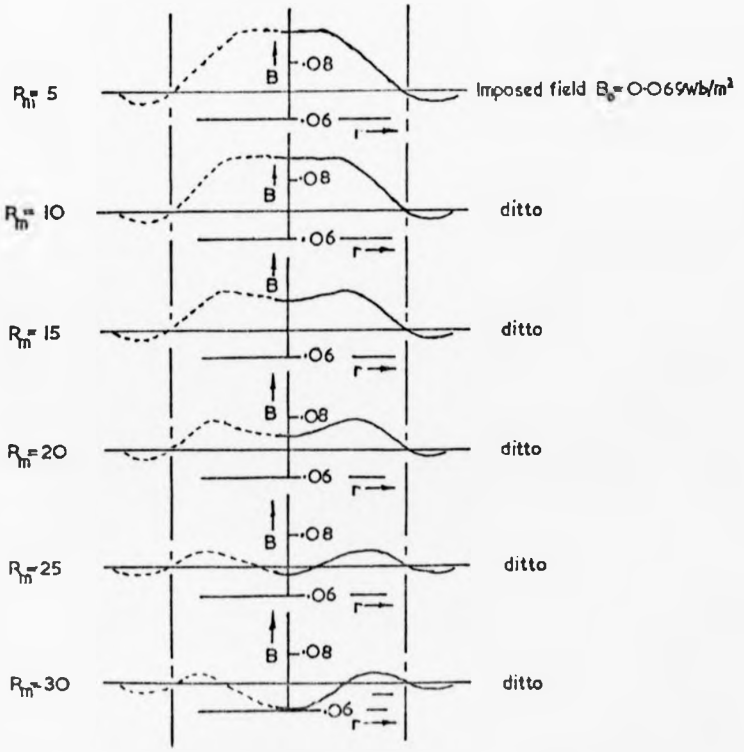

The transverse magnetic field at the exit end of the magnet plotted against radius

fig 14

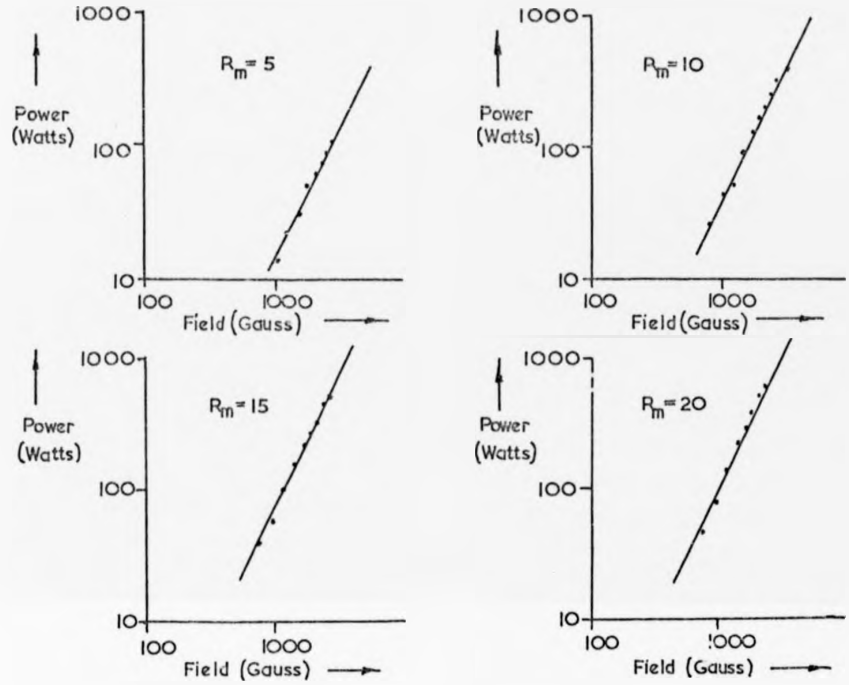

The power dissipation, plotted on a logarithmic scale, against the magnetic field, on a linear scale, for several values of magnetic Reynolds No., each graph has a slope of 2.

fig. 15.

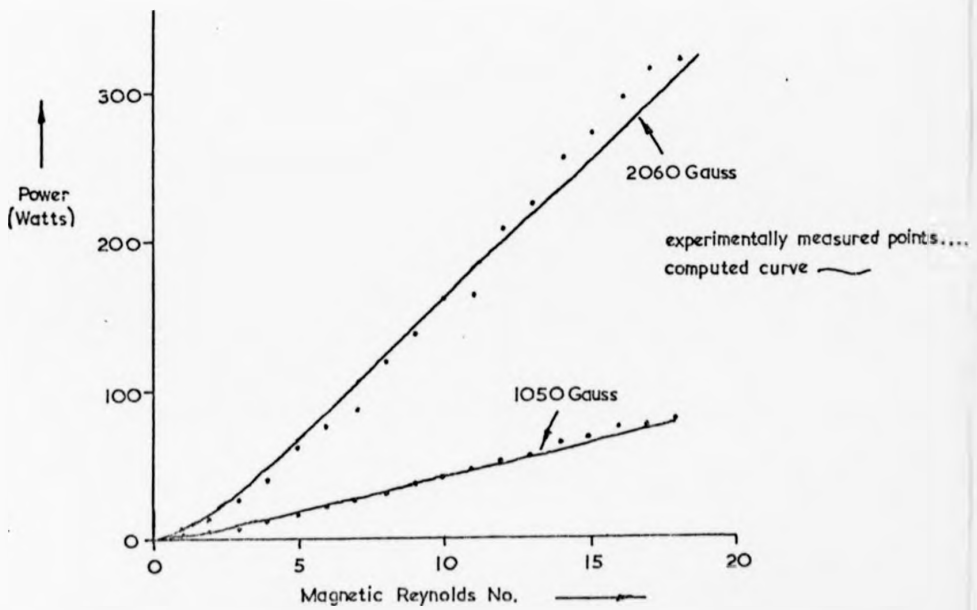

The power dissipation plotted against magnetic Reynolds No for applied magnetic fields of 1050 and 2060 Gauss.

fig. 16.

magnetic Reynolds numbers, in this case $R_m > 10$ the power dissipation is linearly related to R_m.

The accuracy of these power measurements was limited to about 10 or 15% because to calculate the power dissipated at a given value of R_m it was necessary to measure the slope of the graph produced by the tachometer and chart recorder as the wheel slowed down.

Chapter 3

The Magnetic Field and Potential Distribution within a Moving Conductor

3.1 The Magnetic Field

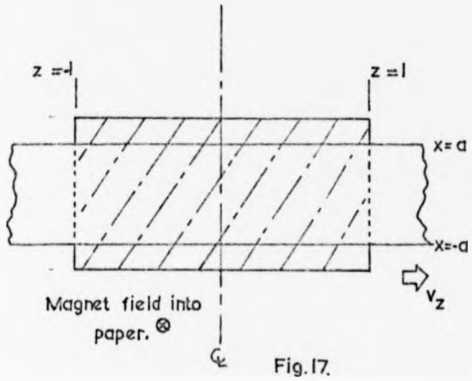

Fig.17.

Figure 17 represents a view, looking in the direction of the magnetic field, of a device in which a conductor passes between the poles of a magnet. The motion is in the positive z-direction. For simplicity it is assumed that the applied magnetic field starts abruptly at z=-l and ends abruptly at z=+l . Eddy currents circulate in the x-z planes within the metal producing an induced magnetic field $\underline{B}_i$ which opposes the applied field at the entrance to the magnet gap and enhances it at the exit.

The relevant equations are the Ohm's law equation, which is:-

$$\frac{\underline{j}}{\sigma} = \underline{E} + \underline{v} \times \underline{B}$$

where $\underline{B}$ is the magnetic field,

$\underline{v}$ is the velocity,

$\underline{E}$ is the electric field,

σ is the conductivity of the moving conductor,

and $\underline{j}$ is the current density, and Maxwell's equations $\text{curl } \underline{B} = \mu \underline{j}$,

$$\text{curl } \underline{E} = -\frac{\partial \underline{B}}{\partial t},$$

$$\text{div } \underline{B} = 0,$$

$$\text{and div } \underline{j} = 0.$$

Because $\text{curl } \underline{B} = \mu \underline{j}$ we may rewrite the Ohm's law equation in the form

$$\frac{1}{\mu\sigma} \text{curl } \underline{B} = \underline{E} + \underline{v} \times \underline{B}. \qquad (1)$$

Taking the curl of Equation(1) we find

$$\frac{1}{\mu\sigma} \text{curl curl } \underline{B} = \text{curl } \underline{E} + \text{curl } \underline{v} \times \underline{B}. \qquad (2)$$

In a stationary frame of reference $\frac{\partial \underline{B}}{\partial t} = 0$

and therefore curl $\underline{E} = 0$.

Using a well known vector identity we write

$$\text{curl } \underline{v} \times \underline{B} = \underline{v}.\text{div } \underline{B} - \underline{B}.\text{ div } \underline{v} + (\underline{B}.\text{grad})\underline{v} - (\underline{v}.\text{ grad})\underline{B}.$$

Because div $\underline{B} = 0$, div $\underline{v} = 0$ and the motion is solely in the z direction the above equation reduces to

$$\text{curl } \underline{v} \times \underline{B} = -v_z \frac{\partial \underline{B}}{\partial z},$$

and because curl curl $\underline{B}$ = grad div $\underline{B} - \nabla^2 \underline{B}$

Equation (2) becomes

$$\nabla^2 \underline{B} = v_z \mu \sigma \frac{\partial \underline{B}}{\partial z}. \qquad (3)$$

We may consider the magnetic flux density $\underline{B}$ as being composed of two parts, that is

$\underline{B} = \underline{B}_i + \underline{B}_a$ where $\underline{B}_a$ is the applied magnetic field

and $\underline{B}_i$ is the induced magnetic field.

We consider the field in three different regions of space. In region I, $z < -1$, the applied field is zero; in region II, $-1 < z < +1$, the applied field is B_o and in region III, $z > +1$, the applied field is zero.

This arrangement is shown in figure 18.

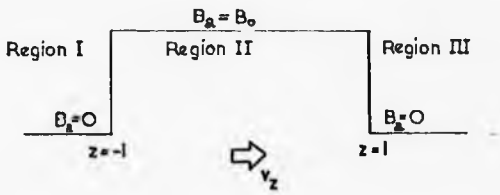

fig.18.

We expect that currents circulating in the magnet gap produce a field which is greater than the field they would have produced in a region well away from the magnet. B_i has two components, part of the induced field ($\underline{B}i_c$) is caused directly by the circulating eddy current whilst part ($\underline{B}i_m$) is caused by the magnetization of the iron magnet, thus,

$$\underline{B}i = \underline{B}i_c + \underline{B}i_m .$$

The field B_{i_z} can be considered as the field due to an equivalent current density j' in the iron and a current sheet of density λ on the surface of the pole pieces. This contribution to the induced magnetic field only exists in the region where the moving metal is within the magnet gap so that upon entering or leaving this region the induced field must change. In general it will be difficult to calculate B_{i_z} because it will depend upon the current distribution within the magnet gap, and the physical properties of both the magnet and the moving conductor.

We have made a coil having a diameter equal to the width of the aluminium rim that was described in the last chapter. A known current was passed through this and the field at its centre was measured when it was first in, and then out, of the magnet gap. The field caused by this coil when in the magnet gap was found to be about twice the field it produced when it was well away from any iron.

We have solved Equation (3), in the two dimensions x and z, by assuming that the transverse magnetic field did not vary in the y-direction and that the reluctance of the external magnetic circuit was everywhere the same, that is to say a circulating eddy current would produce the same magnetic field whether it was in region I, II or III. Later we suggested that the tranverse field caused by the magnetization of the iron would be proportional to the transverse field produced by the circulating eddy currents so that $B_{i_m} = mB_{i_c}$ where m was a constant which would depend upon the dimensions, geometry and physical properties of the magnet and the moving conductor. When the results of this analysis were compared with experimentally measured field profiles it was found that no closer agreement could be obtained than with the former theory in which we assumed that the reluctance of the external magnetic circuit was everywhere the same. This suggests that in order to take full account of the effect of the iron magnet upon the induced magnetic field it is

necessary to solve Equation(3) in three dimensions. Such a solution would be very complex and would necessarily involve the physical properties of the magnet itself. Computed field profiles, based on the theory we present here, which ignores the effect of the iron upon the induced field, agree surprisingly well with the experimentally measured field.

We now consider the case in which the magnetic field is assumed to be transverse and invariant in the y direction. The applied field ($\underline{B}_a$) does not vary in the x direction and is zero except that $\underline{B}_a = \underline{B}_o$ when $1>z>-1$. As we consider only the transverse magnetic field we omit the subscripts and simply refer to the field as B.

Now $\mu\underline{j} = \text{curl } \underline{B} = \text{curl } (\underline{B}_a + \underline{B}_i) = \text{curl } \underline{B}_i$ since curl $\underline{B}_a = 0$. It follows that $j_x = -\frac{1}{\mu}\frac{\partial B_i}{\partial z}$ and $j_z = \frac{1}{\mu}\frac{\partial B_i}{\partial x}$. The streamwise component of the current density, in region I at $z = -1$ must be the same as the streamwise component of the current density at $z = -1$ in region II. Then $\frac{\partial B_i}{\partial x}$ at $z = -1$ in region I $= \frac{\partial B_i}{\partial x}$ at $z = -1$ in region II. Using a similar argument we find that $\frac{\partial B_i}{\partial x}$ at $z = +1$ in region II $= \frac{\partial B_i}{\partial x}$ at $z = +1$ in region III.

It is easily shown that at the top and bottom of the duct ($x = \pm a$) the induced field B_i is zero for all values of z. No current is drawn from the duct and therefore $j_z = 0$ at $x = \pm a$. It follows that $\frac{\partial B_i}{\partial z} = 0$ at $x = \pm a$, but $B_i \to 0$ as $z \to \infty$ so $B_i = 0$ for all z at $x = \pm a$.

The electric potential distribution at $z = -1$ in region I must be the same as electric potential distribution at $z = -1$ in region II, consequently the electric field (ie. minus the potential gradient) at $z = -1$ in region I is the same as the electric field at $z = -1$ in region II.
Then E_x at $z = -1$ in region I $= E_x$ at $z = -1$ in region II for all x,
and E_x at $z = +1$ in region II $= E_x$ at $z = +1$ in region III for all x.
In addition we expect the induced magnetic field to be symmetrical about $x = 0$ so that $\frac{\partial B_i}{\partial x} = 0$ at $x = 0$.

Any solution of equation (3) must now satisfy the following boundary conditions.

(a) $B_i \to 0$ as $z \to \pm\infty$ for all x,

(b) B_i is a maximum at $x = 0$, that is $\frac{\partial B_i}{\partial x} = 0$ at $x = 0$ for all z,

(c) B_i is zero at $x = \pm a$ for all z,

(d) $\frac{\partial B_i}{\partial x}$ at $z = -1$ in region I = $\frac{\partial B_{ii}}{\partial x}$ at $z = -1$ in region II for all x,

and $\frac{\partial B_i}{\partial x}$ at $z = +1$ in region II = $\frac{\partial B_{iii}}{\partial x}$ at $z = +1$ in region III, for all x,

(e) E_x at $z = -1$ in region I = E_x at $z = -1$ in region II for all x

and E_x at $z = +1$ in region II = E_x at $z = +1$ in region III for all x.

Using the method of seperation of variables we look for a solution of the form $B = X(x)Z(z)$ where X is a function of x only and Z is a function of z only.

On substituting into equation (3) we find

$$\frac{1}{X}\frac{\partial^2 X}{\partial x^2} = -\phi^2, \tag{4}$$

$$\text{and } \frac{1}{Z}\frac{\partial^2 Z}{\partial z^2} - \frac{R_m}{a}\frac{\partial Z}{\partial z} - \phi^2 = 0, \tag{5}$$

where ϕ^2 is the seperation constant. ϕ^2 cannot be negative since Equation (4) would then yield solutions growing exponentially with x. ϕ^2 is therefore replaced by C^2 where C is either zero or a real number.

When C = 0 Equations (4) and (5) become

$$\frac{1}{X}\frac{\partial^2 X}{\partial x^2} = 0, \tag{6}$$

$$\text{and } \frac{1}{Z}\frac{\partial^2 Z}{\partial z^2} - \frac{R_m}{a}\frac{\partial Z}{\partial z} = 0. \tag{7}$$

Equations (6) and (7) have solutions $X = Gx + K$ and $Z = E + Fe^{\frac{R_m z}{a}}$ where G,K,E and F are arbitary constants. When C = 0 a solution is

$$B = (Gx + K)(E + Fe^{\frac{R_m}{a} z}).$$

When $C \neq 0$ Equations (4) and (5) become

$$\frac{1}{X}\frac{\partial^2 X}{\partial x^2} = -C^2, \tag{8}$$

and $$\frac{1}{Z}\frac{\partial^2 Z}{\partial z^2} - \frac{R_m}{a}\frac{1}{Z}\frac{\partial Z}{\partial z} - C^2 = 0 \tag{9}$$

Equation (8) has a solution of the form

$$X = A\sin cx + B\cos cx .$$

Looking for solutions to equation (9) of the form $Z = \varepsilon e^{\alpha z}$ we obtain the following auxiliary equation

$$\alpha^2 - \frac{R_m}{a}\alpha - C^2 = 0$$

which has roots

$$\alpha_1 = \frac{R_m}{a} + \sqrt{\frac{R_m^2}{a^2} - 4C^2}$$

and $$\alpha_2 = \frac{R_m}{a} - \sqrt{\frac{R_m^2}{a^2} - 4C^2}$$

Thus when $C \neq 0$ we seek solutions of the form

$$B = \left(He^{\alpha_1 z} + Ie^{\alpha_2 z}\right)\left(A\sin cx + B\cos cx\right).$$

A general solution for all values of C is

$$B = \left(Gx + K\right)\left(E + Fe^{\frac{R_m}{a}z}\right) + \sum_{\text{All } C \neq 0}\left(H_c e^{\alpha_1 z} + I_c e^{\alpha_2 z}\right)\left(A_c\sin cx + B_c\cos cx\right).$$

In order to satisfy boundary condition (b) that $\frac{\partial B}{\partial x} = 0$ at $x = 0$ we take G and each A_c to be zero. Then

$$B = \left(E' + Fe^{\frac{R_m}{a}z}\right) + \sum_{\text{All } C \neq 0}\left(H_c' e^{\alpha_1 z} + I_c' e^{\alpha_2 z}\right)\cos cx$$

where E', F', H_c' and I_c' are arbitary constants.

Boundary condition (c) is that the magnetic field at $x = \pm a$ is the applied field B_a . To satisfy this condition we take F' to be zero and we choose C such that each coscx term is zero at $x = \pm a$. It follows that the constant E' must be equal to the applied magnetic field B_a . For each coscx term to be zero at $x = a$ we put $ca = \frac{n\pi}{2}$ where n is an odd number so that $c = \frac{n\pi}{2a}$ where $n = 1,3,5$ .. etc.

The general solution now becomes:-

$$B = B_a + \sum_{n=1,3,5\ldots} \left(H_n e^{\alpha_1 z} + I_n e^{\alpha_2 z} \right) \cos \frac{n\pi x}{2a} ,$$

where $$\alpha_1 = \frac{1}{2a} \left(R_m + \left(R_m^2 + n^2\pi^2 \right)^{\frac{1}{2}} \right)$$

and $$\alpha_2 = \frac{1}{2a} \left(R_m - \left(R_m^2 + n^2\pi^2 \right)^{\frac{1}{2}} \right).$$

In region I $B_a = 0$ and $B \to 0$ as $z \to -\infty$ so we choose a solution of the form

$$B = \sum_{n=1,3,5\ldots} A_n e^{\alpha_1 z} \cos \frac{n\pi x}{2a} . \qquad (10)$$

In region II $B_a = B_o$ so we choose a solution of the form

$$B = B_o + \sum_{n=1,3,5\ldots} \left(B_n e^{\alpha_1 z} + C_n e^{\alpha_2 z} \right) \cos \frac{n\pi x}{2a} . \qquad (11)$$

In region III $B_a = 0$ and $B \to 0$ as $z \to \infty$ so we choose

$$B = \sum_{n=1,3,5\ldots} D_n e^{\alpha_2 z} \cos \frac{n\pi x}{2a} . \qquad (12)$$

Using boundary condition (d) we find that at $z = -l$

$$-\sum_{n=1,3,5\ldots} A_n e^{-\alpha_1 l} \frac{n\pi}{2a} \sin \frac{n\pi x}{2a} = -\sum_{n=1,3,5\ldots} \left(B_n e^{-\alpha_1 l} + C_n e^{\alpha_2 l} \right) \frac{n\pi}{2a} \sin \frac{n\pi x}{2a} ,$$

multiplying by $\sin \frac{p\pi x}{2a}$ and integrating from $x = 0$ to $x = a$ we find that

$$A_n e^{-\alpha_1 l} = B_n e^{-\alpha_1 l} + C_n e^{\alpha_2 l} . \qquad (13)$$

Similarly at $z = +l$ we find

$$D_n e^{\alpha_2 l} = B_n e^{\alpha_1 l} + C_n e^{\alpha_2 l} . \qquad (14)$$

Boundary condition (e) is that E_x at $z = -l$ in region I = E_x at $z = -l$ in region II. The Ohm's law equation is $\frac{j}{\sigma} = \underline{E} + \underline{v} \times \underline{b}$ which, because curl $\underline{B} = \mu \underline{j}$ we may rewrite in the form

$$\frac{1}{\mu\sigma} \text{ curl } \underline{B} = \underline{E} + \underline{v} \times \underline{B} ,$$

the x component of this is $-\frac{1}{\mu\sigma}\frac{\partial B}{\partial z} = E_x - v_z B$

so that $E_x = v_z B - \frac{1}{\mu\sigma}\frac{\partial B}{\partial z}$. (15)

Then

$$\left[v_z B_i - \frac{1}{\mu\sigma}\frac{\partial B_i}{\partial z}\right] = \left[v_z (B_o + B_i) - \frac{1}{\mu\sigma}\frac{\partial B_i}{\partial z}\right], \quad (16)$$

at $z = -1$ in region I; at $z = -1$ in region II

In order to use Equation (16) it is necessary to express B_o as a function of x by writing it as a Fourier series in terms of $\cos\frac{n\pi x}{2a}$ so that $B_o = B_o \sum_{n=1,3,5\ldots} G_n \cos\frac{n\pi x}{2a}$.

Substituting into Equation (16), multiplying by $\cos\frac{n\pi x}{2a}$ and integrating from x = o to x = a we find that

$$A_n e^{-\alpha_1 l} = -\frac{R_m}{a\alpha_1} B_o G_n + B_n e^{-\alpha_1 l} + \frac{\alpha_2}{\alpha_1} C_n e^{-\alpha_2 l}. \quad (17)$$

By considering the electric field at $z = +1$ in a similar way we find that

$$D_n e^{\alpha_2 l} = -\frac{R_m}{a\alpha_2} B_o G_n + \frac{\alpha_1}{\alpha_2} B_n e^{\alpha_1 l} + C_n e^{\alpha_2 l}. \quad (18)$$

Solving equations (13),(14),(17) and (18) for A_n, B_n, C_n, and D_n, we find that

$$A_n = \frac{B_o R_m G_n}{aK}\left(e^{-\alpha_1 l} - e^{\alpha_1 l}\right), \quad (19)$$

$$B_n = \frac{B_o R_m G_n}{aK} e^{-\alpha_1 l}, \quad (20)$$

$$C_n = -\frac{B_o R_m G_n}{aK} e^{\alpha_2 l}, \quad (21)$$

$$D_n = \frac{B_o R_m G_n}{aK}\left(e^{\alpha_2 l} - e^{\alpha_2 l}\right), \quad (22)$$

where $$\alpha_1 = \frac{1}{2a}\left(R_m + (R_m^2 + n^2\pi^2)^{\frac{1}{2}}\right), \tag{23}$$

$$\alpha_2 = \frac{1}{2a}\left(R_m - (R_m^2 + n^2\pi^2)^{\frac{1}{2}}\right), \tag{24}$$

and $$K = \alpha_1 - \alpha_2 . \tag{25}$$

We have expressed the applied magnetic field as a Fourier series in x, that is

$$B_c = B_0 \sum_{n=1,3,5\ldots} G_n \cos\frac{n\pi x}{2a}$$

$$= B_0 f(x) .$$

To find G_n we consider a magnetic field such that

$f(x) = -1 \qquad x < -a$,

$f(x) = 1 \qquad -a < x < a$,

$f(x) = -1 \qquad x > a$.

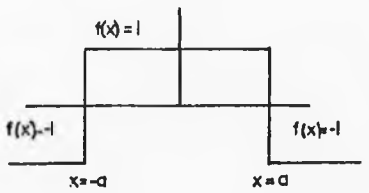

fig 19.

For a half range Fourier series

$$G_n = \frac{1}{a}\int_0^{2a} f(x)\cos\frac{n\pi x}{2a}\,dx$$

$$= \frac{4}{n\pi}\sin\frac{n\pi}{2}$$

so that in Equations (19),(20),(21) and (22) G_n is given by the expression:-

$$G_n = -\frac{4}{n\pi}(-1)^{\frac{n+1}{2}}. \tag{26}$$

We have used Equations (10),(11) and (12) together with the appropriate values of A_n , B_n , C_n and D_n, to calculate the total magnetic field at several values of magnetic Reynolds numbers for an initially uniform magnetic field which starts abruptly at z = -1 metres and ends abruptly at z = +1 metres. Figures 20 shows the computed field profile for an R_m of 10 when l = 0.1m. and a = 0.02 m..

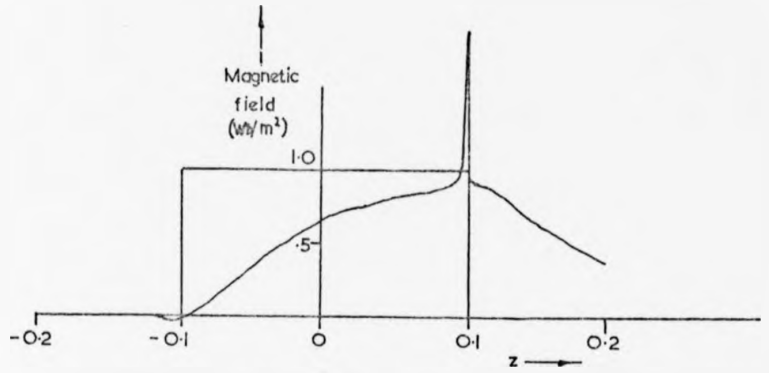

The computed field for an R_m of 10 when $a = 0{\cdot}02m$, $\ell = 0{\cdot}2m$, and the initial magnetic field is $1{\cdot}0 Wb/m^2$.

fig 20.

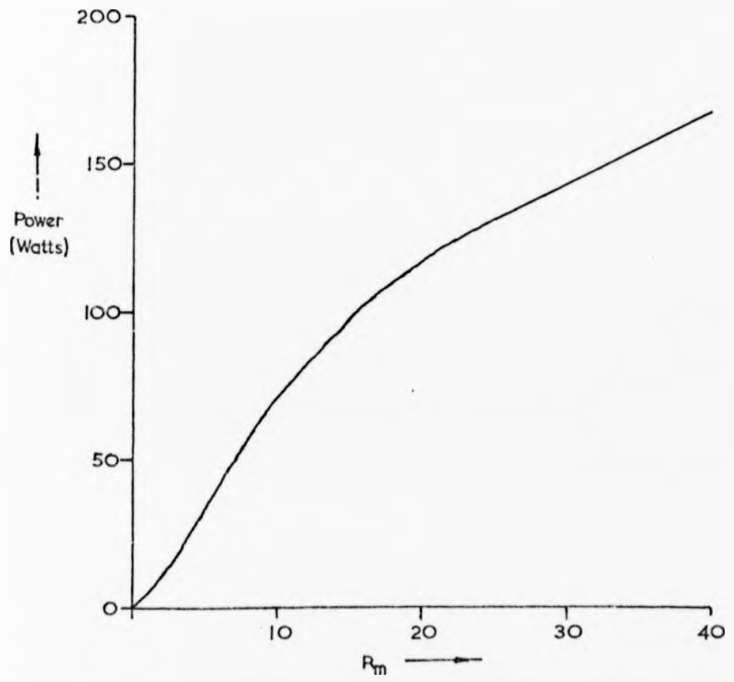

The computed power loss, for an abrupt initial field of $0{\cdot}1 Wb/m^2$, plotted against magnetic Reynolds No. The field region had a length 2ℓ of $0{\cdot}2m$, $a = 0{\cdot}02m$.

fig. 22.

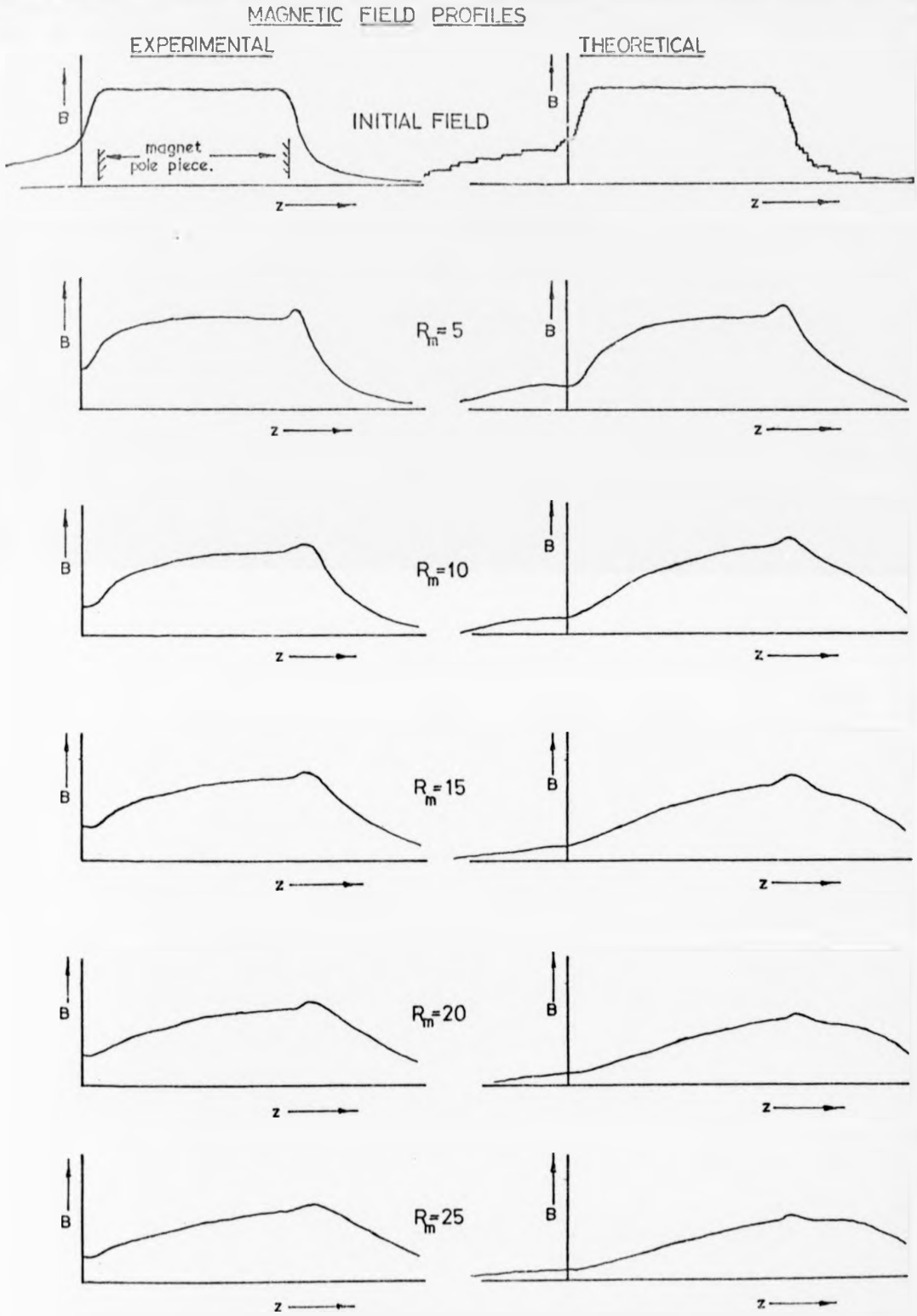

Magnetic field profiles at several values of magnet Reynolds No., the initial field of 0·092Wb/m² was uniform over a length of approx. 0·2m.

fig. 21.

We consider a non-abrupt magnetic field as being composed of many superimposed abruptly ending elements of field extending over different distances in the z - direction. We have used the computer program presented in appendix A to evaluate the induced field which occurs at chosen values of R_m with an initial field profile similar to the experimentally measured profile. Because the radius of curvature of the wheel is large we compare the measured profiles with field profiles which have been computed for the case of a straight conductor. Figure 21 shows the computed and observed profiles side by side. It will be noticed that the agreement between the theoretical and the experimental field profiles is good at R_m's of up to about 5 but is less satisfactory at high R_m. When the magnetic Reynolds number is high an induced field exists well outside the magnet region, the transverse component of the field then varies in the y direction so that our two-dimensional treatment of the problem becomes rather unrealistic.

3.2 The Power Loss

Eddy currents circulating within the conductor cause ohmic heating. The magnitude of this power loss is given by:-

$$P = \int\int\int \frac{j^2}{\sigma} \, dx \, dy \, dz .$$

For a case in which the eddy currents flow solely in the x-z plane and in which the distribution of these currents does not vary in the y-direction,

$$P = \frac{2t}{\sigma} \int_{-\infty}^{+\infty} \int_{0}^{a} j^2 \, dx \, dz . \qquad (27)$$

Because curl $\underline{B} = \mu \underline{j}$ $\quad j_x = \frac{-1}{\mu} \frac{\partial B}{\partial z}$ and $\quad j_z = \frac{1}{\mu} \frac{\partial B}{\partial x}$,

Equation (27) becomes

$$P = \frac{2t}{\mu^2 \sigma} \int_{-\infty}^{+\infty} \int_{0}^{a} \left[\left(\frac{\partial B}{\partial x} \right)^2 + \left(\frac{\partial B}{\partial z} \right)^2 \right] dx \, dz . \qquad (28)$$

We have shown that in region I, $B_z = \sum A_n e^{\alpha_n z} \cos \frac{n\pi x}{2a}$.

If we take the first 10 terms of this series to represent the magnetic field then $\frac{\partial B}{\partial z}$ will be represented by the first 10 terms of $\frac{\partial B_z}{\partial z} = \sum A_n \alpha_n e^{\alpha_n z} \cos \frac{n\pi x}{2a}$ However j_x^2, which is $\left(\frac{1}{\mu}\frac{\partial B_z}{\partial z}\right)^2$, will now be represented by an expression containing 100 terms. It can be seen that it is not simple to calculate the integral in Equation (28) from Equations (10), (11) and (12). We have written a computer program to calculate the magnetic field in the moving conductor for a chosen value of magnetic Reynolds number. Using this program we can calculate $\frac{\partial B}{\partial x}$ and $\frac{\partial B}{\partial z}$ at a large number of places. The integral in Equation (28) is then evaluated by summing the values of $\left(\frac{\partial B}{\partial x}\right)^2$ and $\left(\frac{\partial B}{\partial z}\right)^2$ throughout the moving conductor.

Figure 22 shows how the power loss in the metal, calculated in the above manner, depends upon the magnetic Reynolds number for an initial abrupt field of $0.1 w/m^2$ when $l = 0.1$ m. and $a = 0.02$m.. At high R_m the power loss seems to be linearly related to the magnetic Reynolds number.

The continuous line in fig. 16 shows the power loss which has been calculated, from a theoretical field distribution, for a solid conductor moving through a non abrupt magnetic field similar to the experimentally observed field. The good agreement between theory and experiment may well be fortuitous, it must be remembered that the accuracy of the power measurements is limited to about 15%.

3.3 The Electric Potential Distribution

Once again the relevant equations are $\underline{j} = \underline{E} + \underline{v} \times \underline{B}$, curl $\underline{B} = \mu \underline{j}$, curl $\underline{E} = -\frac{\partial B}{\partial t}$, div $\underline{B} = 0$, and div $\underline{j} = 0$. Taking the divergence of the Ohm's law equation we have $\frac{1}{\sigma} \operatorname{div} \underline{j} = 0 = \operatorname{div} \underline{E} + \operatorname{div}(\underline{v} \times \underline{B})$.
Now $\underline{E} = -\operatorname{grad} U$ and therefore $\operatorname{div} \underline{E} = \operatorname{div}(-\operatorname{grad} U) = -\nabla^2 U$ so that
$\nabla^2 U = \operatorname{div}(\underline{v} \times \underline{B}) = \underline{B}.\operatorname{curl} \underline{v} - \underline{v}.\operatorname{curl} \underline{B}$.

If we consider the velocity to be purely in the z-direction and uniform throughout the channel at a value v_z then $\nabla^2 U = -v_z \frac{\partial B}{\partial x}$ where

the magnetic field $\underline{B}$ is again assumed to be solely in the y-direction.

Because curl $\underline{B} = \mu \underline{j}$, $\mu j_z = \frac{\partial B}{\partial x}$ so that $\nabla^2 U = -v_z \mu j_z$. (29)

From the Ohm's law equation we find that $j_z = \sigma E_z = -\sigma \frac{\partial U}{\partial z}$, Equation (29) now becomes $\nabla^2 U = v_z \mu \sigma \frac{\partial U}{\partial z}$,

or $\nabla^2 U = \frac{R_m}{a} \frac{\partial U}{\partial z}$. (30)

To solve Equation (30) we again let the magnetic field consist of two parts, the applied field $\underline{B}_a$ and an induced field $\underline{B}_i$ so that $B = B_a + B_i$. We choose an applied field B_a such that

$B_a = 0$ in region I, $z < -l$,

$B_a = B_o$ in region II, $-l < z < +l$,

$B_a = 0$ in region III, $z > +l$.

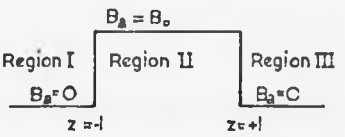

fig. 24.

We have previously shown that when no current is drawn from the duct the induced field at the top and bottom ($x = \pm a$) is zero.

From the Ohm's law equation we find that $\frac{j_x}{\sigma} = -\frac{\partial U}{\partial x} - v_z B$

but because j_x is zero and the induced field is zero, $\frac{\partial U}{\partial x} = -v_z B_a$ at $x = \pm a$ for all z. We require a solution of Equation (30) which satisfies the following boundary conditions.

a) $U \to 0$ as $z \to \pm \infty$ for all x,

b) $U = 0$ at $x = 0$ for all z,

c) $\frac{\partial U}{\partial x} = -v_z B_a$ at $x \pm a$ for all z,

d) U at $z = -1$ in region I = U at $z = -1$ in region II for all x,

U at $z = +1$ in region II = U at $z = +1$ in region III for all x,

e) j_z and hence $\frac{\partial U}{\partial z}$ is continuous for all x at the boundaries $z = \pm 1$, so that $\frac{\partial U}{\partial z}$ at $z = -1$ in region I, = $\frac{\partial U}{\partial z}$ at $z = -1$ in region II, for all x, and $\frac{\partial U}{\partial z}$ at $z = +1$ in region II = $\frac{\partial U}{\partial z}$ at $z = +1$ in region III for all x.

Using the method as separation of variables we look a solution of the form :-

$U = X(x)Z(z)$ where X is a function of x only,

and Z is a function of z only.

On substituting into Equation(1)we find

$$\frac{1}{X}\frac{\partial^2 X}{\partial x^2} = -\lambda \,, \tag{31}$$

and $$\frac{1}{Z}\frac{\partial^2 Z}{\partial z^2} - \frac{R_m}{a}\frac{\partial Z}{\partial z} - \lambda = 0 \,. \tag{32}$$

where λ is the separation constant. λ cannot be negative since Equation (31) would then yield solutions growing exponentially with x. λ is therefore replaced by C^2 where C is either zero or a real number.

When C = 0 Equations (31) and (32) become:-

$$\frac{1}{X}\frac{\partial^2 X}{\partial x^2} = 0 \,, \tag{33}$$

and $$\frac{1}{Z}\frac{\partial^2 Z}{\partial z^2} - \frac{R_m}{a}\frac{\partial Z}{\partial z} - \lambda = 0 \,. \tag{34}$$

Equations (33) and (34) have solutions of the form

$X = Gx + K,$

$Z = E + Fe^{\frac{R_m}{a}z},$

where E,F,G and K are arbitary constants so that

when C = 0 a solution is

$$U = \left(Gx + K\right)\left(E + Fe^{\frac{R_m}{a}z}\right) .$$

When $C \neq 0$ Equations (31) and (32) become

$$\frac{1}{X}\frac{\partial^2 X}{\partial x^2} = -C^2 \,, \tag{35}$$

and $$\frac{1}{Z}\frac{\partial^2 Z}{\partial z^2} - \frac{R_m}{a}\frac{\partial Z}{\partial z} - C^2 = 0 . \qquad (36)$$

Equation (35) has solutions of the form

$X = A\sin cx + B\cos cx.$

Looking for solutions to equation (36) of the form $Z = ke^{\alpha z}$ we obtain the following auxiliary equation

$$\alpha^2 - \frac{R_m}{a}\alpha - C^2 = 0,$$

which has roots $$\alpha_1 = \frac{R_m}{a} + \sqrt{\frac{R_m^2}{a^2} + 4C^2},$$

and $$\alpha_2 = \frac{R_m}{a} - \sqrt{\frac{R_m^2}{a^2} + 4C^2}.$$

Thus when $C \neq 0$ we seek solutions of the form

$$U = \left(He^{\alpha_1 z} + Ie^{\alpha_2 z}\right)\left(A\sin cx + B\cos cx\right).$$

A general solution for all values of C is

$$U = \left(Gx + K\right)\left(E + Fe^{\frac{R_m}{a}z}\right) + \sum_{\text{All } c\neq 0}\left(H_c e^{\alpha_1 z} + I_c e^{\alpha_2 z}\right)\left(A_c\sin cx + B_c\cos cx\right).$$

In order to satisfy boundary condition b), that $U = 0$ at $x = 0$ for all z, we take K and each B_c to be zero. Then

$$U = Gx\left(E + Fe^{\frac{R_m}{a}z}\right) + \sum_{\text{All } c\neq 0}\left(H_c e^{\alpha_1 z} + I_c e^{\alpha_2 z}\right)\sin cx . \qquad (37)$$

Boundary condition c) is $\left(\frac{\partial U}{\partial x}\right)_{x=\pm a} = -V_z B_a$ for all z.

From Equation (37) we have

$$\left(\frac{\partial U}{\partial x}\right)_{x=\pm a} = Ga\left(E + Fe^{\frac{R_m}{a}z}\right) + \sum_{\text{All } c\neq 0}\left(H_c e^{\alpha_1 z} + I_c e^{\alpha_2 z}\right)c\cos ca = -V_z B_a .$$

Now B_x is piece-wise constant, being zero in regions I and III and of value B_o in region II. To satisfy this boundary condition we therefore take F and every cos ca term to be zero.

It follows that $ca = \frac{n\pi}{2}$ where n is an odd number

so that $c = \frac{n\pi}{2a}$ where n = 1,3,5..

The general solution (Equation (37)) now reduces to

$$U = Gx + \sum_{n=1,3,5\ldots} \left(H_n e^{\alpha_1 z} + I_n e^{\alpha_2 z}\right) \sin \frac{n\pi x}{2a} \qquad (38)$$

where $\alpha_1 = \frac{1}{2a}\left(R_m + \left(R_m^2 + n^2\pi^2\right)^{\frac{1}{2}}\right)$,

and $\alpha_2 = \frac{1}{2a}\left(R_m - \left(R_m^2 + n^2\pi^2\right)^{\frac{1}{2}}\right)$,

Now in region I $B_x = 0$, and boundary condition c) becomes $\left(\frac{\partial U}{\partial x}\right)_{x=\pm a} = 0$ so that G in Equation (38) must be zero. We also require that $U \to 0$ as $Z \to -\infty$ so that all values of I_n in Equation (38) must be zero. We therefore choose a solution of the form

$$U = \sum_{n=1,3,5} J_n e^{\alpha_1 z} \sin \frac{n\pi x}{2a} \qquad (39)$$

where J_n is an arbitary constant.

In region II boundary condition c) becomes $\left(\frac{\partial U}{\partial x}\right)_{x=\pm a} = -v_z B_o$. Differentiating Equation (38) and writing $\left(\frac{\partial U}{\partial x}\right)_{x=\pm a} = -v_z B_o$ we find that $G = -v_z B_o$ so that in region II the solution is of the form.

$$U = -v_z B_o x + \sum_{n=1,3,5\ldots} \left(M_n e^{\alpha_1 z} + N_n e^{\alpha_2 z}\right) \sin \frac{n\pi x}{2a} \qquad (40)$$

where M_n and N_n are arbitary constants.

B_x is zero in region III so that $\left(\frac{\partial U}{\partial x}\right)_{x=\pm a} = 0$ and G in Equation (38) must be zero. We require that $U \to 0$ as $Z \to \infty$ so that all values of H_n

in Equation (38) must be zero. The solution in region III is therefore of the form

$$U = \sum_{n=1,3,5\ldots} L_n e^{\alpha_2 z} \sin \frac{n\pi x}{2a} . \qquad (41)$$

The arbitary constants J_n, L_n, M_n, and N_n are found by using boundary conditions d) and e) and are $J_n = \frac{V_2 B_0 8a (-1)^{\frac{n+1}{2}} \alpha_1 \left(e^{-\alpha_1 l} - e^{\alpha_1 l}\right)}{n^2 \pi^2 K}$,

$$M_n = \frac{V_2 B_0 8a (-1)^{\frac{n+1}{2}} \alpha_2 e^{-\alpha_1 l}}{n^2 \pi^2 K} ,$$

$$N_n = \frac{-V_2 B_0 8a (-1)^{\frac{n+1}{2}} \alpha_1 e^{\alpha_2 l}}{n^2 \pi^2 K} ,$$

$$L_n = \frac{V_2 B_0 8a (-1)^{\frac{n+1}{2}} \alpha_1 \left(e^{-\alpha_2 l} - e^{\alpha_2 l}\right)}{n^2 \pi^2 K} ,$$

where $\alpha_1 = \frac{1}{2a}\left(R_m + \left(R_m^2 + n^2\pi^2\right)^{\frac{1}{2}}\right)$,

$$\alpha_2 = -\frac{1}{2a}\left(R_m - \left(R_m^2 + n^2\pi^2\right)^{\frac{1}{2}}\right),$$

and $K = \alpha_1 - \alpha_2$.

Substituting for J_n, M_n, N_n, and L_n in Equations (39),(40) and (41) we have :-

$$U = -V_2 B_0 a \frac{16}{\pi^2} \sum_{n=1,3,5\ldots} \frac{(-1)^{\frac{n+1}{2}}}{n^2 K} \alpha_2 \sinh \alpha_1 l \exp \alpha_1 z \sin \frac{n\pi x}{2a} \quad \text{in region I} , \qquad (42)$$

$$U = -V_2 B_0 a \left[\frac{x}{a} - \frac{8}{\pi^2} \sum_{n=1,3,5} \frac{(-1)^{\frac{n+1}{2}}}{n^2 K} \left(\alpha_2 e^{-\alpha_1 (1-z)} - \alpha_1 e^{\alpha_2 (1+z)}\right) \sin \frac{n\pi x}{2a}\right] \text{ in region II} \qquad (43)$$

$$U = -V_2 B_0 a \frac{16}{\pi^2} \sum_{n=1,3,5\ldots} (-1)^{\frac{n+1}{2}} \alpha_2 \sinh \alpha_2 l \exp \alpha_2 z \sin \frac{n\pi x}{2a} \quad \text{in region III} \qquad (44)$$

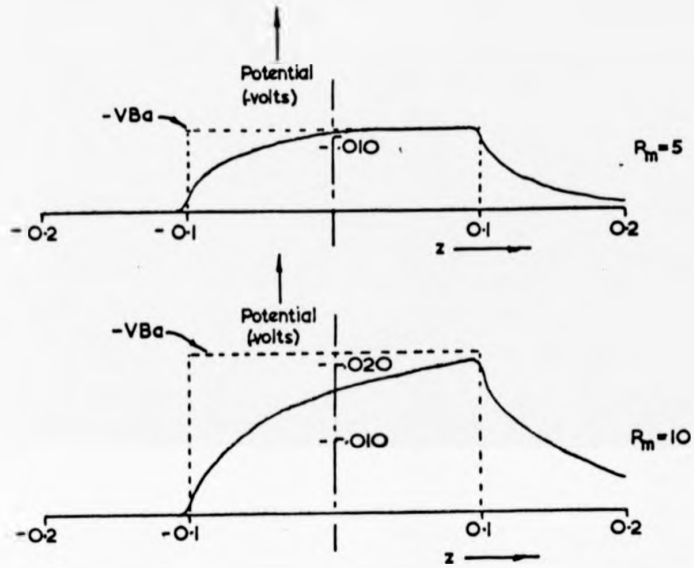

The potential distribution on the surface of a moving conductor, a is 0·02m, ℓ is 0·1m.

fig. 25.

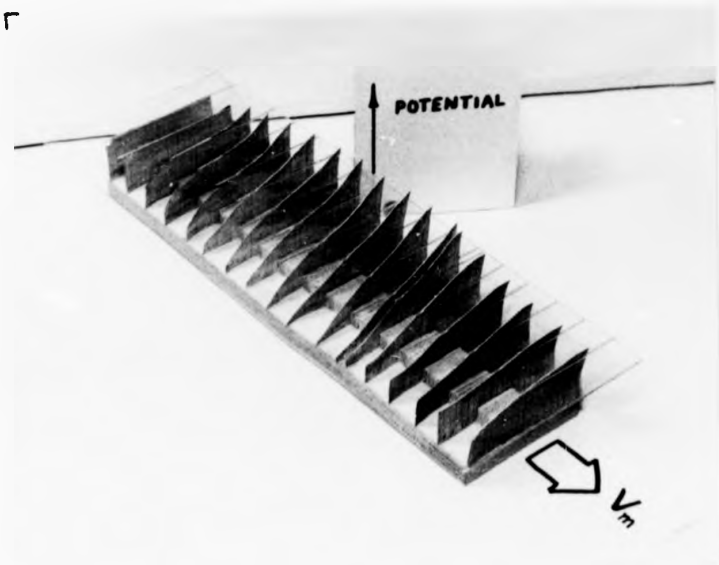

fig. 26.

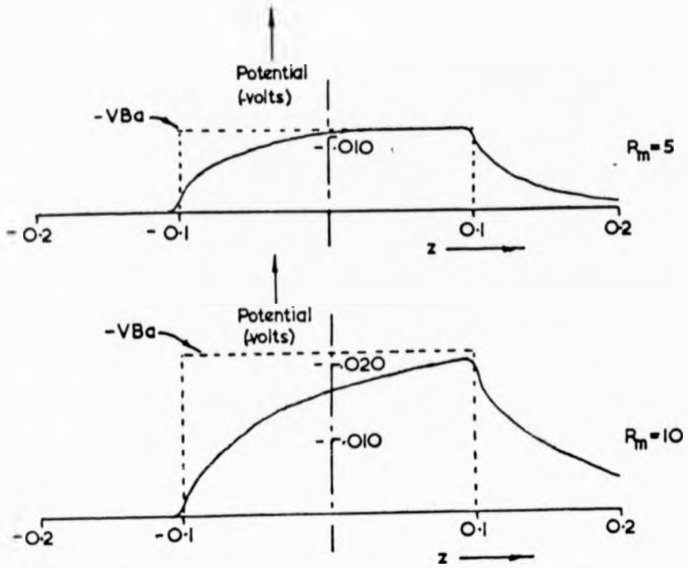

The potential distribution on the surface of a moving conductor, a is 0·02m, ℓ is 0·1m.

fig. 25.

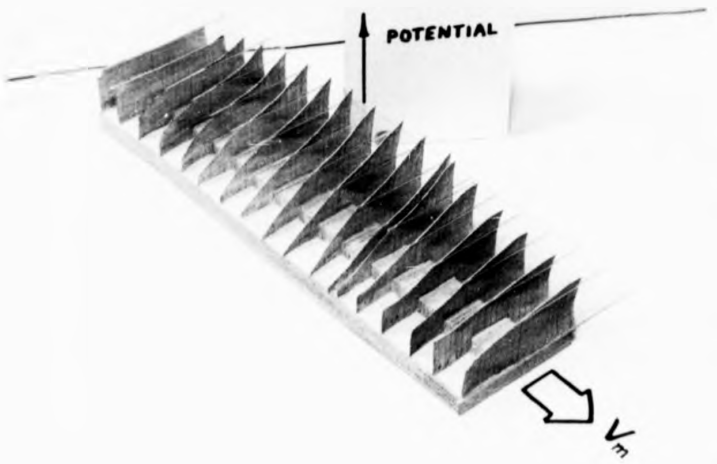

fig. 26.

If we allow R_m to be small these equations become identical to those found by Shercliff[9] for the low R_m case.

Equations (42),(43) and (44) can also be derived from the calculated magnetic field (Equations (10) to (12) and (19) to (25)). Because curl $\underline{B} = \mu \underline{j}$ we can rewrite the Ohm's law equation in the form.

$$\frac{1}{\mu\sigma} \text{curl } \underline{B} = \underline{E} + \underline{v} \times \underline{B}. \tag{45}$$

The x component of this may be written as

$$-\frac{1}{\mu\sigma} \frac{\partial B}{\partial z} = -\frac{\partial U}{\partial x} - v_z B_y, \tag{46}$$

because B is solely in the y-direction and $v_x = v_y = 0$. Using the above mentioned equations for B we can integrate Equation (46) to find U. Using the boundary condition that U = 0 at x = o for all z we obtain expressions for U which are identical to Equations (42),(43) and (44).

Figure 25 shows the computed potential at x = a for a duct where a = 0.02 metres in which the metal moves with slug flow through a field of length 0.2 metres. The two cases shown are for magnetic Reynolds numbers of 5 and 10. If the magnetic field region were infinitely long one would expect voltages of $\pm v_z B_o a$ at the electrodes. It can be seen that when $R_m = 5$ the potential only rises to the expected value at the exit end of the magnetic field whilst when $R_m = 10$ the expected potential of $v_z B_o a$ is never achieved.

Figure 25 is a photograph of a cardboard model showing the calculated electric potential distribution across a straight conductor as it moves through a field of 0.1 w/m^2 of length 0.2 metres when $R_m = 10$.

Electromagnetic Flowmeters Used at High R_m

It is now well known that flowmeters for use at high R_m must be provided with a magnetic field of great length so that the electrodes are

well away from any disturbance of the potential due to circulating currents at the ends of the device. A flow meter used on the Enrico-Fermi reactor employing a short permanent magnet is described in reference 10. It was found that the output of this device was not proportional to the volume throughput. Using the data given in this reference we have computed the output of this device for various throughputs of sodium assuming once again a slug flow and a rectangular field profile. Figure 27 shows the manufacturer's calibration curve together with the experimentally measured calibration and our computed calibration for this device. The sensitivity of such a short flowmeter will depend upon the distribution of the magnetic field provided by the permanent magnet. It is expected that computing the calibration curve for such a device using a real field profile would provide a more accurate calibration than our assumed "square field" case, unfortunately we were unable to obtain the necessary detailed information about the field used for the Enrico-Fermi flowmeter.

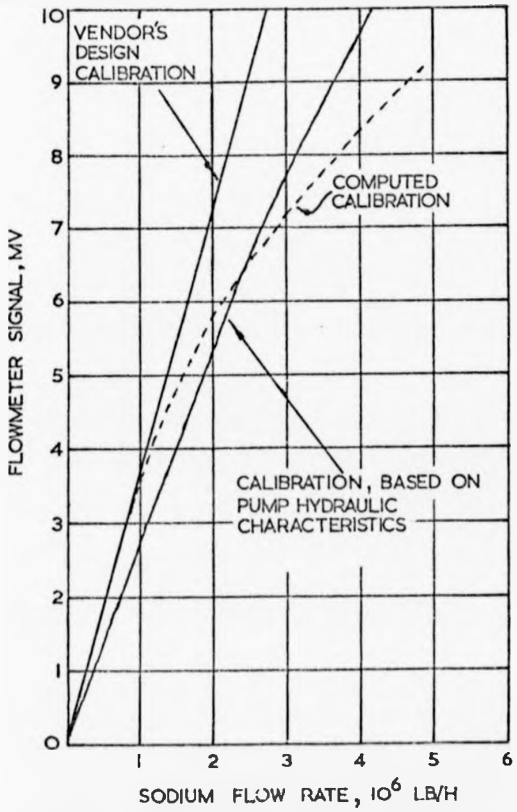

fig. 27.

Chapter 4

A First Order Theory for the Velocity Perturbation caused by the Interaction of the Induced Eidy Currents with the Magnetic Field in an M.H.D. Device.

Once again we consider, in a two dimensional way, the case of a fluid flowing through a transverse magnetic field which falls abruptly to zero at $z = \pm l$. The theory closely follows that used by Shercliff[11] for the low R_m case.

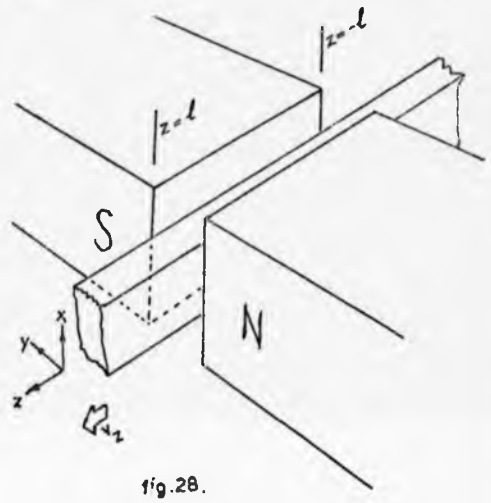

fig.28.

The Navier-Stokes equation, modified to include the electromagnetic body force is, for an incompressible fluid,

$\rho \frac{D\underline{v}}{Dt} + \text{grad}\, p = \underline{j} \times \underline{B} + \eta \nabla^2 \underline{v}$ where ρ is the density of the fluid, η is the viscosity of the fluid and p is the pressure in the fluid. Taking the curl of this equation and ignoring the viscous forces we have, for a steady state:-

$$\rho \frac{D\underline{\omega}}{Dt} = \rho (\underline{v}.\text{grad})\underline{\omega} = \text{curl}\ \underline{j} \times \underline{B}$$
$$= (\underline{B}.\text{grad})\underline{j} - (\underline{j}.\text{grad})\underline{B},$$

taking the y-component we get, to the first order,

$$\rho v_z \frac{\partial \omega_y}{\partial z} = -j_x \frac{\partial B}{\partial x} - j_z \frac{\partial B}{\partial z}. \qquad (47)$$

Now B is the sum of the applied magnetic field B_a and an induced field B_i so that $B = B_a + B_i$.

Equation (47) now becomes.

$$\rho v_z \frac{\partial \omega_y}{\partial z} = -j_x \frac{\partial (B_a + B_i)}{\partial x} - j_z \frac{\partial (B_a + B_i)}{\partial z}$$

$$\text{or}\ \rho v_z \frac{\partial \omega_y}{\partial z} = -j_x \frac{\partial B_a}{\partial x} - j_x \frac{\partial B_i}{\partial x} - j_z \frac{\partial B_a}{\partial z} - j_z \frac{\partial B_i}{\partial z}. \qquad (48)$$

We consider an applied field which is uniform in x and such that

$B_a = 0$ if $z < -l$,

$B_a = B_o$ if $-l < z < +l$,

and $B_a = 0$ if $z > +l$.

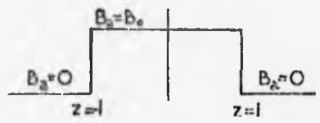

fig.29.

As the applied magnetic field is uniform in x $\frac{\partial B_a}{\partial x} = 0$ so Equation (48) now becomes

$$\rho v_z \frac{\partial \omega_y}{\partial z} = - j_x \frac{\partial B_i}{\partial x} - j_z \frac{\partial B_o}{\partial z} - j_z \frac{\partial B_i}{\partial x} .$$

Curl $\underline{B}_i = \mu \underline{j}$ so that $j_x = - \frac{1}{\mu} \frac{\partial B_i}{\partial z}$ and $j_z = \frac{1}{\mu} \frac{\partial B_i}{\partial x}$, consequently we find that

$$\rho v_z \frac{\partial \omega_y}{\partial z} = - j_x \frac{\partial B_o}{\partial z} ; \qquad (49)$$

so curl $\underline{j} \times \underline{B}$ is zero except where there is a z-wise variation in the applied magnetic field. This equation is precisely that found by Shercliff. It appears that the only difference between the low R_m case and the high R_m case is that at high R_m j_z is strongly dependent upon the length of the field region and upon the magnetic Reynolds number. We see that curl $\underline{j} \times \underline{B}$ is zero except at the ends of the magnet so the vorticity must change abruptly as the liquid enters or leaves the field. In the limit of an abrupt edge Equation (49) becomes:-

$$\rho v_z \Delta \omega_y = - j_z \Delta B_o , \qquad (50)$$

because v_z and j_z are continuous across the edge; $\Delta\omega$ is the change in vorticity and ΔB_o is the change in the applied magnetic field.

To proceed with the analysis of the problem we use the solution of $\nabla^2 U = \frac{R_m}{a} \frac{\partial U}{\partial z}$ and Ohm's law equation to find j_z. When a fluid crosses an edge into a region of applied magnetic field the quantities p, v_x, v_z and $\frac{\partial v_z}{\partial x}$ are continuous but ω_y and hence $\frac{\partial v_x}{\partial z}$ change abruptly. From Equation (50) we find that the vorticity changes by an amount $\Delta\omega$ where

$$\Delta \omega = - j_z \frac{\Delta B_o}{\rho v_z} . \qquad (51)$$

We now let $v_z = v_m + w$ where v_m is the undisturbed uniform velocity and w is a z-wise perturbation velocity small in comparison with v_m. We introduce a stream function so that:-

$$v_x = \frac{\partial \psi}{\partial z} \quad \text{and} \quad w = -\frac{\partial \psi}{\partial x},$$

then $$\omega_y = -\frac{\partial w}{\partial x} + \frac{\partial v_x}{\partial z} = +\frac{\partial^2 \psi}{\partial x^2} + \frac{\partial^2 \psi}{\partial z^2} = \nabla^2 \psi .$$

The vorticity changes abruptly at the entrance and exit of the field so that well inside the field region $v_x = 0$ but because $v_x = \frac{\partial \psi}{\partial z}$, $\frac{\partial^2 \psi}{\partial z^2} = 0$. Then inside the field $\omega_y = \frac{\partial^2 \psi}{\partial x^2}$.

If we assume that the liquid had slug flow before entering the field then ω_y and hence $\frac{\partial^2 \psi}{\partial x^2} = 0$ when $z<-1$. ω_y increases by an amount $\Delta\omega$ on entering the field so that

$$\omega_y(x) = \Delta\omega_y(x) = -j_z \frac{\Delta B_o}{\rho v_m} \quad \text{when} \quad -1 < z < 1 .$$

Using the solution of $\nabla^2 U = \frac{R_m}{a}\frac{\partial U}{\partial z}$ for a slug flow, and the Ohm's law equation we find that at $z = -1$

$$j_z = -\sigma v_m B_o 2 \sum_{n=1,3,5\ldots} \frac{(-1)^{\frac{n+1}{2}}\left(1 - e^{-2\alpha_1}\right)}{\left(R_m + n^2\pi^2\right)^{\frac{1}{2}}} \sin\frac{n\pi x}{2a}, \text{ where } \alpha_1 = \frac{1}{2a}\left(R_m + \left(R_m^2 + n^2\pi^2\right)^{\frac{1}{2}}\right).$$

We may rewrite this as:-

$$j_z = -\sigma v_m B_o 2 \sum_{n=1,3,5\ldots} \frac{(-1)^{\frac{n+1}{2}}\left(1 - e^{-N\beta_1}\right)}{\left(R_m + n^2\pi^2\right)^{\frac{1}{2}}} \sin\frac{n\pi x}{2a} \quad \text{where } \beta_1 = R_m + \left(R_m^2 + n^2\pi^2\right)^{\frac{1}{2}}$$

and $N = \frac{1}{a}$.

From Equation (51) we find that the vorticity inside the field is given by

$$\omega_y(x) = \frac{\sigma B_o^2 2}{\rho} \sum_{n=1,3,5\ldots} \frac{(-1)^{\frac{n+1}{2}}\left(1 - e^{-N\beta_1}\right)}{\left(R_m + n^2\pi^2\right)^{\frac{1}{2}}} \sin\frac{n\pi x}{2a} = \frac{\partial^2 \psi}{\partial x^2} \qquad (52)$$

When $z < -1$ the liquid has slug flow so that $\frac{\partial^2 \psi}{\partial x^2} = 0$ and the perturbation velocity $w = -\frac{\partial \psi}{\partial x} = 0$, we therefore choose ψ the stream function, to be zero when $z \to -\infty$. w and v_x, that is $-\frac{\partial \psi}{\partial x}$ and $\frac{\partial \psi}{\partial z}$, are always zero at the duct walls $(x = \pm a)$. It follows that $\psi = 0$ at $x = \pm a$. Solving equation (52) subject to these boundary conditions we have:-

$$\psi = -\frac{\sigma B_o 2}{\rho} \sum_{n=1,3,5\ldots} \frac{(1-e^{-N\beta_1})\,4a^2}{(R_m + n^2\pi^2)^{\frac{1}{2}} n^2\pi^2} \left(\frac{x}{a} + (-1)^{\frac{n+1}{2}} \sin \frac{n\pi x}{2a} \right)$$

The z-wise velocity perturbation $w = -\frac{\partial \psi}{\partial x}$

and therefore $$w = \frac{\sigma B_o^2 \delta a}{\rho \pi^2} \sum_{n=1,3,5\ldots} \frac{(1-e^{-N\beta_1})}{(R_m^2 + n^2\pi^2)^{\frac{1}{2}}} \cdot \frac{1}{n^2} \left(1 + (-1)^{\frac{n+1}{2}} \frac{n\pi}{2} \cos \frac{n\pi x}{2a} \right). \quad (53)$$

As the fluid leaves the magnetic field the vorticity again changes so that once outside the field:-

$$\omega_y = \underset{\text{INSIDE FIELD}}{\omega_y} - \frac{j_z \Delta B_o}{\rho V_m} .$$

Once again using the solution of $\nabla^2 U = \frac{R_m}{a} \frac{\partial U}{\partial z}$ and the Ohm's law equation we find that at z = + 1

$$j_z = -\sigma v_m B_o 2 \sum_{n=1,3,5\ldots} \frac{(-1)^{\frac{n+1}{2}} \left(e^{N\beta_2} - 1 \right)}{(R_m^2 + n^2\pi^2)^{\frac{1}{2}}} \sin \frac{n\pi x}{2a} \quad \text{where } \beta_2 = R_m - \left(R_m^2 + n^2\pi^2 \right)^{\frac{1}{2}}$$

and $N = \frac{1}{a}$.

$$\text{Then } \underset{\text{OUTSIDE FIELD}}{\omega_y} = \frac{\sigma B_o^2 2}{\rho} \sum_{n=1,3,5\ldots} \frac{(-1)^{\frac{n+1}{2}} \left(1 - e^{-N\beta_1} \right)}{(R_m^2 + n^2\pi^2)^{\frac{1}{2}}} \sin \frac{n\pi x}{2a} - \frac{\sigma B_o^2 2}{\rho} \sum_{n=1,3,5\ldots} \frac{(-1)^{\frac{n+1}{2}} \left(e^{N\beta_2} - 1 \right)}{(R_m^2 + n^2\pi^2)^{\frac{1}{2}}} \sin \frac{n\pi x}{2a}$$

$$= -\frac{\sigma B_o^2 2}{\rho} \sum_{n=1,3,5\ldots} \frac{(-1)^{\frac{n+1}{2}} \left(e^{N\beta_2} + e^{-N\beta_1} - 2 \right)}{(R_m^2 + n^2\pi^2)^{\frac{1}{2}}} \sin \frac{n\pi x}{2a} = \frac{\partial^2 \psi}{\partial x^2} .$$

If we integrate the above expression and use the boundary condition $\psi = 0$ at $x = \pm a$ we find:-

$$\psi = \frac{\sigma B_o^2 2}{\rho} \sum_{n=1,3,5\ldots} \frac{\left(e^{N\beta_2} + e^{-N\beta_1} - 2 \right)}{(R_m + n^2\pi^2)^{\frac{1}{2}}} \frac{4a^2}{n^2\pi^2} \left(\frac{x}{a} + (-1)^{\frac{n+1}{2}} \sin \frac{n\pi x}{2a} \right).$$

The perturbation velocity w is then found to be:-

$$w = -\frac{\sigma B_o^2 2}{\rho} \sum_{n=1,3,5} \frac{\left(e^{N\beta_2} + e^{N\beta_1} - 2 \right)}{(R_m^2 + n^2\pi^2)^{\frac{1}{2}}} \frac{4a}{n^2\pi^2} \left(1 + (-1)^{\frac{n+1}{2}} \frac{n\pi}{2} \cos \frac{n\pi x}{2a} \right).$$

Figure 30 shows how the slug flow is perturbed as the fluid passes

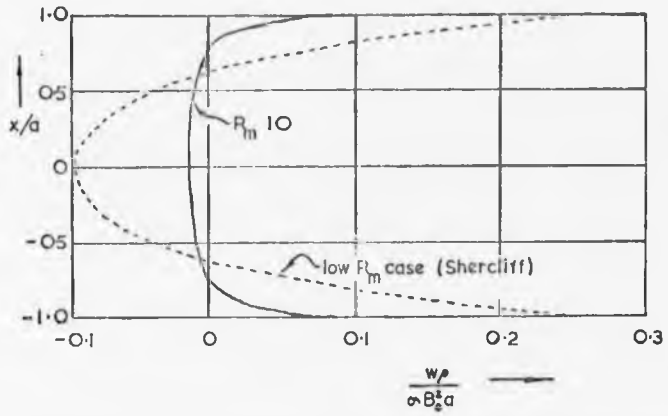

The perturbation of the velocity profile at the entrance of an abrupt magnetic field.

fig. 30.

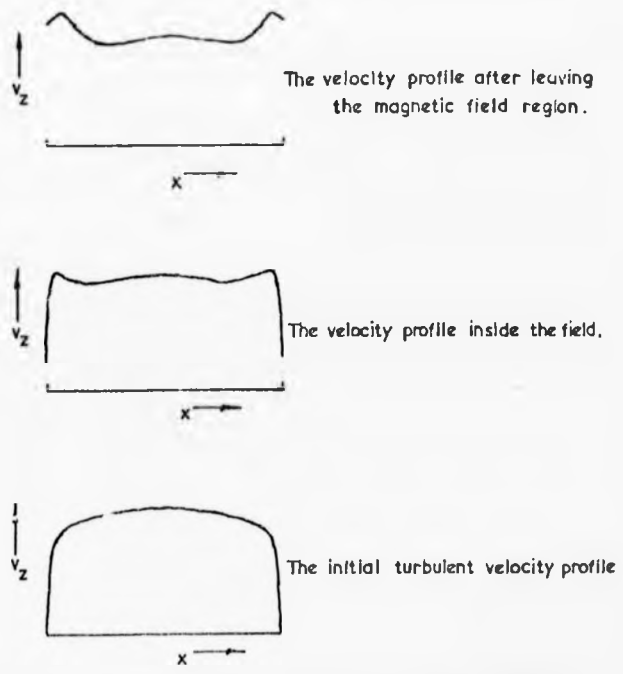

The computed velocity profiles for a turbulent flow passing through an abruptly edged magnetic field where ℓ = 1·0m, a = 0·2m, R_m = 10 and B = 0·1wb/m².

fig. 32.

through a field such that $\frac{l}{a} = 5$ and the magnetic Reynolds number is 10. The effect of the electromagnetic forces in the fluid is to increase the velocity at the edges of the duct and to decrease the velocity at the centre of the duct. The velocity perturbation at the centre when R_m is small is found to be the same as that predicted by Shercliff and is of order $\frac{\sigma B_o^2 a}{10\rho}$, which is independent of the mean velocity. When R_m is large the perturbation is of order $\frac{\sigma B_o^2 a}{10\rho R_m}$ which is inversly proportional to v_m, suggesting that the $\underline{j} \times \underline{B}$ forces although themselves larger produce a smaller change in the velocity.

The ratio of the $\underline{j} \times \underline{B}$ forces to the inertia force (the interaction parameter) is given at low R_m by the expression

$S = \frac{\sigma B_o^2 b}{\rho v_m}$ where b is a scale length of the system,

and at high R_m by the expression:-

$$S = \frac{B_o^2}{\mu \rho v_m^2} = \frac{\mu \sigma^2 B_o^2 b^2}{\rho R_m^2}.$$

Shercliff has shown that the fractional perturbation at low R_m is of order $\frac{\sigma B_o^2 a}{10\rho v_m}$ which is 1/10 x the interaction parameter. We have shown that at high R_m the velocity perturbation is of order $\frac{\sigma B_o^2 a}{10\rho R_m}$ so that the fractional perturbation is $\frac{\mu \sigma^2 B_o^2 a^2}{10\rho R_m^2}$ which is, once again, 1/10 x the interaction parameter.

This first order analysis becomes unrealistic as soon as the fractional perturbation becomes larger than about 10 or 20%, that is the interaction parameter is greater than 1 or 2.

We now perform a similar calculation for a fluid which has vorticity before it enters the magnetic field region. We represent the turbulent flow of the fluid by a simple power law which is $\frac{U}{U_1} = \left(\frac{y}{a}\right)^n$ where U_1 is the velocity at the centre of the duct, U is the velocity

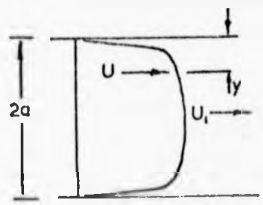

fig. 31.

at a distance y from the duct wall and n is a power which depends upon the Reynolds number. Nikuradse[12] gives n for a round pipe as $\frac{1}{10}$ when the Reynolds number is greater than 1.6×10^6 and we use this value in our approximate theory. In our system of co-ordinates $\frac{u}{u_1} = \left(\frac{y}{a}\right)^n$ becomes

$$\frac{u}{u_1} = \left(1-\frac{x}{a}\right)^n. \tag{55}$$

For a two dimensional flow in a duct of thickness 't', throughput $2atv_m = 2t\int_0^a U\,dx$ where v_m = mean velocity.

Therefore $2atv_m = 2t\int_0^a u_1\left(1-\frac{x}{a}\right)^n dx$

or $v_m = \frac{1}{a}\int_0^a u_1\left(1-\frac{x}{a}\right)^n dx.$

Performing the integral we find

$$v_m = \frac{u_1}{n+1}.$$

For sodium flow in a duct 0.40 metres high x 0.2 metres thick, such that $R_m = 10$, we find the Reynolds number is 3.28×10^6. Nikuradse gives the value of n at this Reynolds number as 0.1 so that $v_m = \frac{u_1}{1.1}$ or

$$u_1 = 1.1\,\frac{R_m}{\mu\sigma a}.$$

Equation (55) now becomes

$$U = 1.1\,\frac{R_m}{\mu\sigma a}\left(1-\frac{x}{a}\right)^{0.1}. \tag{56}$$

We again consider an abruptly edged field stretching from $z = -1$ to $z = +1$. Before the fluid enters the field it has a vorticity which is $-\frac{\partial v_z}{\partial x}$, that is

$$\omega_y = 1.1\,\frac{R_m}{\mu\sigma a^2}\cdot\frac{1}{10}\left(1-\frac{x}{a}\right)^{-\frac{9}{10}}. \tag{57}$$

We let v_z be $v_m + w$ where v_m is the mean velocity and w is the perturbation velocity and we choose a stream function so that

$$w = -\frac{\partial\psi}{\partial x} \quad \text{and} \quad v_x = \frac{\partial\psi}{\partial z}.$$

Then $\omega_y = -\frac{\partial}{\partial x}(v_m + w) + \frac{\partial v_x}{\partial z}$

$$= \frac{\partial^2 \psi}{\partial x^2} + \frac{\partial^2 \psi}{\partial z^2} .$$

When the fluid is outside the magnetic field region the flow profile does not vary in the z direction so that the vorticity is not a function of z, that is $\omega_y = f(x) = \frac{\partial^2 \psi}{\partial x^2}$. Integrating Equation (57) and using the boundary condition that v_z is zero at $x = \pm a$ (that is $-\frac{\partial \psi}{\partial x} = 0$ at $x = \pm a$) we find that before the fluid enters the magnetic field

$$\psi = \frac{R_m}{\mu\sigma a}\left(1{\cdot}1\, a \cdot \frac{10}{11}\left(1 - \frac{x}{a}\right)^{\frac{11}{10}} + x\right). \qquad (58)$$

At the walls of the duct the x-component of the velocity is always zero so that $\frac{\partial \psi}{\partial z} = 0$ for all z at $x = \pm a$. From Equation (58) we find that at $x = \pm a$, $\psi = \frac{R_m}{\mu\sigma}$. We have already shown (Equation (51)) that the velocity changes abruptly at when the liquid enters or leaves the magnetic field by an amount $\Delta\omega_y$ where

$$\Delta\omega_y = -j_z \frac{\Delta B_a}{\rho v_z} .$$

We again use the solution of $\nabla^2 U = \frac{R_m}{a}\frac{\partial U}{\partial z}$ for a slug flow, together with the Ohm's law equation, to find j_z . We find that upon entering the field region:-

$$\omega_y = 1{\cdot}1\frac{R_m}{\mu\sigma a^2} \cdot \frac{1}{10}\left(1 - \frac{x}{a}\right)^{-\frac{9}{10}} + \frac{\sigma B_a^2 2}{\rho}\sum_{n=1,3,5\ldots}\frac{(-1)^{\frac{n-1}{2}}\left(1 - e^{-N\beta_1}\right)}{\left(R_m^2 + n^2\pi^2\right)^{\frac{1}{2}}}\sin\frac{n\pi x}{2a} = \frac{\partial^2 \psi}{\partial x^2}$$

where $\beta_1 = R_m + \left(R_m^2 + n^2\pi^2\right)^{\frac{1}{2}}$ and $N = \frac{1}{a}$. Integrating and using the boundary condition that $\psi = \frac{R_m}{\mu\sigma}$ at $x = a$ we have

$$\psi = \frac{1{\cdot}1\, R_m}{\mu\sigma} \cdot \frac{10}{11}\left(1 - \frac{x}{a}\right)^{\frac{11}{10}} + \frac{R_m x}{\mu\sigma a} - \frac{\sigma B_a^2 2}{\rho}\sum_{n=1,3,5\ldots}\frac{\left(1 - e^{-N\beta_1}\right)4a^2}{\left(R_m^2 + n^2\pi^2\right)^{\frac{1}{2}} n^2\pi^2}\left(\frac{x}{a} + (-1)^{\frac{n+1}{2}}\sin\frac{n\pi x}{2a}\right).$$

The perturbation velocity $w = -\frac{\partial \psi}{\partial x}$ so that

$$w = \frac{R_m}{\mu\sigma a}\left[1{\cdot}1\left(1 - \frac{x}{a}\right)^{0{\cdot}1} - 1\right] - \frac{\sigma B_a^2 8a}{\rho\pi^2}\sum_{n=1,3,5\ldots}\frac{\left(1 - e^{-N\beta_1}\right)}{\left(R_m^2 + n^2\pi^2\right)^{\frac{1}{2}}} \cdot \frac{1}{n^2}\left(1 + (-1)^{\frac{n+1}{2}}\frac{n\pi}{2}\cos\frac{n\pi x}{2a}\right). \qquad (59)$$

Using a similar method we find that when the liquid leaves the magnetic field the perturbation is given by:-

$$w = \frac{R_m}{\mu\sigma a}\left[\frac{n+1}{n}\left(1-\frac{x}{a}\right)^{n+1} - 1\right] - \frac{\sigma B_0^2 8a}{\rho\pi^2}\sum \frac{\left(e^{\beta_1 d} + e^{-\beta_2 N} - 2\right)}{\left(R_m^2 + n^2\pi^2\right)^{\frac{1}{2}}} \cdot \frac{1}{n^2}\left(1+(-1)^{\frac{n+1}{2}}\frac{n\pi}{2}\cos\frac{n\pi x}{2a}\right), \quad (60)$$

where $\beta_1 = R_m + \left(R_m^2 + n^2\pi^2\right)^{\frac{1}{2}}$, $\beta_2 = R_m - \left(R_m^2 + n^2\pi^2\right)^{\frac{1}{2}}$ and $N = \frac{1}{a}$.

Before the fluid enters the magnetic field the velocity profile is that of a slug flow modified by an amount w where $w = \frac{R_m}{\mu\sigma a}\left[\frac{n+1}{n}\left(1-\frac{x}{a}\right)^{n+1} - 1\right]$. Equations (59) and (60) show that the electromagnetic perturbation which takes place upon entering the magnetic field is the same for both the slug flow and the turbulent flow cases described here. Both are approximate because $\frac{1}{\mu}$ is derived from the solution of $\nabla^2 U = \frac{R_m}{a}\frac{\partial U}{\partial z}$ for a slug flow and both cases fail at the walls of the duct where the velocity of the fluid must be zero.

Figure 32 shows the computed velocity profiles for a turbulent flow passing through an abruptly edged magnetic field of length 2 metres, the magnetic Reynolds number is 10 and the magnetic field is 0.1 Wb/m^2. From this first order analysis it is evident that the perturbation increases the velocity of the liquid at the top and bottom of the duct and decreases the velocity at the centre.

Part II

Chapter 5

Experiments to Investigate the Magnetic Field Perturbation when Large Currents are allowed to Enter and Leave the M.H.D. Duct and when two Streams of Moving Conductor pass through a common Magnetic Field.

5.1 The Apparatus

In all the theoretical and experimental work described in Part I of this thesis the electric currents were confined entirely to the moving conductor. Many M.H.D. devices have external circuits through which currents may enter and leave the duct. Consequently Part I, whilst providing a qualitative understanding of the magnetic field perturbation, is not directly applicable to such things as pumps and generators. The flow coupler is more complicated than either an M.H.D. pump or generator because the magnetic field in a flow coupler may be modified by the induced field caused by eddy currents circulating in each of the streams of moving conductors. These streams may be travelling at different velocities.

The apparatus described in Part I of this thesis was designed and built as quickly as possible because at that time it was thought that work on this project might end after a period of one year. In 1971 we needed an experimental rig with which we could study the magnetic field perturbation which occurred when large, externally applied, currents flowed through an M.H.D. duct and when two conductors moved through a common magnetic field at different speeds. Once again it was not possible to build a model in which sodium was represented by some other liquid and so once again we used solid conductors to represent the streams of liquid sodium. Because it was not possible to modify the original apparatus it was necessary for us to design and build a new rig. This would consist of a pair of annular discs of aluminium which would rotate side by side in a magnetic field and be

electrically interconnected so that currents could flow from one disc to other.

In real sodium-filled devices large currents can be drawn from the moving sodium through copper electrodes brazed onto the duct walls. In our experimental rig the only method of inserting or extracting electrical power from the moving conductors would be to have brushes rubbing against the inner and outer edges of the aluminium rims. We appreciated that if meaningfull results were to be obtained there should be very little contact resistance between the brush gear and the moving aluminium.

We used the rig described in Part I of this thesis for testing several different types of brush material. Brush holders were made and these were mounted in pairs so that they rubbed against the outer edge of the aluminium. We then measured the contact resistance between each brush and the moving aluminium whilst maintaining the current density in the brushes at about that which we expected in the new experimental rig. The task of selecting a suitable brush material was made easier because, as we only required a life of a few hours, the wearing properties of the brushes were relatively unimportant. As a result of these tests we selected a material known as LINK SM9162 which was manufactured by Morganite Carbon Limited. These silver graphite brushes were made from a sintered material which has a composition of 85% silver and 15% carbon.

The new apparatus, which is shown diagrammatically in fig. 13 is a solid analogue of a flow coupler and consists of two large Tufnol discs each of which carries an annular tyre of aluminium. One of the discs is bolted securely to an axle whilst the other is mounted on bearings which run upon the axle. In this way the two wheels may be rotated at different speeds. The bearing block which carries the left hand wheel has a vee-bolt groove so that it may be rotated by an electric motor mounted above

electrically interconnected so that currents could flow from one disc to other.

In real sodium-filled devices large currents can be drawn from the moving sodium through copper electrodes brazed onto the duct walls. In our experimental rig the only method of inserting or extracting electrical power from the moving conductors would be to have brushes rubbing against the inner and outer edges of the aluminium rims. We appreciated that if meaningfull results were to be obtained there should be very little contact resistance between the brush gear and the moving aluminium.

We used the rig described in Part I of this thesis for testing several different types of brush material. Brush holders were made and these were mounted in pairs so that they rubbed against the outer edge of the aluminium. We then measured the contact resistance between each brush and the moving aluminium whilst maintaining the current density in the brushes at about that which we expected in the new experimental rig. The task of selecting a suitable brush material was made easier because, as we only required a life of a few hours, the wearing properties of the brushes were relatively unimportant. As a result of these tests we selected a material known as LINK SM9162 which was manufactured by Morganite Carbon Limited. These silver graphite brushes were made from a sintered material which has a composition of 85% silver and 15% carbon.

The new apparatus, which is shown diagrammatically in fig. 33 is a solid analogue of a flow coupler and consists of two large Tufnol discs each of which carries an annular tyre of aluminium. One of the discs is bolted securely to an axle whilst the other is mounted on bearings which run upon the axle. In this way the two wheels may be rotated at different speeds. The bearing block which carries the left hand wheel has a vee-bolt groove so that it may be rotated by an electric motor mounted above

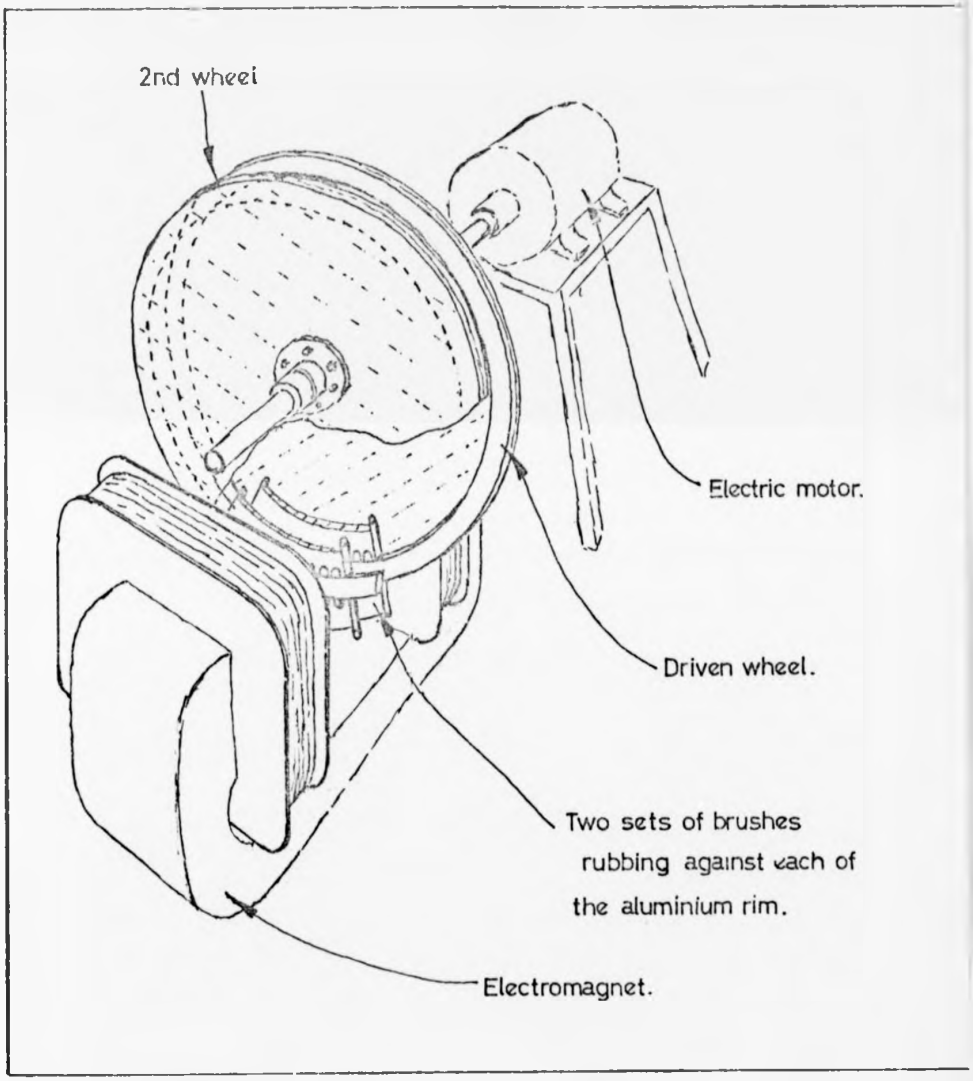

A schematic diagram of the 2nd experimental apparatus.

figure 33.

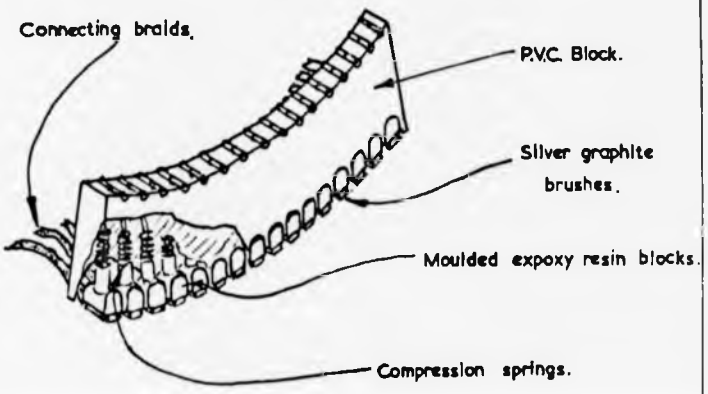

Fig 34 An upper brush block.

Figure 35.

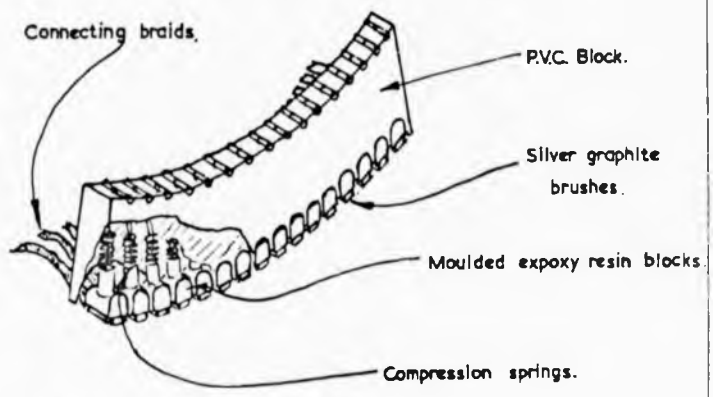

Fig 34 An upper brush block.

Figure 35.

the apparatus. The axle, to which the other wheel is attached, is driven, through a gear box, by a variable speed electric motor.

The aluminium tyres, which have an outside diameter of 0.9m and an inside diameter of 0.82m, are each constructed from two pieces of metal glued either side of a thin Tufnol spacer, so that the complete rims have deep slots in their outer edges. The tyres are fixed to the adjacent faces of the two Tufnol discs which rotate so that the metal rims pass between the poles of an electromagnet. This magnet is watercooled and is powered by a 60 kw motor generator set. Brush gear has been made which can rub against the top and bottom faces of the aluminium in the magnetic field region. The brushes are arranged in four sets, each set containing 15 seperately mounted brushes. The two inner sets bear upon the inner faces of the aluminium tyres whilst the other two sets bear on the outer faces of the rims. Each of the 60 individual brushes has its own copper connecting braid so that they may be interconnected in many different ways. Each brush is held in contact with the moving metal by a compression spring, figure 34 shows a sketch of one brush block, whilst figure 35 is a photograph of a block in which one brush has been removed to show the copper connecting braid and spring.

Each individual brush is made from a piece of silver graphite measuring 20mm x 10mm x 3mm. The pieces of brush material were silver plated by coating them with a compound, purchased from Melton Metallurgical Laboratories Limited, and heating them to a temperature of about 550°C. They were then soldered onto pieces of copper braid 10mm wide and 1mm thick so that a good electrical contact could be made with the brush material. The pieces of silver graphite and the copper braids were then mounted on small shaped pieces of epoxy resin.

The brush blocks, which each contained 15 brushes, were manufactured from unplastigized P.V.C. The individual brushes where spring loaded so

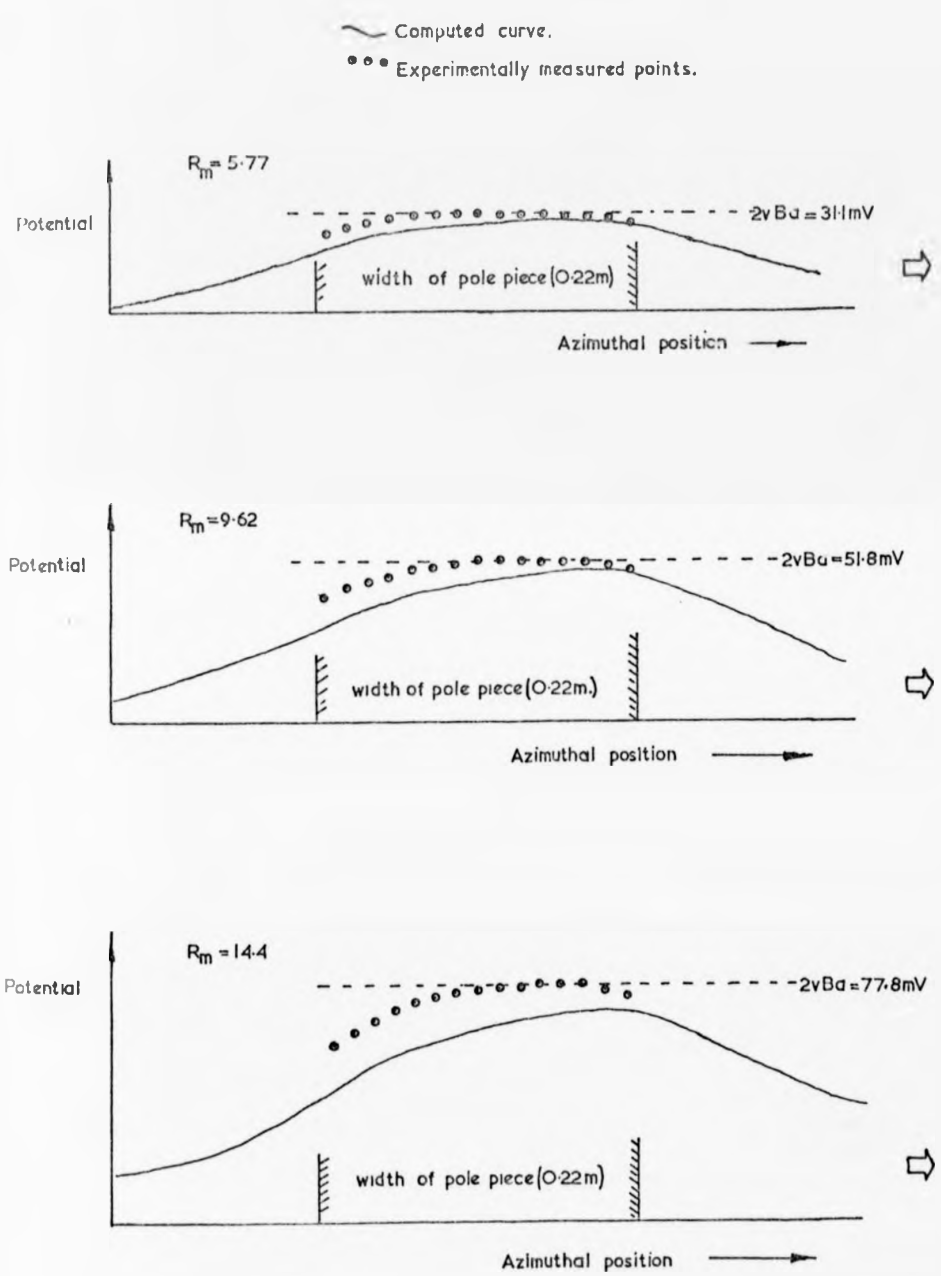

FIG. 36 Showing how the potential difference between the edges of the metal was found to vary with azimuthal position for several values of magnetic Reynolds number In each case the magnetic field was 0·115Wb/m^2.

that a constant force of about 30N kept them in good contact with the moving aluminium.

The components of this second rig were manufactured partly in the U.K.A.E.A. workshops at Risley and partly in the workshops of the Department of Engineering at the University of Warwick.

5.2 The Electric Potential.

The apparatus was assembled with one wheel rotating so that its rim passed through the centre of the magnet gap. Brush gear was installed between the poles of the magnet so that brushes rubbed against the inner and outer edges of the aluminium rim. A digital voltmeter was used to measure the potential difference between pairs of brushes on opposite sides of the aluminium. Each piece of silver graphite was connected to a 15 way switch so that by changing the position of this switch it was possible to find the potential differences between each of the pairs of brushes. In this way the voltage difference between the inner and outer edge of the rim was measured. The wheel was rotated at a chosen speed with the magnetic field set at some convenient value. Figure 36 shows how the potential difference between the edges of the conductor was found to vary in the azimuthal direction, for several values of magnetic Reynolds number. The continous lines are computed curves based upon the theory presented in Chapter 3. Once again these curves were calculated for the case of a straight conductor passing through a field which is similar to the observed magnetic field.

Although the agreement between theory and experiment is not good it can be seen that the potential at the entrance to the field region is significantly reduced at high R_m . The theory overestimates the effect of the induced eddy currents upon the potential distribution within the conductor.

5.3 The Magnetic Field Perturbation when Large Externally Applied Electric Currents Flow.

In M.H.D. devices such as pumps and generators large currents may circulate around an external circuit and through the M.H.D. duct. It is important to know in what way, if any, these currents effect the perturbation of the magnetic field.

Experiments in which the current density in the external circuit was small, when compared with the eddy current circulating in the conductor, might not be very meaningful. Once again the apparatus was assembled with one wheel rotating so that its rim passed through the centre of the magnet gap. We passed currents through the moving rim whilst simultaneously measuring the magnetic field. The magnitude of the externally applied current was limited by the contact resistance between the brush gear and the moving conductor. This was measured and was initially found to be 0.46×10^{-3} ohms. Later we found that although this resistance did not seem to depend upon the speed of rotation of the wheel it did depend upon the condition of the surface of the aluminium. The resistance between the brushes and the wheel was generally found to be about $1 \times 10^{-3}\Omega$.

It was desirable that neither the metal rim nor the brush gear should get hot because a large thermal expansion would probably break the araldite bond which held the rim onto the rotating wheel and a high temperature in the brush gear would probably melt some of the soldered connections. For these reasons we decided to limit the electrical power dissipation in the brush gear to about 350 watts. This dissipation would be produced by an externally applied current of about 600 amps.

If the magnetic field is considered to be solely in the y direction we find, from curl $\underline{B} = \mu \underline{j}$, that $j_x = -\frac{1}{\mu}\frac{\partial B}{\partial z}$. That is the x-component of the current density has a magnitude of order

$$\frac{\text{the induced field}}{\mu \times \text{length of the field region}}$$

In our earlier experiments the maximum observed magnetic field perturbation was about $0.05 Wb/m^2$ for an initial field of $0.1 Wb/m^2$ and of total length about 0.22 metres. Using these figures we find that the x-component of the current density was of order 1.8×10^5 amps/m^2. An applied brush current of 600 amps would give a current density in the aluminium of approximately 1.5×10^5 amps/m^2. Using a current of this size ensures that the applied current density is of the same order as the eddy current density.

A lead acid motor car battery, which had external links between each of the cells, was modified so that its cells were connected in parallel. In this way we aquired a 2 volt battery which would give a current of about 600 amps when short circuited. The brush gear was installed in the magnet gap and the copper braids from each brush in the same block were connected together on a copper plate. Copper busbars connected the two plates, one inside the wheel and one out, to the battery. We also included, in the external circuit, a watercooled variable resistor (0.5mΩ to 5.19mΩ) and a switch.

The variable resistor was in principal a brass U-tube through which water flowed. Electrical connections were made to the ends of the two arms of this tube. A brass bridge slid up and down between these two arms effectively varying the length of the brass tubing in the electrical circuit.

When we first tried to pass large currents through the rim of the rotating wheel we discovered that, after a period of a few minutes, the contact resistance would suddenly rise to an unacceptable value as the surface became very rough. The instant before this happened we had observed arcing taking place between the brush gear and the metal.

It appeared that when the wheel first started to rotate the applied current was well distributed between the brushes. As soon as an arc formed between the metal and a brush the local contact resistance fell dramatically so that a very large current flowed into one small area of the aluminium. This caused local melting and oxidation which rapidly destroyed the polished surface of the rim. One way of overcoming this problem would have been to have electronically controlled the current taken through each brush. Because building an electronic control would have been time consuming and expensive we decided to try to prevent arcs forming.

We thought that if the brushes could be kept in contact with the aluminium there could be no arcing. We tried several commercially available lubricants which were designed to decrease the resistance between sliding contacts. Using these we found that we could run the apparatus for longer periods of time. These lubricants were very expensive. One of our technicians informed us that a mixture of 3 in 1 oil and parafin had in the past been used to suppress noise in carbon track variable resisters. On his suggestion we tried lubricating the aluminium rim with this mixture. This produced a great improvement so that it was possible to run the experiment for about 20 minutes continuously. One then had to stop and repolish the aluminium rim. Arcs are only established when a brush carrying an electric current ceases to make contact with the metal. It appears that when the rim was covered with oil and parafin the arcing was suppressed because when a brush left the surface of the aluminium a thin layer of oil insulated the bare metal. This prevented currents being drawn from the surface of the metal and thus prevented arcing. Currents could only flow when the brush gear made good contact with the surface of the moving conductor. It seems paradoxical that in this way covering the metal with an insulating film ultimately

decreased the contact resistance.

With the brush gear in place it was difficult to measure the magnetic field in the slot between the two halves of the metal rim. One of the brushes had to be removed and the Hall probe was then threaded through the brush block until the sensitive tip of the probe projected into the slot. In order to change the azimuthal position of this probe it was necessary to completely dismantle the brush gear and then to replace the probe in a different brush hole. For this reason we have compared field profiles constructed from measurements taken with the Hall probe in the slot (position A in figure 37) with those field profiles constructed from measurements taken when the Hall probe was at the side of the aluminium rim (position B in figure 37). These measurements were made with several different values of magnetic Reynolds numbers but without the brush gear in place. No current entered or left the moving conductor. It was found that the field in position A was the same as the field in position B. We then assembled the brush gear and passed large currents through the metal rim whilst the wheel rotated. By inserting the probe, in 3 different azimuthal positions, into the slot in the centre of the rim we checked that the field at the centre (position A) was the same as the field at the edge (position B). From that time on, whenever the brush gear was in place, field measurements were made with the Hall probe at the edge of the aluminium (position B).

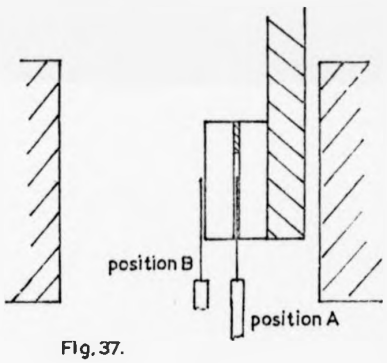

Fig. 37.

In M.H.D. pumps and generators the external circuits in the duct region are usually arranged so that the devices operate in a compensated mode, that is to say the currents in the external circuit produce a magnetic field parallel to the direction of the fluid flow and are thus incapable of modifying the transverse magnetic field. In a similar way the currents

which circulate between the two channels of a flow coupler produce a field which is parallel to the direction of fluid flow and thus do not modify the transverse field. Two experiments were therefore performed. In the first the external circuit was connected to the brush gear so that the apparatus represented an uncompensated device and in the second the external circuit resembled that of a compensated device. The arrangement of the conductors is shown in figure 38

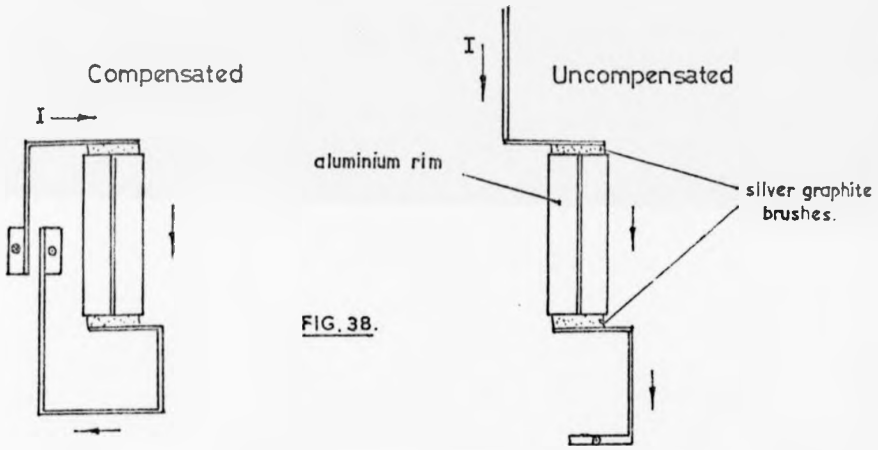

FIG. 38.

The Hall probe was placed at a known position along the side of the aluminium rim. The field was then measured whilst no current flowed from the battery and the wheel was stationary. This field was then recorded as the applied magnetic field. A large current, typically 500 amps, was then passed through the metal rim and the magnetic field was once again recorded. The wheel was then rotated and the field was measured at several chosen values of magnetic Reynolds number. The externally applied current was carefully maintained at the chosen value. This procedure was repeated many times with the Hall probe at a succession of places in the magnetic field region. Field profiles were constructed which showed how the transverse magnetic field varied in the azimuthal and the radial direction. Figure 39 shows how the initial and the convected field was found to vary in the azimuthal direction for an uncompensated device when there was no

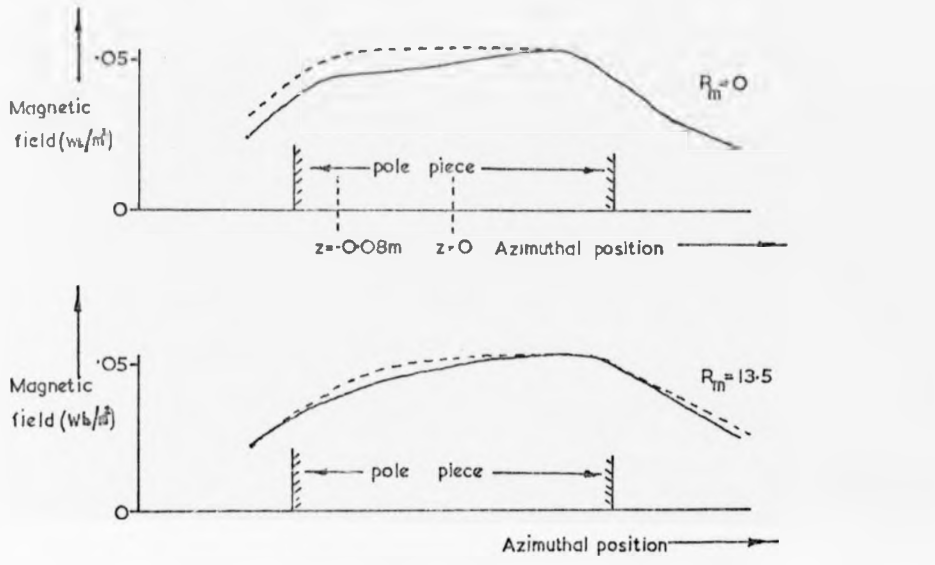

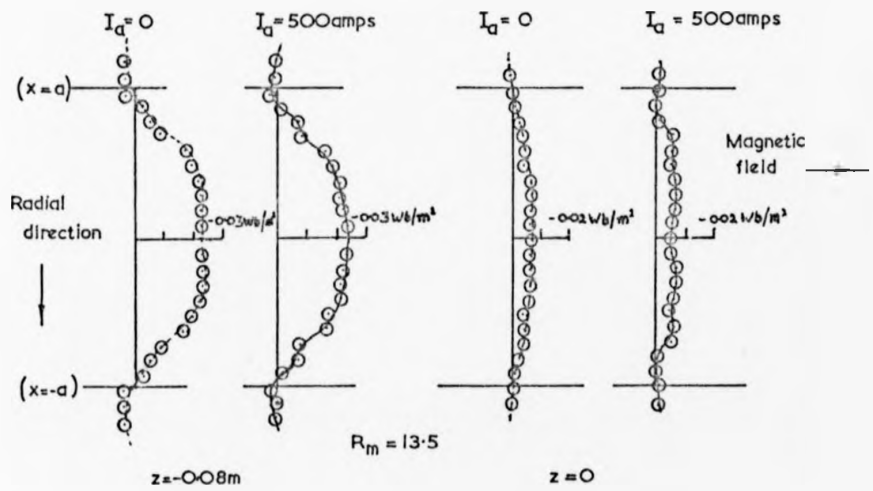

FIG 39. Showing the azimuthal distribution of the magnetic field when R_m=0 and 13·5 and when the applied current is zero and 500amps (upper) and the radial distribution of the field at two azimuthal positions when R_m=13·5 and the applied current is zero and 500amps (lower).

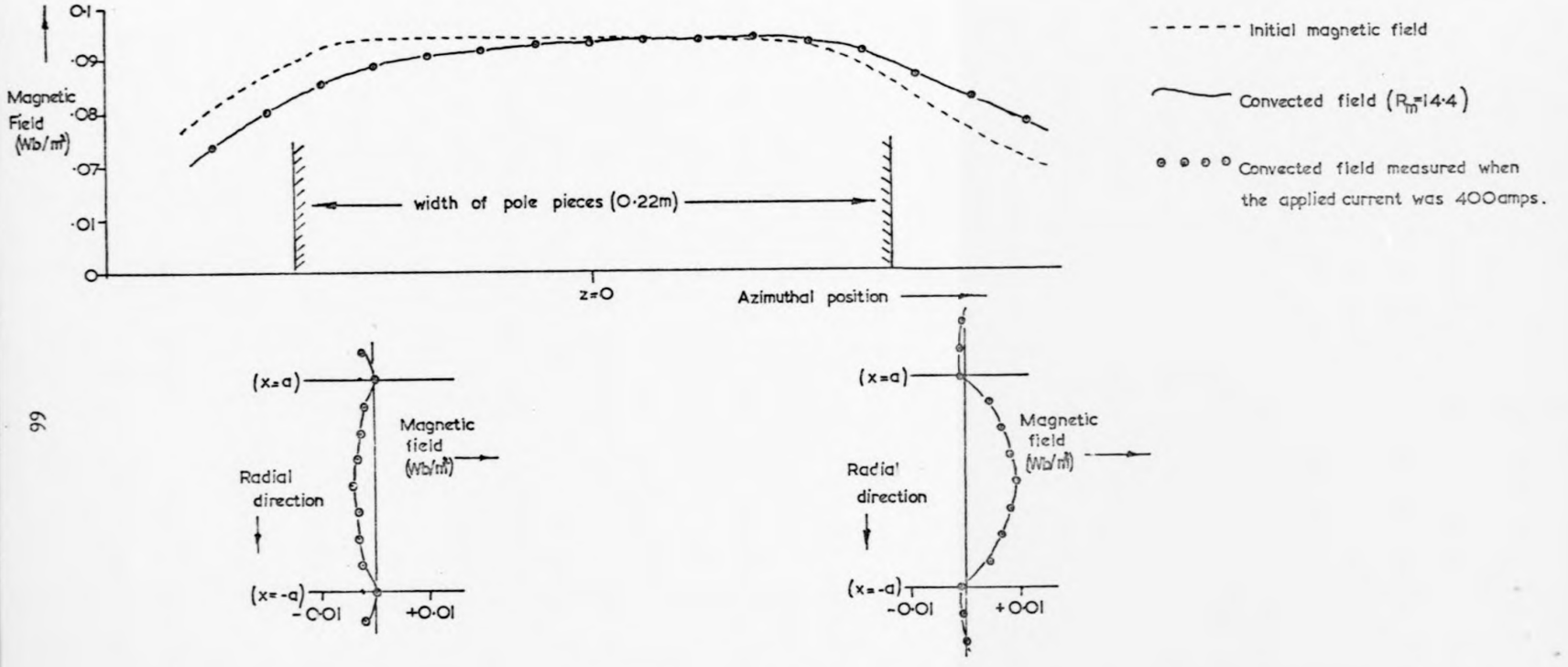

The azimuthal and radial distribution of the magnetic field in a compensated device when there is an applied current of 500amps.

FIG. 40.

brush current, and when the brush current was 500 amps. The magnetic Reynolds number was 13.5. In this case, as in other similar cases which we examined, the induced field which occurred when there was no brush current seemed to be very similar to the induced field which occurred when a current of 500 amps was passed through the moving conductor. This could have been because the initial magnetic field profile was only slightly distorted by a current of this size flowing through the circuit.

The apparatus was rebuilt to resemble a compensated device and the experiment was then repeated. It was found that the magnetic field in the compensated device was the same as the field which occurred when the current was confined within the moving conductor and that it did not depend upon the magnitude of the externally applied current. Figure 40 shows the initial field profile and the converted field profiles which occurred when no current flowed through the external circuit. Superimposed upon the convected field profile are the measured values of the field which occurred when a current of 400 amps flowed through the external circuit and through the aluminium. Also shown upon this diagram are field profiles which show the variation of the transverse magnetic field in the radial direction with an without the applied current of 400 amps. It is evident that when a device operates in a compensated mode the external currents are incapable of modifying the transverse magnetic field and that the induced component of the transverse field is the same as that which would occur if no current entered or left the moving conductor.

5.4 The Electrical Output of a Simple Generator.

Until this time the single wheel apparatus had been operating as a kind of M.H.D. pump. Unfortunately a current of 500 amps in a magnetic field of about 0.1 Wb/m^2 would produce only a small force in the conductor. Typically the interaction between a current of this size and the magnetic field would produce a force in the metal rim about $\frac{1}{30}$th of that required

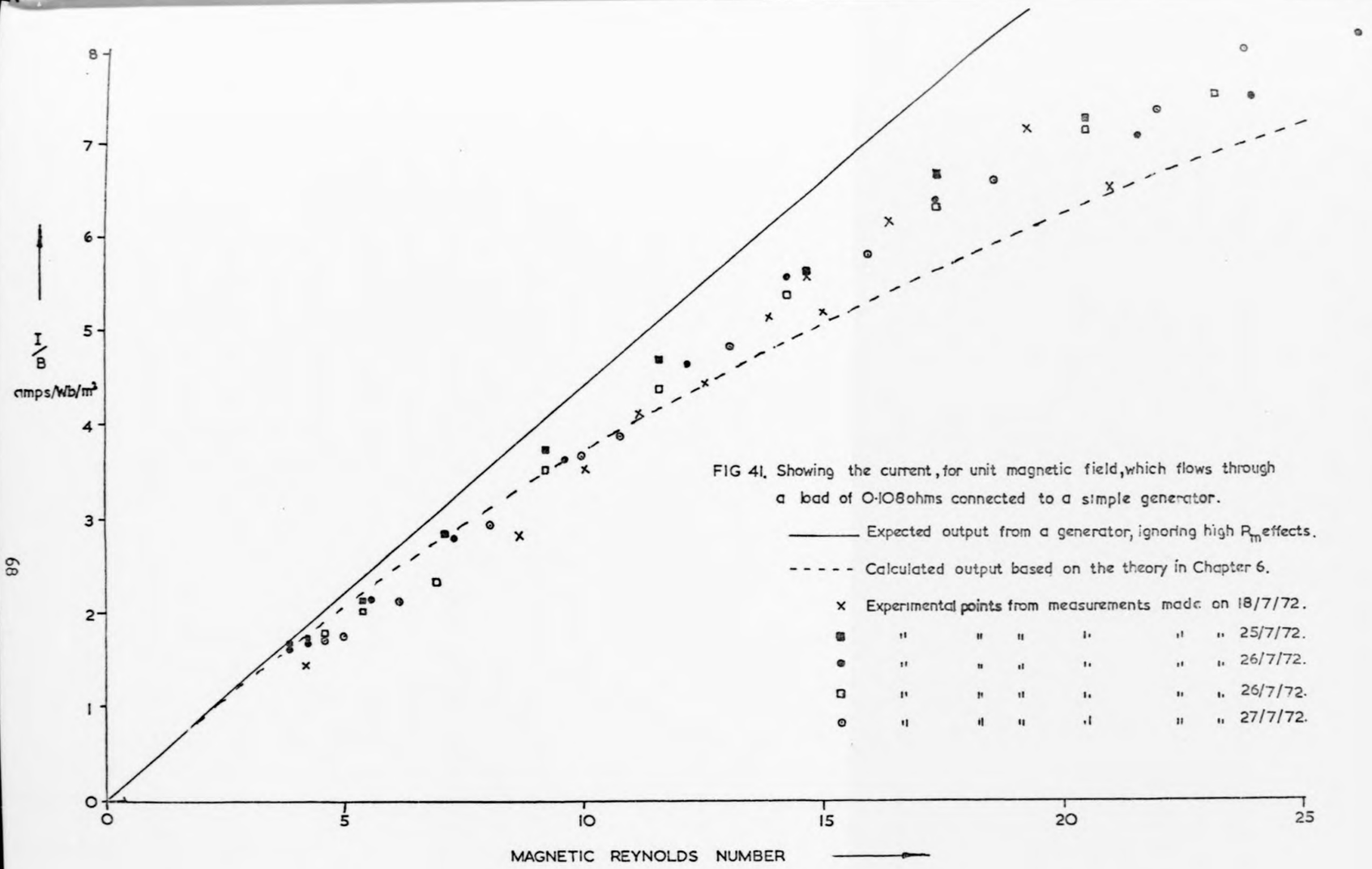

FIG 41. Showing the current, for unit magnetic field, which flows through a load of 0·108ohms connected to a simple generator.

——— Expected output from a generator, ignoring high R_m effects.

- - - - - Calculated output based on the theory in Chapter 6.

× Experimental points from measurements made on 18/7/72.

■ " " " " " " 25/7/72.

● " " " " " " 26/7/72.

□ " " " " " " 26/7/72.

⊙ " " " " " " 27/7/72.

to overcome the friction between the brush gear and the moving conductor. When operating an M.H.D. pump one would normally apply a known voltage to the terminals of the device. The current drawn would depend upon the velocity of the fluid travelling through the pump so that its apparent electrical resistance would depend upon the throughput. In our apparatus most of the voltage drop occurred across the brush gear; this would have made it difficult to measure any small changes in the apparent resistance of the moving aluminium. For these reasons we did not attempt to study in detail the performance of this device when it was operating as a pump.

We have investigated the performance of a simple M.H.D. generator by connecting the brush gear to a resistance which is large compared to the contact resistance between the brushes and the aluminium rim. Any change in the contact resistance between the brushes and the moving conductor are then small in comparison with the total resistance in the external circuit. During this experiment the apparatus was operated in a compensated mode with the brushes connected to a resister of 0.108Ω . Figure 41 shows how the output of this generator was found to vary with magnetic Reynolds number. The scattered points are the accumulated results of 5 different experiments and the dotted curve is a curve calculated from a theory presented in Chapter 6. The straight line indicates the way in which the output would vary if it were possible to ignore high magnetic Reynolds number effects. Because of the high frictional losses in the system we have not attempted to investigate the efficiency of this apparatus as a pump.

5.5 The Magnetic Field Perturbation When Two Conductors Move with Different Velocities Through a Common Magnetic Field.

The apparatus was now reassembled with two wheels rotating so that their rims passed between the poles of an electromagnet. The brush gear was not installed because we had already shown that the field perturbation in a compensated device, such as a flow coupler, does not depend upon the

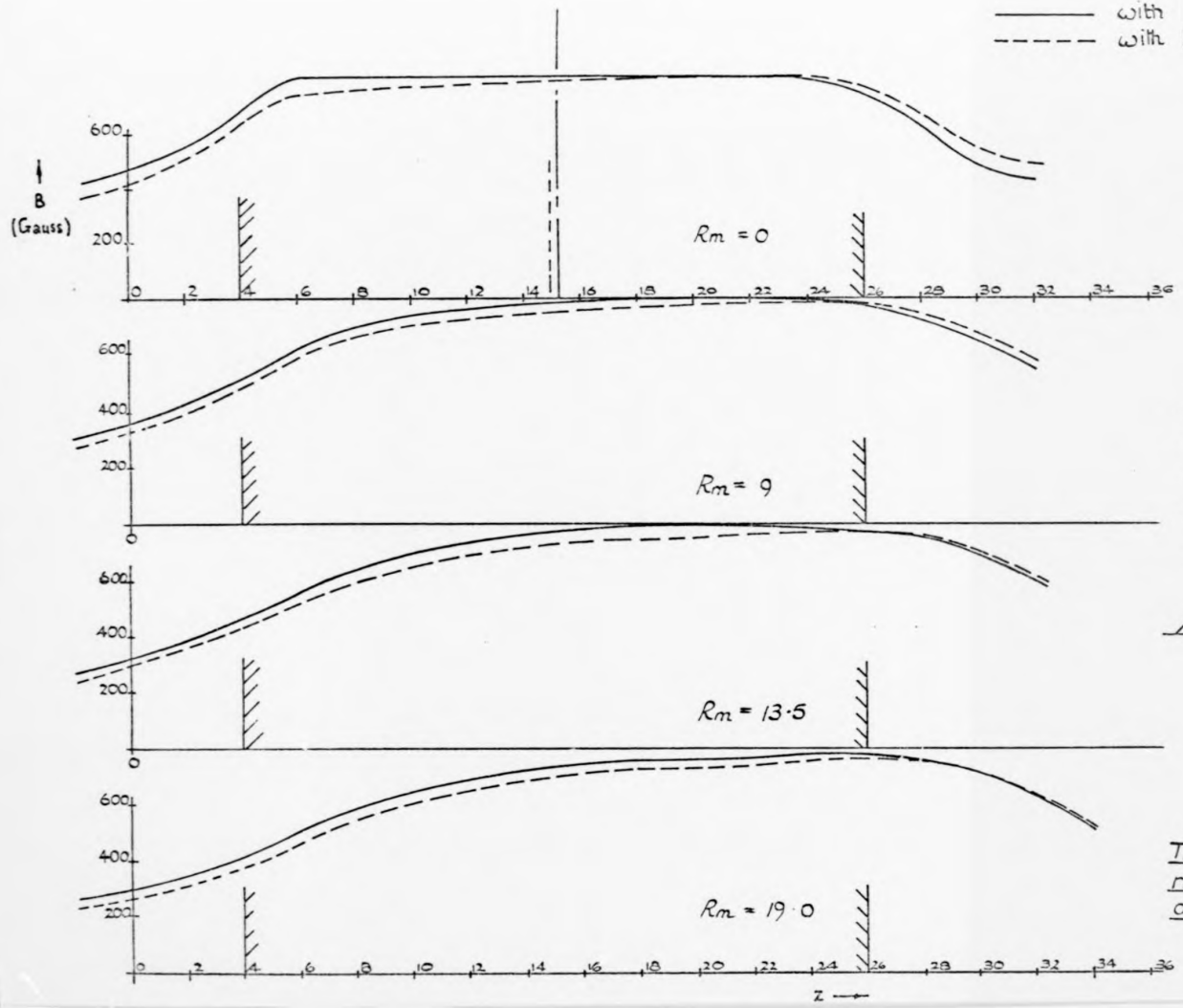

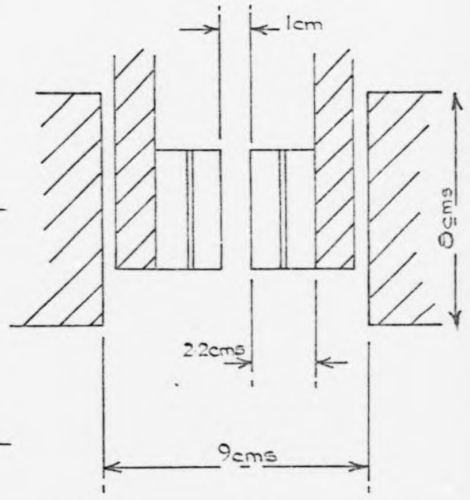

The total magnetic field within the right hand wheel for 4 different values of Rm for this wheel.

FIG. 42.

current which flows through the stationary external circuit. The magnetic field was measured, at a succession of different places, with the Hall probe located in the slots of the moving metal rims.

Many field profiles were constructed which showed how the field in each wheel depended upon the speed of that wheel and upon the speed of its neighbour. These results are summarized in figure 42. This figure shows how the magnetic field at the centre of the rim of the right hand wheel varied in the azimuthal direction, for several values of R_m, when the left hand wheel was first stationary and then moving very quickly. It can be seen that the change in field in this wheel which occurs when the magnetic Reynolds number in the rim of the left hand wheel is changed from zero to 19 is only of the order of 6%. Figure 42 also includes a sketch which shows the arrangement of the conductors within the magnet gap. Unfortunately we have been unable to investigate the way in which the modification of the magnetic field in one conductor due to the motion of its neighbour, depends upon the separation of the two conductors. The results we have presented suggest that it is unlikely that this modification is very great. In Chapter 7, which is the theoretical work concerning flow couplers, we therefore assume that the field in one channel of the flow coupler is not affected by the motion of its neighbour.

Chapter 6.

M.H.D. Pumps and Generators.

In this chapter we consider, in a two dimensional way, devices in which a conductor moves in the z-direction through a transverse magnetic field. This field is considered to be uniform in the y-direction. Currents may enter and leave through electrodes which are in contact with the moving metal at $x = \pm a$.

In 6.1 we calculate the potential at the surface of a moving conductor when the applied magnetic field, which is uniform in the electrode region, drops abruptly to zero at the ends of the electrodes. In 6.2 we calculate this potential for cases in which the applied magnetic field does not change abruptly at the ends of the device. We use this information in section 6.3 to calculate the electric current which flows through an external circuit connected between the two electrodes. We compare the computed output current of a simple generator with the experimentally measured current. Finally we attempt to calculate the efficiency of an M.H.D. pump which is similar to that described by D.A. Watt[6]. We then compare our results with those of Watt.

6.1 The Potential at the Electrodes of a Device in which the Applied Magnetic Field ends abruptly at $z = \pm l$

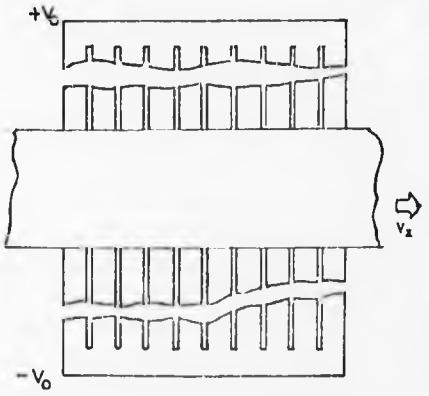

FIG. 43.

We consider devices in which the electrodes are segmented or have a high resistance to currents flowing in the z-direction. Electrodes such as this might consist of a solid piece of metal in which thin slots have been cut. The free ends of the electrodes are maintained at potentials of $\pm V_0$ volts and the faces of the electrodes which

are in contact with the moving conductor at $x=\pm a$ will be at a potential U_a where U_a is an unknown function of z. The current flowing in the moving conductor can be regarded as the sum of an applied current $\underline{j}_a$, which circulates through the duct and the external circuit, and an induced current $\underline{j}_i$ which arises because of the motion of the conductor through a magnetic field, that is $\underline{j} = \underline{j}_a + \underline{j}_i$. If the electrodes are arranged so that the device operates in a compensated mode the applied current produces a magnetic field in the z-direction and cannot modify the transverse magnetic field except at the ends of the device. Figure 44 is a sketch which represents a compensated device. The applied current I_a flows upwards through the M.H.D. duct and downwards through the return conductors. Applying Ampere's Law to the circuit A.B.C.D. we find that the contribution to transverse field at the ends of the electrode region is of order $\frac{\mu I_a}{2 \times \text{length of electrodes}}$

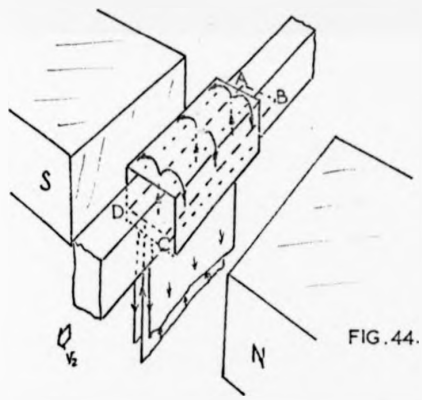

FIG.44.

We consider here only those cases in which this contribution to the transverse field is small in comparison to the applied field, that is $I_a < \frac{4 B_a l}{\mu}$ where B_a is the applied magnetic field, l is the half length of the electrodes and μ is the permeability of the moving conductor.

Because curl $\underline{B} = \mu \underline{j}$, $j_x = \frac{1}{\mu}\left(\frac{\partial B_z}{\partial y} - \frac{\partial B_y}{\partial z}\right)$

and $j_x = j_{x_a} + j_{x_i} = \frac{1}{\mu}\frac{\partial B_z}{\partial y} - \frac{1}{\mu}\frac{\partial B_y}{\partial z}$ (61)

Inside a compensated device the applied current can only produce fields in the z-direction so that B_y and therefore $\frac{\partial B_y}{\partial z}$ does not depend upon j_{x_a}. The induced currents do not in general produce z-wise fields in the moving conductor so that B_z and hence $\frac{\partial B_z}{\partial y}$ do not depend upon j_{x_i}. We therefore conclude that in Equation (61)

$$j_{x_2} = \frac{1}{\mu} \frac{\partial B_z}{\partial y} \tag{62}$$

and $$j_{x_i} = -\frac{1}{\mu} \frac{\partial B_y}{\partial z} \tag{63}$$

Our experimental observations confirm that the induced component of the magnetic field is independant of the applied current.

We consider cases in which the electrodes are much longer in the z-direction than the duct is wide, in the x-direction. We then ignore the fringing of the applied current distribution at the ends of the device and assume that the distribution of the applied current within the moving conductor is the same as that in the electrodes.

From the Ohm's law equation we find that the current density in the electrodes is given by $j_{x_2} = \sigma_\varepsilon E_x$, where σ_ε is the conductivity of the electrode material.

Then $$j_x = j_{x_2} + j_{x_i}$$

$$= -\frac{\sigma_\varepsilon (V_0 - U_2)}{d} - \frac{1}{\mu} \frac{\partial B_y}{\partial z} . \tag{65}$$

Where U_2 is the potential at the surface of the moving conductor and is a function of z, and d is a length associated with the electrode.

The Ohms law equation for the moving conductor is

$$\frac{\underline{j}}{\sigma_m} = \underline{E} + \underline{v} \times \underline{B} ,$$

the x component of which is:-

$$\frac{j_x}{\sigma_m} = E_x - v_z B_y , \quad \text{where } \sigma_m \text{ is the conductivity of the moving metal.} \tag{66}$$

Then $$-\frac{\sigma_\varepsilon (V_0 - U_2)}{\sigma_m \, d} - \frac{1}{\mu \sigma_m} \frac{\partial B_y}{\partial z} = -\frac{\partial U}{\partial x} - v_z B_y , \tag{67}$$

where B_y is the sum of the applied transverse magnetic field B_a and the induced transverse magnetic field B_i.

We have shown in Chapter 3 that the induced magnetic field in a conductor which moves through an abruptly ending magnetic field may be considered in three regions of space and that the induced magnetic field, which is independant of the applied current, is

$$B_i = \sum_{n=1,3,5\ldots} A_n e^{\alpha_1 z} \cos \frac{n\pi x}{2a} \qquad \text{when} \quad z < -1 \ ,$$

$$B_i = \sum_{n=1,3,5\ldots} \left(B_n e^{\alpha_1 z} + C_n e^{\alpha_2 z}\right) \cos \frac{n\pi x}{2a} \qquad \text{when} \quad -1 < z < +1 \ ,$$

$$\text{and } B_i = \sum_{n=1,3,5\ldots} D_n e^{\alpha_2 z} \cos \frac{n\pi x}{2a} \qquad \text{when} \quad z > +1 \ ,$$

where α_1, α_2, A_n, B_n, C_n, and D_n are given in Equations (23),(24),(19),(20),(21) and (22) respectively.

We here consider devices in which the electrodes extend from $z = -1$ to $z = +1$ and we rewrite Equation (67) in the form

$$-\frac{\sigma_2}{\sigma_m}\frac{(V_0 - U_2)}{d} - \frac{1}{\mu\sigma_m}\sum_{n=1,3,5\ldots}\left(B_n \alpha_1 e^{\alpha_1 z} + C_n \alpha_2 e^{\alpha_2 z}\right)\cos\frac{n\pi x}{2a}$$
$$= -\frac{\partial U}{\partial x} - v_2 B_a - v_2 \sum_{n=1,3,5\ldots}\left(B_n e^{\alpha_1 z} + C_n e^{\alpha_2 z}\right)\cos\frac{n\pi x}{2a} \qquad (68)$$

By collecting terms and writing v_2 as $\frac{R_m}{\mu\sigma_m a}$ we find that

$$\frac{\partial U}{\partial x} = \frac{\sigma_2}{\sigma_m}\frac{(V_0 - U_2)}{d} + \frac{1}{\mu\sigma_m}\sum_{n=1,3,5\ldots}\left(-\alpha_2 B_n e^{\alpha_1 z} - \alpha_1 C_n e^{\alpha_2 z}\right)\cos\frac{n\pi x}{2a} - \frac{R_m B_0}{\mu\sigma_m a} \ .$$

Integrating w.r.t. x we have

$$U = \frac{\sigma_2}{\sigma_m}\frac{(V_0 - U_2)}{d} - \frac{1}{\mu\sigma_m}\sum_{n=1,3,5\ldots}\left(\alpha_2 B_n e^{\alpha_1 z} + \alpha_1 C_n e^{\alpha_2 z}\right)\frac{2a}{n\pi}\sin\frac{n\pi x}{2a} - \frac{R_m B_0 x}{\mu\sigma_m a} + \text{const} \qquad (69)$$

We require that $U = 0$ at $x = 0$ and we therefore choose the constant to be zero.

At x = a U = U_a and Equation (69) becomes

$$U_a = \frac{\sigma_\varepsilon}{\sigma_m}\left(\frac{V_o - U_a}{d}\right).a - \frac{1}{\mu\sigma_m}\left[\sum_{n=1,3,5}\left(\alpha_1 B_n e^{\alpha_1 z} + \alpha_1 C_n e^{\alpha_2 z}\right)\frac{2a}{n\pi}\sin\frac{n\pi}{2} - \frac{R_m B_o}{\mu\sigma_m}\right.$$

We substitute for B_n and C_n using Equations (20),(21), and (26), to be found on Chapter 3, and we then find

$$U_a = \frac{\sigma_\varepsilon}{\sigma_m}\left(\frac{V_o - U_a}{d}\right).a - \frac{B_o R_m 8a}{\mu\sigma_m}\left[\sum_{n=1,3,5}\frac{\left(\alpha_2 e^{\alpha_1(z-l)} - \alpha_1 e^{\alpha_2(z+l)}\right)}{n^2\pi^2\left(R_m^2 + n^2\pi^2\right)^{1/2}}\right] - \frac{R_m B_o}{\mu\sigma_m}. \quad (70)$$

We have shown in Equation (43) of Chapter 3 that the potential within a moving conductor which has no electrodes is

$$U = -V_2 B_o a\left[\frac{x}{a} - \frac{8}{\pi^2}\sum_{n=1,3,5}\frac{(-1)^{\frac{n+1}{2}}}{n^2 K}\left(\alpha_2 e^{-\alpha_1(l-z)} - \alpha_1 e^{\alpha_2(l+z)}\right)\sin\frac{n\pi z}{2a}\right] \text{ when } -l < z < +l.$$

At x = a this equation may be written in the form,

$$U_a = -\frac{R_m B_o}{\mu\sigma_m} - \frac{R_m B_o 8a}{\mu\sigma_m}\left[\sum_{n=1,3,5}\frac{\left(\alpha_2 e^{\alpha_1(z-l)} - \alpha_1 e^{\alpha_2(l+z)}\right)}{n^2\pi^2\left(R_m^2 + n^2\pi^2\right)^{1/2}}\right].$$

In the present case currents cannot flow in the z-direction within the electrodes so that if the electrodes are not connected to a load the potential along the surface at x = ± a will be the same as that at the surface of an electrodeless moving conductor. We see by comparing the above expression with Equation (70) that we may express U_a in the form

$$U_a = \frac{\sigma_\varepsilon}{\sigma_m}\left(\frac{V_o' - U_a}{d}\right).a + \left[\text{OPEN CIRCUIT POTENTIAL}\right]$$

or

$$U_a\left(1 + \frac{\sigma_\varepsilon}{\sigma_m}.\frac{a}{d}\right) = \frac{\sigma_\varepsilon}{\sigma_m} V_o \frac{a}{d} + \left[\text{OPEN CIRCUIT POTENTIAL}\right]$$

If we consider the resistance of the moving conductor to the flow of current in the x direction, then, ignoring the fringing effects at the ends of the device, the resistance Rd between x = 0 and x = a is :-

$$R_d = \frac{1}{\sigma_m}\,\frac{a}{2lt}$$ where t is the thickness of the duct in the y-direction.

The resistance of the electrode (R_e) is

$$R_e = \frac{1}{\sigma_e}\,\frac{d}{2lt} \quad \text{and so} \quad \frac{R_d}{R_e} = \frac{\sigma_e}{\sigma_m}\cdot\frac{a}{d}.$$

Equation (71) now becomes

$$U_3\left(1+\frac{R_d}{R_e}\right) = \frac{R_d}{R_e}\cdot V_0 + \left[\text{OPEN CIRCUIT POTENTIAL}\right]$$

or $$U_3 = \frac{R_d}{(R_e+R_d)}\cdot V_0 + \frac{R_e}{(R_e+R_d)}\left[\text{OPEN CIRCUIT POTENTIAL}\right].$$ When R_e is large compared with R_d, the potential at the surface of the moving conductor, U_3, is effectively the open circuit potential.

6.2 The Potential at the Electrodes of a Device in which the Applied Magnetic Field is Uniform in the Electrode Region but in which the Field does not end Abruptly.

We consider the initial magnetic field to be composed of p abrupt fields, each of magnitude $\frac{B_3}{p}$ and of length L_p so that the total applied field $(B_3) = B_{L_1} + B_{L_2} + B_{L_3} \ldots\ldots B_{L_p}$.

We let the electrodes extend from $z = -l$ to $z = +l$ in a region in which the total applied magnetic field is uniform. The induced magnetic field due to each element is

$$B_{i_{L_p}} = \sum_{n=1,3,5\ldots} \left(B_n e^{\alpha_n z} + C_n e^{\alpha_n z}\right) \cos\frac{n\pi x}{2a}$$

where $B_n = -\frac{B_0}{P} \cdot R_m \frac{4}{n\pi} \frac{(-1)^{\frac{n+1}{2}} e^{-\alpha_1 L_\rho}}{\left(R_m^2 + n^2\pi^2\right)^{1/2}}$,

and $C_n = \frac{B_0}{P} \cdot R_m \frac{4}{n\pi} \frac{(-1)^{\frac{n+1}{2}} e^{\alpha_2 L_\rho}}{\left(R_m^2 + n^2\pi^2\right)^{1/2}}$

or $B_{i_{L_\rho}} = \frac{B_0}{P} \cdot R_m \sum_{n=1,3,5\ldots} -\frac{4}{n\pi} (-1)^{\frac{n+1}{2}} \frac{\left(e^{\alpha_1(z-L_\rho)} - e^{\alpha_2(z+L_\rho)}\right)}{\left(R_m^2 + n^2\pi^2\right)^{1/2}} \cos\frac{n\pi x}{2a}$.

Once again we find from the Ohm's law equation that $\frac{j_x}{\sigma} = E_x - v_z B_y$

and $j_x = -\sigma_e \frac{(V_0 - U_1)}{d} - \frac{1}{\mu} \frac{\partial B_y}{\partial z}$

so that $-\frac{\sigma_e (V_0 - U_1)}{\sigma_m \; d} - \frac{1}{\mu\sigma_m} \frac{\partial B_y}{\partial z} = E_x - v_z B_y$ where $B_y = B_1 + B_i$.

Substituting for B_y and $\frac{\partial B_y}{\partial z}$ and collecting terms we find

$$-\frac{\sigma_e}{\sigma_m} \frac{(V_0 - U_1)}{d} - \frac{1}{\mu\sigma_m} \cdot \frac{B_0}{P} \cdot R_m \sum_{n=1,3,5\ldots} \sum_{P=1-\rho} -\frac{4}{n\pi} \frac{(-1)^{\frac{n+1}{2}} \left(e^{\alpha_1(z-L_\rho)\left(\alpha_1 - \frac{R_m}{a}\right)} - e^{\alpha_2(z+L_\rho)\left(\alpha_2 - \frac{R_m}{a}\right)} \right)}{\left(R_m^2 + n^2\pi^2\right)^{1/2}} \cos\frac{n\pi x}{2a}$$

$$= -\frac{\partial U}{\partial x} - \frac{R_m}{\mu\sigma_m a} B_0 . \qquad (72)$$

Because $\alpha_1 - \frac{R_m}{a} = -\alpha_2$ and $\alpha_2 - \frac{R_m}{a} = -\alpha_1$

we rearrange Equation (72) and integrate with w.r.t x and find that

where $B_n = -\frac{B_0}{P} \cdot R_m \frac{4\,(-1)^{\frac{n+1}{2}}\, e^{-\alpha_1 L_\rho}}{n\pi\left(R_m^2 + n^2\pi^2\right)^{\frac{1}{2}}}$,

and $C_n = \frac{B_0}{P} \cdot R_m \frac{4\,(-1)^{\frac{n+1}{2}}\, e^{\alpha_2 L_\rho}}{n\pi\left(R_m^2 + n^2\pi^2\right)^{\frac{1}{2}}}$

or $B_{i_{L_\rho}} = \frac{B_0}{P} \cdot R_m \left[\sum_{n=1,3,5\ldots} -\frac{4}{n\pi}(-1)^{\frac{n+1}{2}} \frac{\left(e^{\alpha_1(z-L_\rho)} - e^{\alpha_2(z+L_\rho)}\right)}{\left(R_m^2 + n^2\pi^2\right)^{\frac{1}{2}}} \cos\frac{n\pi x}{2a} \right]$.

Once again we find from the Ohm's law equation that $\frac{j_x}{\sigma} = E_x - v_z B_y$

and $j_x = -\sigma_e\left(\frac{V_0 - U_1}{d}\right) - \frac{1}{\mu}\frac{\partial B_y}{\partial z}$

so that $-\frac{\sigma_e}{\sigma_m}\left(\frac{V_0 - U_1}{d}\right) - \frac{1}{\mu\sigma_m}\frac{\partial B_y}{\partial z} = E_x - v_z B_y$ where $B_y = B_a + B_i$.

Substituting for B_y and $\frac{\partial B_y}{\partial z}$ and collecting terms we find

$$-\frac{\sigma_e}{\sigma_m}\left(\frac{V_0 - U_1}{d}\right) - \frac{1}{\mu\sigma_m} \cdot \frac{B_0}{P} \cdot R_m \left[\sum_{n=1,3,5\ldots} -\frac{4}{n\pi} \frac{(-1)^{\frac{n+1}{2}}\left(e^{\alpha_1(z-L_\rho)\left(\alpha_1 - \frac{R_m}{a}\right)} - e^{\alpha_2(z+L_\rho)\left(\alpha_2 - \frac{R_m}{a}\right)}\right)}{\left(R_m^2 + n^2\pi^2\right)^{\frac{1}{2}}} \cos\frac{n\pi x}{2a} \right]_{P=1-\rho}$$

$$= -\frac{\partial U}{\partial x} - \frac{R_m}{\mu\sigma_m a} B_0 . \qquad (72)$$

Because $\alpha_1 - \frac{R_m}{a} = -\alpha_2$ and $\alpha_2 - \frac{R_m}{a} = -\alpha_1$

we rearrange Equation (72) and integrate with w.r.t x and find that

$$U = \frac{\sigma_2}{\sigma_m}\frac{(V_0 - U_a)}{d}x + \frac{B_0}{P}\cdot\frac{R_m}{\mu\sigma_m}\left[\sum_{n=1,3,5\ldots}\left[\sum_{p=1\ldots\infty}-\frac{4}{n\pi}(-1)^{\frac{n+1}{2}}\frac{\left(-\alpha_2 e^{\alpha_1(z-Lp)}+\alpha_1 e^{\alpha_2(z+Lp)}\right)}{\left(R_m^2+n^2\pi^2\right)^{1/2}}\right]\frac{2a}{n\pi}\sin\frac{n\pi x}{2a}\right] - \frac{R_m B_0 x}{\mu\sigma_m a}$$

$$+ \text{const.} \quad \ldots\ldots \quad (73)$$

We require that U = 0 at x = 0 so that the constant in Equation (73) is zero, Then at x = a U = U_a and

$$U_a = \frac{\sigma_2}{\sigma_m}\left(V_0 - U_a\right)\frac{a}{d} + \frac{B_0}{P}\cdot\frac{R_m}{\mu\sigma_m}\left[\sum_{n=1,3,5\ldots}\left[\sum_{p=1\ldots\infty}-\frac{4}{n\pi}(-1)^{\frac{n+1}{2}}\frac{\left(-\alpha_2 e^{\alpha_1(z-Lp)}+\alpha_1 e^{\alpha_2(z+Lp)}\right)}{\left(R_m^2+n^2\pi^2\right)^{1/2}}\right]\frac{2a}{n\pi}\sin\frac{n\pi}{2}\right] - \frac{R_m B_0}{\mu\sigma_m},$$

which is:-

$$U_a = \frac{\sigma_2}{\sigma_m}\left(V_0 - U_a\right)\frac{a}{d} - \frac{R_m B_0}{\mu\sigma_m}\left[1 + \frac{1}{P}\left[\sum_{n=1,3,5\ldots}\left[\sum_{p=1\ldots\infty}\frac{8a}{n^2\pi^2}\frac{\left(\alpha_2 e^{\alpha_1(z-Lp)}-\alpha_1 e^{\alpha_2(z+Lp)}\right)}{\left(R_m^2+n^2\pi^2\right)^{1/2}}\right]\right]\right]. \quad (74)$$

The electrical resistance of the electrode to currents entering the duct is $R_E = \frac{1}{\sigma_2}\cdot\frac{d}{2lt}$ and the resistance of the duct from x = 0 to x = a is $R_d = \frac{1}{\sigma_m}\cdot\frac{a}{2lt}$ so that $\frac{R_d}{R_E} = \frac{\sigma_2}{\sigma_m}\cdot\frac{a}{d}$.

Then $$U_a\left(1+\frac{R_d}{R_E}\right) = \frac{R_d}{R_e}V_0 - \frac{R_m B_0}{\mu\sigma_m}\left[1 + \frac{1}{P}\left[\sum_{n=1,3,5\ldots}\left[\sum_{p=1\ldots\infty}\frac{8a}{n^2\pi^2}\frac{\left(\alpha_2 e^{\alpha_1(z-Lp)}-\alpha_1 e^{\alpha_2(z+Lp)}\right)}{\left(R_m^2+n^2\pi^2\right)^{1/2}}\right]\right]\right]$$

or $$U_a = \frac{R_d}{R_E+R_d}\cdot V_0 - \frac{R_e}{R_e+R_d}\cdot\frac{R_m B_0}{\mu\sigma_m}\left[1 + \frac{1}{P}\left[\sum_{n=1,3,5\ldots}\left[\sum_{p=1\ldots\infty}\frac{8a}{n^2\pi^2}\frac{\left(\alpha_2 e^{\alpha_1(z-Lp)}-\alpha_1 e^{\alpha_2(z+Lp)}\right)}{\left(R_m^2+n^2\pi^2\right)^{1/2}}\right]\right]\right] \quad (75)$$

Once again when R_L is large compared with R_d the potential U_a is effectively the open circuit potential which in this case is the sum of the potentials due to each small element of field.

6.3 The Electric Current through the Electrodes of a Device in Which the Applied Magnetic Field is Uniform in the Electrode Region but in which the Field does not end Abruptly.

The total current flowing through an electrode will be given by

$$I_x = \int_{-l}^{+l} j_x \, t \, dz .$$

We have previously shown that $j_{x_a} = -\sigma_2 \frac{(V_0 - U_a)}{d}$, that is

$$j_{x_a} = -\frac{\sigma_2 V_0}{d} + \frac{\sigma_2 R_d V_0}{d(R_d + R_\varepsilon)} - \frac{\sigma_2 R_\varepsilon R_m B_0}{d(R_\varepsilon + R_d)\mu\sigma_m}\left[1 + \frac{1}{\rho}\sum_{n=1,3,5}^{\infty}\sum_{p=1,-\rho}^{\rho}\frac{8a}{n^2\pi^2}\frac{\left(\alpha_2 e^{\alpha_1(z-l_\rho)} - \alpha_1 e^{\alpha_2(z+l_\rho)}\right)}{(R_m^2 + n^2\pi^2)^{1/2}}\right] \quad (76)$$

Integrating over the length of the electrode and writing $R_\varepsilon = \frac{1}{\sigma_\varepsilon}\frac{d}{2lt}$ we find that

$$I_x = \frac{-V_0}{(R_d + R_\varepsilon)} - \frac{R_m B_0}{\mu\sigma_m}\cdot\frac{1}{(R_d + R_\varepsilon)}\left[1 + \frac{1}{2l\rho}\sum_{n=1,3,5}^{\infty}\sum_{p=1,-\rho}^{\rho}\frac{8a}{n^2\pi^2}\frac{\left[\frac{\alpha_2}{\alpha_1}\left(e^{\alpha_1(l-l_\rho)} - e^{-\alpha_1(l+l_\rho)}\right) - \frac{\alpha_1}{\alpha_2}\left(e^{\alpha_2(l+l_\rho)} - e^{-\alpha_2(l-l_\rho)}\right)\right]}{(R_m + n^2\pi^2)^{1/2}}\right] \quad (77$$

If the two electrodes of the device are connected to a load resistor of value $2R_L$ the device acts as a generator. The voltage across this resistor will be $2V_0$ so that $\frac{2V_0}{I_x} = 2R_L$ or $V_0 = R_L I_x$. Substituting into Equation (76) and writing $R_d + R_\varepsilon + R_L = \frac{R_c}{2}$ where R_c is the total resistance in the circuit we find that

$$I_x = -\frac{2 R_m B_0}{R_c \mu\sigma_m}\left[1 + \frac{1}{2l\rho}\sum_{n=1,3,5}^{\infty}\sum_{p=1,-\rho}^{\rho}\frac{8a}{n^2\pi^2}\frac{\left[\frac{\alpha_2}{\alpha_1}\left(e^{\alpha_1(l-l_\rho)} - e^{-\alpha_1(l+l_\rho)}\right) - \frac{\alpha_1}{\alpha_2}\left(e^{\alpha_2(l+l_\rho)} - e^{-\alpha_2(l-l_\rho)}\right)\right]}{(R_m^2 + n^2\pi^2)^{1/2}}\right] \quad (78)$$

We have used Equation (78) to calculate the current which one would expect when a resistor of 0.108Ω was connected as a load resistor to a simple generator which had an applied magnetic field similar to the measured field in our apparatus. In figure 41 we contrast the calculated current with the observed current. There is reasonable agreement between experiment and theory when Rm is less than about 12 or 13; when R_m is higher than this the theory underestimates the output of the device.

Equation 77 may also be used to study the behaviour of an M.H.D. pump in which there is slug flow. When operating a pump we apply a known voltage to the electrodes, the current drawn depends upon the velocity of the fluid in the duct and upon the magnetic field. If we represent the whole pump as a resistor, which has a value of 2Rp, then Rp will depend upon Rm. An applied current in the positive x-direction in the presence of the applied magnetic field in the y-direction, produces a force in the fluid in the z-direction. We consider devices in which the potential at the centre of the duct (x = o) is zero. To obtain a current in the positive x-direction it is necessary to apply a negative voltage to the electrode which touches the moving metal at x = a. Therefore for an M.H.D. pump we write Vo = $-I_x R_p$. Equation 77 now becomes

$$I_x = \frac{I_x R_p}{(R_d + R_\ell)} - \frac{R_m B_o}{\mu \sigma_m} \cdot \frac{1}{(R_d + R_\ell)} \left[1 + \frac{1}{2\ell_p} \sum_{n=1,3,5\ldots} \frac{8a}{n^2\pi^2} \frac{\left[\frac{\alpha_2}{\alpha_1} \left(e^{\alpha_1(l-l_p)} - e^{-\alpha_1(l+l_p)} \right) - \frac{\alpha_1}{\alpha_2} \left(e^{\alpha_2(l+l_p)} - e^{-\alpha_2(l-l_p)} \right) \right]}{\left(R_m^2 + n^2\pi^2 \right)^{1/2}} \right] \quad (79)$$

Rearranging Equation (79) we find

$$R_p = \frac{1}{I_x} \cdot \frac{R_m B_o}{\mu \sigma_m} \left[1 + \frac{1}{2\ell_p} \sum_{n=1,3,5\ldots} \frac{8a}{n^2\pi^2} \frac{\left[\frac{\alpha_2}{\alpha_1} \left(e^{\alpha_1(l-l_p)} - e^{-\alpha_1(l+l_p)} \right) - \frac{\alpha_1}{\alpha_2} \left(e^{\alpha_2(l+l_p)} - e^{-\alpha_2(l-l_p)} \right) \right]}{\left(R_m^2 + n^2\pi^2 \right)^{1/2}} \right]$$

$$+ R_d + R_\ell . \qquad (80).$$

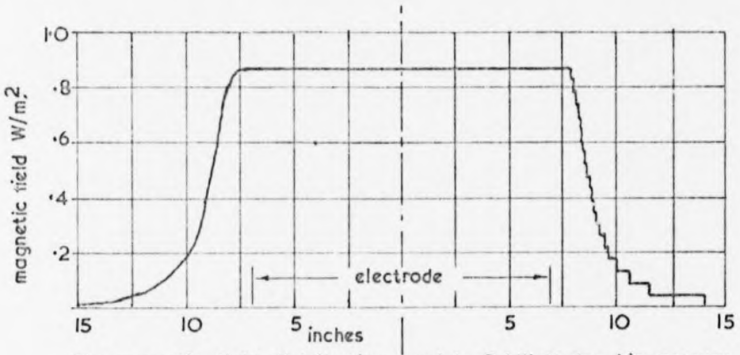

The magnetic field distribution used by D.A.Watt for his mercury experiments (left) and the magnetic field distribution used for this theory (right).

fig 45.

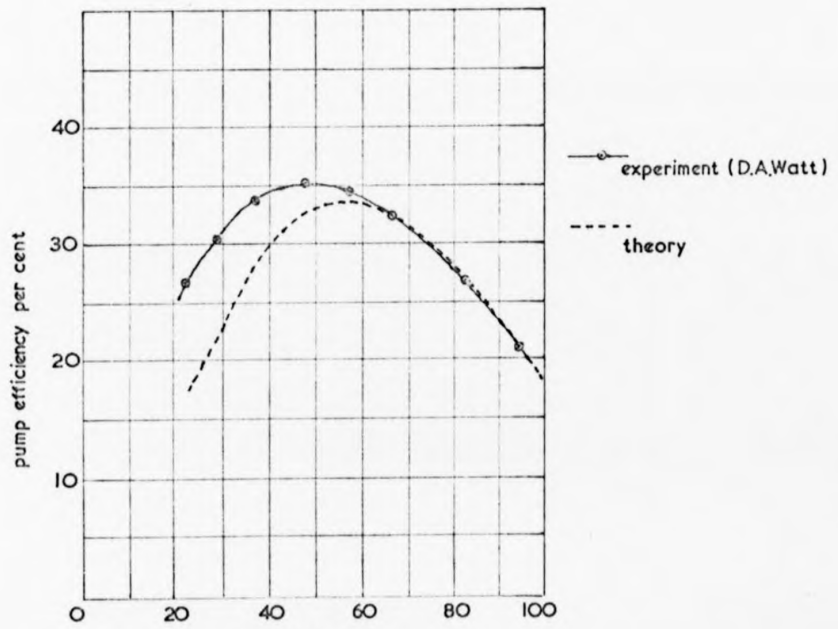

Graph showing how the measured and calculated efficiency of the mercury pump varies with the flow rate.

fig 46.

It is evident that we may represent a pump as a device whose total resistance is composed of three parts, that is:- $R_p = R_{dm} + R_d + R_E$ where R_d is the resistance of the stationary liquid, R_{dm} is an extra resistance caused by the motion of the liquid through the magnetic field and R_E is the resistance of the electrode. The apparent resistance of the liquid in the duct is then R_{app} where

$$R_{app} = \frac{1}{I_x} \cdot \frac{R_m B_0}{\mu \sigma_m} \left[1 + \frac{1}{2\ell_p} \sum_{\text{poles}} \frac{B_n}{n^2 \pi^2} \frac{\left[\frac{\alpha_2}{\alpha_1} \left(e^{\alpha_1 (l-l_f)} - e^{-\alpha_1 (l-l_f)} \right) - \frac{\alpha_1}{\alpha_2} \left(e^{\alpha_2 (l-l_f)} - e^{-\alpha_2 (l-l_f)} \right) \right]}{\left(R_m^2 + n^2 \pi^2 \right)^{\frac{1}{2}}} \right] + R_d \quad (81)$$

In real devices the total current supplied to the electrodes (I_T) is divided into two parts, part flows through the fluid in the duct (I_x) whilst part (I_w) flows through the duct wall. It is easily shown that

$$I_x = \frac{R_w}{(R_{app} + R_w)} \cdot I_T \qquad \text{and} \qquad I_w = \frac{R_{app}}{(R_{app} + R_w)} \cdot I_T .$$

As the fluid in the pump increases its velocity Rapp increases so that a greater proportion of the total current flows through the duct wall.

D.A. Watt has performed detailed tests upon a large M.H.D. mercury pump. The pump consisted of a stainless steel duct having internal dimensions of 0.152 metres in a direction perpendicular to the magnetic field and 0.0151 metres in the direction of the field. The duct had copper electrodes, attached to the thin edges, which extended for a distance of 0.356 metres in the flow direction. The pump was compensated by passing the return conductors along each side of the duct. Figure 45 shows how the transverse magnetic field was found to vary in the direction of the flow. Flow rates of up to about 100 gallons per minute were achieved using this pump. Watt measured the resistance (2Rw) of the stainless steel duct when it was empty and found that it was $2.37 \times 10^{-4} \Omega$. The resistance when filled with stationary mercury was found to be $19.3 \times 10^{-6} \Omega$. From these two measurements we calculate that the resistance of the stationary mercury (2Rd) was $0.21 \times 10^{-4} \Omega$.

We have calculated the theoretical efficiency of this pump by assuming that the liquid in the duct moves with slug flow. We also assume that the resistance of the electrodes to currents flowing in the x-direction was negligible when compared with the resistance of the duct and the liquid it contained. One half of the total resistance of the pump is then R_p where $R_p = \frac{R_w R_{eff}}{(R_w + R_{eff})}$. The total power supplied to the pump is $I_T^2 R_p$. There are three different mechanisms which cause losses in the pump. Part of the total current flows uselessly through the duct walls and causes ohmic heating; this we call the wall loss. The induced currents and the applied current within the moving conductor cause ohmic heating, which we call the duct loss. There is also a hydraulic loss because power is required to overcome the viscous forces in the liquid within the pump. We calculate the efficiency of this device by evaluating each of these losses. The useful power available for pumping mercury is then the total input power minus the power losses. The percentage efficiency we define as $\frac{\text{useful power output}}{\text{total power input}} \times 100$.

Watt performed water tests upon the pump channel. He used the results of these tests to calculate the pressure drop which would occur if mercury instead of water was made to flow through the duct. We use this calculated pressure drop to evaluate the hydraulic loss in the duct.

We use Equation (81) to calculate the apparent resistance of the mercury in the duct. Watt presents graphs which show how the efficiency of the pump depends upon the flow rate when to total current through the pump is maintained at any one of several chosen values. In these tests the magnetic field was 0.88 $/m^2$.

We use the expression $I_x = \frac{R_w}{(R_{eff} + R_w)} I_T$ to rewrite Equation (81) in terms of the total current.

Then R_{app} =

$$= \frac{(R_{app} + R_w)}{R_w I_T} \cdot \frac{R_m B_0}{\mu \sigma_m} \left[1 + \frac{1}{2 l_p} \sum_{\substack{n=1,3,5,\ldots \\ p=1,\ldots p}} \frac{8 a}{n^2 \pi^2} \frac{\left[\frac{\alpha_2}{\alpha_1} \left(e^{\alpha_1 (l-l_p)} - e^{-\alpha_1 (l+l_p)} \right) - \frac{\alpha_1}{\alpha_2} \left(e^{\alpha_2 (l+l_p)} - e^{-\alpha_2 (l-l_p)} \right) \right]}{\left(R_m^2 + n^2 \pi^2 \right)^{1/2}} \right]$$

$$+ R_d \qquad (82)$$

Rearranging Equation (82) we find

$$R_{app} = \frac{R'_{dm} + R_d}{1 - \frac{R'_{dm}}{R_w}} \quad \text{where} \quad R'_{dm} = \frac{1}{I_T} \cdot \frac{R_m B_0}{\mu \sigma_m} \left[1 + \frac{1}{2 l_p} \sum_{\substack{n=1,3,5,\ldots \\ p=1,\ldots p}} \frac{8 a}{n^2 \pi^2} \frac{\left[\frac{\alpha_2}{\alpha_1} \left(e^{\alpha_1 (l-l_p)} - e^{-\alpha_1 (l+l_p)} \right) - \frac{\alpha_1}{\alpha_2} \left(e^{\alpha_2 (l+l_p)} - e^{-\alpha_2 (l-l_p)} \right) \right]}{\left(R_m^2 + n^2 \pi^2 \right)^{1/2}} \right].$$

The <u>total resistance of the pump</u> is then given by the expression

$$R_p = \frac{R_w R_{app}}{(R_w + R_{app})}$$

and the total power input to the pump is then $I_T^2 2 R_p$.

The current which flows through the duct wall is given by

$$I_w = \frac{R_{app}}{(R_w + R_{app})} ,$$

and the power dissipated in the walls is given by the expression $2 I_w^2 R_w$. The applied current flowing through the duct (I_λ) is $I_T - I_w$.

The ohmic heating within the moving conductor is caused by a current density which is the sum of the applied current density and the induced current density. This power loss is given by:-

$$P = \int\int\int \frac{j^2}{\sigma} \, dx \, dy \, dz .$$

If we assume that these currents flow solely in the x-z plane and that their distribution does not vary in the y-direction then

$$P = \frac{2t}{\sigma_m} \int_{-\infty}^{+\infty} \int_{0}^{a} \left(j_x^2 + j_z^2 \right) dx \, dz . \qquad (83)$$

The z-component of the current density may be found from the equation curl $\underline{B} = \mu \underline{j}$ and is $j_z = \frac{1}{\mu}\frac{\partial B}{\partial x}$, and the x component of the current density j_x is the sum of the x-component of the induced current density and the applied current density j_{x_a}. Thus $j_x = j_{x_a} - \frac{1}{\mu}\frac{\partial B}{\partial z}$.

We rewrite Equation (76) in the form

$$j_{x_a} = -V_o \frac{\sigma_z}{d} \cdot \frac{R_\epsilon}{(R_\epsilon + R_d)} - \frac{\sigma_z}{d} \cdot \frac{R_f}{(R_\epsilon + R_d)} \cdot \frac{R_m B_o}{\mu \sigma_m} \left[1 + \frac{1}{P} \sum_{p=1 \ldots P} \sum_{n=1,3,5 \ldots} \frac{8a}{n^2\pi^2} \frac{\left(\alpha_2 e^{\alpha_1(z-L)} - \alpha_1 e^{\alpha_2(z+L)}\right)}{\left(R_m^2 + n^2\pi^2\right)^{\frac{1}{2}}} \right].$$

If we substitute $V_o = -I_x$ and $R_\epsilon = \frac{1}{\sigma_z}\frac{d}{2lt}$ into this equation we find that

$$j_{x_a} = \frac{I_x R_{app}}{2lt(R_\epsilon + R_d)} - \frac{1}{2lt(R_\epsilon + R_d)} \cdot \frac{R_m B_o}{\mu \sigma_m} \left[1 + \frac{1}{P} \sum_{p=1 \ldots P} \sum_{n=1,3,5 \ldots} \frac{8a}{n^2\pi^2} \frac{\left(\alpha_2 e^{\alpha_1(z-L_p)} - \alpha_1 e^{\alpha_2(z+L_p)}\right)}{\left(R_m^2 + n^2\pi^2\right)^{\frac{1}{2}}} \right] \quad (84)$$

We now assume that the resistance of the electrode R_ϵ is small so that the x-component of the current density is

$$j_x = j_{x_a} + j_{x_i} = \frac{I_x R_{app}}{2lt\, R_d} - \frac{1}{2lt\, R_d} \cdot \frac{R_m B_o}{\mu \sigma_m} \left[1 + \frac{1}{P} \sum_{p=1 \ldots P} \sum_{n=1,3,5 \ldots} \frac{8a}{n^2\pi^2} \frac{\left(\alpha_2 e^{\alpha_1(z-L_p)} - \alpha_1 e^{\alpha_2(z+L_p)}\right)}{\left(R_m^2 + n^2\pi^2\right)^{\frac{1}{2}}} \right] - \frac{1}{\mu}\frac{\partial B}{\partial z}.$$

The integral in Equation (83) was calculated using a digital computer. The computer calculated the induced magnetic field B_i at 1111 places in a solid moving conductor, and then evaluates the integral by calculating j_x and j_z in the many small elements within the moving metal.

Table 1 shows computed values of the apparent resistance of the duct $2R_{app}$, the apparent resistance of the pump $2R_p$, the total input power, the wall loss, the duct loss, and the hydraulic loss. Figure 45 shows how the computed efficiency compares with Watt's experimentally measured efficiency.

Mercury Throughput Gals/min	R_m	Apparent Resistance of Duct ($\times 10^{-4}\Omega$)	Apparent Resistance of Pump ($\times 10^{-4}\Omega$)	Total Input Power (Watts)	Wall Current (Amps)	Wall Loss (Watts)	Duct Loss (Watts)	Hydraulic Loss (Watts)	Total Loss (Watts)	Efficiency %
0	0	0.21	0.193	1.24	0.647	99	—	—	—	—
10	0.0332	0.27	0.242	1.53	0.815	157	—	—	—	—
20	0.0664	0.332	0.29	1.84	0.975	225	1332	7.3	1564	15
30	0.0996	0.397	0.34	2.15	1.14	308	1336	24	1668	24.2
40	0.132	0.467	0.39	2.47	1.31	405	1266	63	1734	29.8
50	0.166	0.539	0.44	2.78	1.48	518	1224	126	1868	32.8
60	0.199	0.613	0.486	3.08	1.63	630	1216	220	2066	33
70	0.232	0.695	0.538	3.41	1.8	770	1240	330	2340	31.4
80	0.265	0.778	0.586	3.71	1.97	920	1252	502	2674	28.2
90	0.298	0.868	0.637	4.03	2.14	1090	1288	725	3103	23
100	0.332	0.962	0.686	4.34	2.3	1250	1320	995	3565	17.9

TABLE. I.

Part III

Chapter 7.

Flow Couplers.

In this chapter we calculate the efficiency of several flow couplers which are similar in design to that suggested by Davidson and Thatcher.[2] Each flow coupler consists of two identical ducts placed side by side in the gap of a magnet so that the field, which is in the y-direction, passes through both ducts.

The liquid metal inside the ducts is considered to flow in the z-direction. The two streams of liquid are connected electrically by segmented electrodes which make contact with the tops and bottoms of the channels at $x = \pm a$ in the region $-l < z < +l$. In this region the applied magnetic field is considered to be uniform.

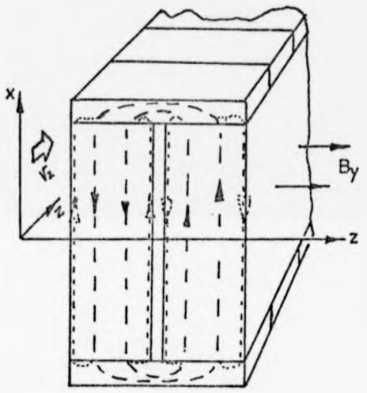

FIG. 47.

The motion of the liquid through the field produces a voltage between the top and bottom of the ducts. The fluid in one channel moves faster than the fluid in its neighbour so that this channel acts as a generator whilst its neighbour becomes a pump. In our calculations we have considered the left hand channel to be a generator through which the liquid moves at a known and constant velocity. This generator drives a current through the liquid in the neighbouring duct. This liquid then moves at a slower velocity.

The current which circulates between the two channels also modifies the eddy current distribution within the moving liquids so that the ohmic power dissipation increases in one duct and decreases in the other. Ohmic heating also occurs in the electrodes and in the side walls of the ducts. There is also a hydraulic loss in each duct. In this chapter we

calculate the power which is transferred from one channel to the other and the losses in the system. The useful hydraulic power output from the pump is equal to the electrical power transferred from the generator to the pump minus the losses in the electrodes and in the pump channel. The hydraulic power input to the system is equal to the electrical power transferred from the generator to the pump plus the losses in the generator channel. The percentage efficiency is $\frac{\text{hydraulic power output} \times 100}{\text{power input}}$

In our experiments we observed that when two conductors move with dissimilar speeds through a magnetic field the motion of one conductor does not seriously affect the magnetic field in its neighbour. We now therefore assume that the field in each channel is the same field which would occur if each stream moved individually through the magnet gap and that each field is solely in the y-direction.

We consider electrodes, of conductivity σ_e , which have an effective length in the y-direction of d and have a thickness of t_e in the x-direction. We then calculate the power transferred from one channel to the other by finding, for each duct the potential at $x = \pm a$, which is a function z.

In order to find U_{a_L} , the potential at $x = a$ in the left hand channel, we consider the x-component of the current density inside each duct to be the sum of the applied current density (j_{x_a}) and the induced current density (j_{xi}). In order that we may ignore the fringing of the applied current at the ends of the device we consider only those cases in which the electrodes are long in the z-direction when compared with the height of the duct in the x-direction (i.e., $\ell \gg a$).

Using the Ohm's law equation we find the current density in the electrode to be $+\sigma_e \left(\frac{U_{a_L} - U_{a_R}}{d} \right)$. This current will produce a contribution to the x component of the current density in the duct of $\sigma_e \left(\frac{U_{a_L} - U_{a_R}}{d} \right) \frac{t_e}{t_m}$, where t_m is the thickness of the duct. If the duct has vertical walls

of thickness w and of conductivity σ_w , the current density in the walls of the left hand channel (j_{xw}) will be $j_{xw} = -\sigma_w \frac{\partial U}{\partial x} = -\sigma_w \frac{U_{2L}}{a}$. This will produce a further contribution of magnitude $+\sigma_w \frac{U_{2L}}{a} \cdot \frac{w}{t_m}$ to the x component of the current density. The x component of the current density within the left hand channel will now be

$$j_{x1} = -\sigma_f \frac{(U_{2R} - U_{2L})}{d} \frac{t_f}{t_m} + \sigma_w \frac{U_{2L}}{a} \cdot \frac{w}{t_m} .$$

From Maxwell's equation curl $\underline{B} = \mu \underline{j}$ we find that j_{xi} , the x-component of the induced current density, is given by $j_{xi} = -\frac{1}{\mu} \frac{\partial B_L}{\partial z}$.

The total current density inside the left hand moving conductor is,

$$j_x = j_{x2} + j_{xi} = +\sigma_f \frac{(U_{2L} - U_{2R})}{d} \frac{t_f}{t_m} + \sigma_w \frac{U_{2L}}{a} \cdot \frac{w}{t_m} - \frac{1}{\mu} \frac{\partial B_L}{\partial z} , \qquad (85)$$

where B_L is the field in the left hand channel. The current density in the right hand conductor is

$$j_x = j_{x3} + j_{xi} = +\sigma_f \frac{(U_{2R} - U_{2L})}{d} \frac{t_f}{t_m} + \sigma_w \frac{U_{2R}}{a} \cdot \frac{w}{t_m} - \frac{1}{\mu} \frac{\partial B_R}{\partial z} , \qquad (86)$$

where B_R is the field in the right hand channel.

We have previously shown that the induced field caused by the motion of a solid conductor through an abruptly ending field of length L may be represented by the equation.

$$B_{iL} = \sum_{n=1,3,5\ldots}^{\infty} (B_{Ln} e^{\alpha_n z} + C_{Ln} e^{-\alpha_n z}) \cos \frac{n\pi x}{2a} \quad \text{when } -l < z < l,$$

where B_{Ln} and C_{Ln} are given in Equations (20) and (21). We now assume that the flow coupler has slug flow in each of the ducts and we consider the initial non abrupt or fringed magnetic field to be composed of p abrupt fields of magnitude $\frac{B_0}{p}$ superimposed upon each other. Then the total magnetic field in the electrode region of the left hand duct is:

$$B_L = B_o + \sum_{p=1\ldots\rho}\sum_{n=1,3,5\ldots} \left(B_{Lpn}\, e^{\alpha_1 z} + C_{Lpn}\, e^{\alpha_2 z}\right) \cos\frac{n\pi x}{2a}, \quad \text{where } \alpha_1 = \frac{1}{2a}\left(R_L + (R_L^2 + n^2\pi^2)^{1/2}\right)$$

and $\alpha_2 = \frac{1}{2a}\left(R_L - (R_L^2 + n^2\pi^2)^{1/2}\right)$

and the total magnetic field in the electrode region of the right hand duct is:

$$B_R = B_o + \sum_{p=1\ldots\rho}\sum_{n=1,3,5} \left(B_{Rpn}\, e^{\beta_1 z} + C_{Rpn}\, e^{\beta_2 z}\right) \cos\frac{n\pi x}{2a}, \quad \text{where } \beta_1 = \frac{1}{2a}\left(R_R + (R_R^2 + n^2\pi^2)^{1/2}\right)$$

and $\beta_2 = \frac{1}{2a}\left(R_R - (R_R^2 + n^2\pi^2)^{1/2}\right)$.

R_L is the magnetic Reynolds number for the left hand duct, R_R is the magnetic Reynolds number for the right hand duct.

Using the Ohm's law equation $\frac{\underline{j}}{\sigma} = \underline{E} + \underline{v} \times \underline{B}$ together with Equations (85) and (86) we find that

$$\sigma_E \frac{(U_{3L} - U_{3R})}{d}\frac{t_c}{t_m} + \sigma_w \frac{U_{3L}}{a}\frac{w}{t_m} - \frac{1}{\mu}\frac{\partial B_L}{\partial z} = -\sigma_m \frac{\partial U_L}{\partial x} - \sigma_m v_{1z} B_L, \qquad (87)$$

and $$\sigma_E \frac{(U_{3R} - U_{3L})}{d}\frac{t_c}{t_m} + \sigma_w \frac{U_{3R}}{a}\frac{w}{t_m} - \frac{1}{\mu}\frac{\partial B_R}{\partial z} = -\sigma_m \frac{\partial U_R}{\partial x} - \sigma_m v_{2z} B_R, \qquad (88)$$

where U_L is the potential at a general point within the left hand duct and v_{1z} is the velocity of the conductor in the left hand duct. U_R is the potential at a point in the right hand duct, v_{2z} is the velocity in the right hand duct.

Substituting for B_L and B_R and integrating w.r.t. x we find

$$U_L = \frac{\sigma_E}{\sigma_m}\frac{(U_{3R} - U_{3L})}{d}\frac{t_c}{t_m}\cdot x - \frac{\sigma_w}{\sigma_m}\cdot\frac{U_{3L}}{a}\cdot\frac{w}{t_m}\cdot x - \frac{R_L B_o}{\mu\sigma_m}\frac{x}{a} - \frac{1}{\mu\sigma_m}\sum_{p=1\ldots\rho}\sum_{n=1,3,5\ldots}\left(B_{Lpn}\alpha_1 e^{\alpha_1 z} + C_{Lpn}\alpha_2 e^{\alpha_2 z}\right)\frac{2a}{n\pi}\sin\frac{n\pi x}{2a} + \text{constant}, \qquad (89)$$

and $$U_R = \frac{\sigma_E}{\sigma_m}\frac{(U_{3L} - U_{3R})}{d}\frac{t_c}{t_m}\cdot x - \frac{\sigma_w}{\sigma_m}\frac{U_{3R}}{a}\frac{w}{t_m}\cdot x - \frac{R_R B_o}{\mu\sigma_m}\frac{x}{a} - \frac{1}{\mu\sigma_m}\sum_{p=1\ldots\rho}\sum_{n=1,3,5\ldots}\left(B_{Rpn}\beta_1 e^{\beta_1 z} + C_{Rpn}\beta_2 e^{\beta_2 z}\right)\frac{2a}{n\pi}\sin\frac{n\pi x}{2a} + \text{constant}. \qquad (90)$$

The constants in Equations (89) and (90) must be zero because we require the potential at x = 0 to be zero. The potential at x = a in the left hand duct is U_3, so that we may rewrite Equation (89) in the form:

$$U_{2L}\left(1+\frac{\sigma_2}{\sigma_m}\cdot\frac{t_\epsilon}{t_m}\cdot\frac{a}{d}+\frac{\sigma_d}{\sigma_m}\cdot\frac{w}{t_m}\right)=\frac{\sigma_2}{\sigma_m}\frac{t_\epsilon}{t_m}\frac{a}{a}U_{2R}-\frac{R_L B_0}{\mu\sigma_m}-\frac{1}{\mu\sigma_m}\sum_{p=1}^{p=f}\sum_{n=1,3,5}^{n=\infty}\left(B_{Lp}\alpha_2 e^{\alpha_1 z}+C_{Lp}\alpha_1 e^{\alpha_2(2a-z)}\right)\frac{2a}{n\pi}\sin\frac{n\pi}{2} \qquad (91)$$

The resistance (R_L) of a duct between x = 0 and x = a to a current flowing in the x-direction is given approximately by $R_L = \frac{a}{\sigma_2 2lt_m}$ and the resistance (R_w) of a duct wall between x = 0 and x = a is approximately $\frac{a}{\sigma_d 2lw}$. Then $\frac{R_L}{R_w}=\frac{\sigma_d}{\sigma_2}\cdot\frac{w}{t_m}$. The resistance of an electrode (R_ϵ) is $\frac{1}{\sigma_\epsilon}\frac{d}{2lt_\epsilon}$. We now find that $\frac{R_d}{R_\epsilon}=\frac{\sigma_2}{\sigma_m}\frac{t_\epsilon}{t_m}\cdot\frac{a}{d}$. Equation (91) now becomes,

$$U_{2L}\left(1+\frac{R_L}{R_\epsilon}+\frac{R_L}{R_w}\right)=\frac{R_d}{R_\epsilon}U_{2R}-\frac{R_L B_0}{\mu\sigma_m}-\frac{1}{\mu\sigma_m}\sum_{p=1}^{p=f}\sum_{n=1,3,5}^{n=\infty}\left(B_{Lp}\alpha_2 e^{\alpha_1 z}+C_{Lp}\alpha_1 e^{\alpha_2(2a-z)}\right)\frac{2a}{n\pi}\sin\frac{n\pi}{2}.$$

One usually chooses a wall material such that $\frac{R_L}{R_w}\ll 1$. Then from the above equation we have

$$U_{2L}=\frac{R_L}{(R_\epsilon+R_d)}\cdot U_{2R}-\frac{R_\epsilon}{(R_\epsilon+R_d)}\cdot\frac{R_L B_0}{\mu\sigma_m}-\frac{R_\epsilon}{(R_\epsilon+R_d)}\cdot\frac{1}{\mu\sigma_m}\sum_{p=1}^{p=f}\sum_{n=1,3,5}^{n=\infty}\left(B_{Lp}\alpha_2 e^{\alpha_1 z}+C_{Lp}\alpha_1 e^{\alpha_2(2a-z)}\right)\frac{2a}{n\pi}\sin\frac{n\pi}{2}. \qquad (92)$$

In a similar way we may find

$$U_{2R}=\frac{R_d}{(R_\epsilon+R_d)}\cdot U_{2L}-\frac{R_\epsilon}{(R_\epsilon+R_d)}\cdot\frac{R_\epsilon B_0}{\mu\sigma_m}-\frac{R_\epsilon}{(R_\epsilon+R_d)}\frac{1}{\mu\sigma_m}\sum_{p=1}^{p=f}\sum_{n=1,3,5}^{n=\infty}\left(B_{Rp}\beta_2 e^{\beta_1 z}+C_{Rp}\beta_1 e^{\beta_2(2a-z)}\right)\frac{2a}{n\pi}\sin\frac{n\pi}{2}. \qquad (93)$$

Solving equations (92) and (93) and substituting the appropriate values for B_{Lf}, B_{Rp}, C_{Lp} and C_{Rp} (Equations (20), (21) and (26)) we find

$$U_{2R}=-\frac{R_d}{(R_\epsilon+2R_d)}\cdot\frac{R_L}{\mu\sigma_m}\cdot\frac{B_0}{f}\sum_{p=1}^{p=f}\sum_{n=1,3,5}^{n=\infty}\frac{8}{n^2\pi^2}\frac{\left(\alpha_2 e^{\alpha_1(2-\epsilon_p)}-\alpha_1 e^{\alpha_2(2+\epsilon_p)}\right)}{(\alpha_1-\alpha_2)}$$

$$-\frac{R_\epsilon+R_w}{(R_\epsilon+2R_d)}\cdot\frac{R_\epsilon}{\mu\sigma_m}\cdot\frac{B_0}{f}\sum_{p=1}^{p=f}\sum_{n=1,3,5}^{n=\infty}\frac{8}{n^2\pi^2}\frac{\left(\beta_2 e^{\beta_1(2-\epsilon_p)}-\beta_1 e^{\beta_2(2+\epsilon_p)}\right)}{(\beta_1-\beta_2)}-\frac{B_0}{\mu\sigma_m}\frac{\left(R_\epsilon R_w+R_\epsilon(R_\epsilon+R_d)\right)}{(R_\epsilon+2R_d)}, \qquad (94)$$

and

$$U_{2L}=-\frac{R_d}{(R_\epsilon+2R_d)}\cdot\frac{R_\epsilon}{\mu\sigma_m}\cdot\frac{B_0}{f}\sum_{p=1}^{p=f}\sum_{n=1,3,5}^{n=\infty}\frac{8}{n^2\pi^2}\frac{\left(\beta_2 e^{\beta_1(2-\epsilon_p)}-\beta_1 e^{\beta_2(2+\epsilon_p)}\right)}{(\beta_1-\beta_2)}$$

$$-\frac{R_\epsilon+R_d}{(R_\epsilon+2R_d)}\cdot\frac{R_\epsilon}{\mu\sigma_m}\cdot\frac{B_0}{f}\sum_{p=1}^{p=f}\sum_{n=1,3,5}^{n=\infty}\frac{8}{n^2\pi^2}\frac{\left(\alpha_2 e^{\alpha_1(2-\epsilon_p)}-\alpha_1 e^{\alpha_2(2+\epsilon_p)}\right)}{(\alpha_1-\alpha_2)}-\frac{B_0}{\mu\sigma_m}\frac{\left(R_\epsilon R_L+R_\epsilon(R_\epsilon+R_d)\right)}{(R_\epsilon+2R_d)}. \qquad (95)$$

We then find that the potential difference (ΔV_d) between the "tops" of the

two ducts at a position z is

$$(U_{aL} - U_{aR}) = \frac{R_E}{(R_E + 2R_a)} \cdot \frac{1}{\mu_0 \omega_m} \cdot \frac{B_0}{P} \sum_{p=1}^{\infty} \frac{8}{n^2\pi^2} \left[\frac{R_E}{(\beta_1 - \beta_2)} \left(\beta_2 e^{\beta_1(z-l)} - \beta_1 e^{\beta_2(z+l)} \right) + \frac{R_L}{(\alpha_1 - \alpha_2)} \left(\alpha_1 e^{\alpha_2(z+l)} - \alpha_2 e^{\alpha_1(z-l)} \right) \right] + \frac{R_E}{(R_E + 2R_a)} \cdot \frac{B_0}{\mu_0 \omega_m} (R_R - R_L), \quad -(96)$$

In order to find the power extracted from the left hand channel of the flow coupler it is necessary to know to current density and the potential at the electrode. The current density in the electrode (j_E) is $-\sigma_E \frac{(U_{aR} - U_{aL})}{d}$ which is $\sigma_E \frac{\Delta V_a}{d}$. We calculate half of the power extracted from the generator channel by computing the integral in the equation

$$P_T = \int_{-l}^{+l} U_{aL} j_E \, t_E \, dz .$$

If we consider the currents in the walls of the duct as flowing solely in the x-direction then the power dissipated in an element of length dz of a wall of the left hand duct is $2(U_{aL})^2 \frac{\sigma_W w}{a} dz$ and the total dissipation in this wall (P_{LW}) is

$$2 \frac{\sigma_W w}{a} \int_{-\infty}^{+\infty} (U_{aL})^2 \, dz .$$

We expect most of the power dissipation in the wall to occur in the electrode region where the magnetic field is greatest. In our calculations we have therefore integrated from $z = -l$ to $z = +l$ and not from $z = -\infty$ to $z = +\infty$. This greatly simplifies the computer program necessary to evaluate this integral and is equivalent to computing the wall loss in a device in which the walls are conducting only in the electrode region. In a similar way we have taken the dissipation in the right hand duct (P_{RW}) to be $2 \frac{\sigma_W w}{a} \int_{-l}^{+l} (U_{aR})^2 \, dz$.

The power dissipated in an element of length dz of the upper electrode is $\Delta V_2 j_e t_e dz$, but since $j_e = \sigma_e \frac{\Delta V_2}{d}$ this is $(\Delta V_2)^2 \frac{\sigma_e}{d} t_e dz$. The power dissipated in the whole of the upper electrode (P_e) is

$$\int_{-\ell}^{+\ell} (\Delta V_2)^2 \frac{\sigma_e}{d} t_e \, dz \quad \text{which is} \quad \int_{-\ell}^{+\ell} \frac{(\Delta V_2)^2}{2\ell R_e} dz.$$

Inside one of the ducts the total ohmic power dissipation is

$$2\int_{-\infty}^{\infty}\int_{0}^{a}\int_{0}^{c} \frac{j^2}{\sigma} dx\,dy\,dz \qquad \text{which is} \qquad 2\int_{-\infty}^{\infty}\int_{0}^{c}\int_{0}^{a} (j_x^2 + j_z^2)\, dx\,dy\,dz.$$

The x-component of the current density has two parts. These are the induced current density, which is $-\frac{1}{\mu}\frac{\partial B_y}{\partial z}$, and the applied current density, which is $j_e \cdot \frac{t_e}{t_m}$.

We ignore the very small contribution to the applied current caused by the existence of the current in the duct walls. There are no applied currents flowing in the z-direction so that j_z is just $\frac{1}{\mu}\frac{\partial B_y}{\partial x}$. Then in the left hand duct ,

$$j_x = j_e \frac{t_e}{t_m} - \frac{1}{\mu}\frac{\partial B_x}{\partial z} = \frac{1}{\mu}\left(j_e \frac{t_e}{t_m}\mu - \frac{\partial B_x}{\partial z}\right) \qquad \text{between the electrodes}$$

and $j_x = -\frac{1}{\mu}\frac{\partial B_x}{\partial z}$ outside the electrodes; j_z is always $\frac{1}{\mu}\frac{\partial B_x}{\partial x}$. In the right hand duct $j_x = -j_e \frac{t_e}{t_m} - \frac{1}{\mu}\frac{\partial B_x}{\partial z} = -\frac{1}{\mu}\left(j_e \frac{t_e}{t_m}\mu + \frac{\partial B_x}{\partial z}\right)$ between the electrodes

and $j_x = -\frac{1}{\mu}\frac{\partial B_x}{\partial z}$ outside the electrodes; j_z is always $\frac{1}{\mu}\frac{\partial B_x}{\partial x}$.

To find the power dissipation in the top half of a duct we first compute the current density in the electrodes and the magnetic field in the moving conductor at a large number of different x- and z- positions. We use these values to find j_x and j_z in the moving metal and we then evaluate the integral $\int_{-\ell}^{+\ell}\int_{0}^{a} (j_x^2 + j_z^2) t_m \, dx\,dz.$

We do not know the hydraulic loss which occurs when a conducting liquid flows through a field when the magnetic Reynolds number is high. We therefore assume that the hydraulic loss in a flow coupler duct is the same as that which would occur in any normal rectangular duct. We then consider a rectangular channel as being equivalent to a circular pipe whose diameter D is $\frac{4 \times \text{cross sectional area.}}{\text{wetted perimeter}}$ For one channel of a flow coupler of dimensions 0.4m x 0.2m, this equivalent diameter is 0.2667m. The Reynold's number is $\frac{\rho D v_z}{\eta}$ where η is the viscosity and v_z is $\frac{R_m}{\mu\sigma a}$.

Taking σ the conductivity of sodium as 5×10^6 mho/m and μ the permeability at $4\pi \times 10^{-7}$ we find that a magnetic Reynolds number of 25 corresponds to an ordinary Reynolds number of about 10^{-7}. From tables[13] we find that in smooth pipes a skin friction coefficient C_f for a Reynolds number of 10^7 is approximately 2×10^{-3} and the pressure drop along a pipe is given by $\Delta_p = 2 C_f \frac{L}{D} \rho u_m^2$ where U_m is the mean velocity, and L is the total length of the device. In the flow coupler $U_m = v_z = \frac{R_m}{\mu\sigma a}$ so that $\Delta_p = 2 C_f \frac{L}{D} \rho \frac{R_m^2}{\mu^2\sigma^2 a^2}$. The power needed to overcome this pressure drop (the hydraulic loss) is $4 C_f \frac{L}{D} \rho \frac{R_m^3}{\mu^3\sigma^3 a}$.

We consider flow couplers, with ducts whose dimensions are 0.4m in a direction perpendicular to the magnetic field and 0.2m in the field direction, in which the electrodes extend for distances of 2, 3, and 4 metres in the z-direction. The applied magnetic field, B_o, is always considered to be uniform at 0.3 Wb/m^2 or 0.6 Wb/m^2 in the electrode region, falling to zero in a distance of 0.5m at each end of the device. We use the computer program, which is presented in appendix B to calculate the results which are given in Tables, 2, 3, 4, 5 and 6. These tables show the ohmic power dissipation in sodium, the approximate wall loss and the hydraulic loss in each duct together with the power transferred from one channel to the other, and the

$B = 0.3 Wb/m^2$

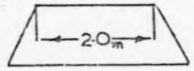

R_m Left	R_m Right	Power Transfer (MW)	Power Dissipation L.H.Duct (MW)	Hydraulic Loss in L.H.Duct (MW)	Wall Loss L.H. Duct (MW)	Total Input Power (MW)		Power Dissipation in electrode (MW)	Power Dissipation in R.H.Duct (MW)	Hydraulic Loss in R.H.Duct (MW)	Wall Loss in R.H.Duct (MW)	Total Power Loss(MW)		Useful Power Output(MW)		Efficiency %	
						t=0	t=0·005m					t = 0	t=0·005m	t = 0	t=0·005m	t = 0	t=0·00
27	26	0.084	0.074	0.035	0.092	0.193	0.285	0.0001	0.077	0.030	0.092	0.217	0.401	-	-	-	-
27	25	0.168	0.077	0.035	0.090	0.280	0.371	0.0006	0.091	0.026	0.090	0.230	0.411	0.05	-	17.85	-
27	24	0.253	0.082	0.035	0.089	0.370	0.458	0.0016	0.116	0.023	0.088	0.257	0.434	0.112	0.025	30.4	5.36
27	23	0.338	0.088	0.035	0.087	0.461	0.548	0.0029	0.154	0.020	0.086	0.300	0.477	0.161	0.076	34.9	13.78
27	22	0.425	0.097	0.035	0.085	0.556	0.642	0.0048	0.205	0.018	0.084	0.360	0.529	0.197	0.113	35.3	17.65
27	21	0.512	0.108	0.035	0.083	0.642	0.725	0.071	0.272	0.016	0.081	0.438	0.603	0.204	0.123	31.8	16.9
27	20	0.599	0.121	0.035	0.082	0.755	0.837	0.0099	0.356	0.013	0.079	0.535	0.696	0.220	0.141	29.1	16.85

TABLE 2.

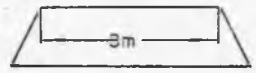

R_m Left	R_m Right	Power Tr	ciency % t=0 OC
27	26	0	-
27	25	0	9.05
27	24	0	13.1
27	23	0.	20.2
27	22	0.	23.1
27	21	1.	21.1
27	20	1.524	17.0

TEXT OFF THE EDGE OF THE PAGE IN THE ORIGINAL

TABLE 3.

B=0·3Wb/m²

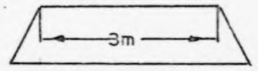

R_m eft	R_m Right	Power Transfer (MW)	Power Dissipation L.H.Duct (MW)	Hydraulic Loss in L.H.Duct (MW)	Wall Loss L.H. Duct (MW)	Total Input Power (MW) t=0	Total Input Power (MW) t=0·005m	Power Dissipation in electrode (MW)	Power Dissipation in R.H.Duct (MW)	Hydraulic Loss in R.H.Duct (MW)	Wall Loss in R.H.Duct (MW)	Total Power Loss(MW) t = 0	Total Power Loss(MW) t=0·005m	Useful Power Output(MW) t = 0	Useful Power Output(MW) t=0·005m	Efficiency % t = 0	Efficiency % t=0·00
27	26	0.185	0.089	0.046	0.188	0.32	0.508	0.0004	0.094	0.039	0.187	0.268	0.643	0.052	-	16.1	-
27	25	0.371	0.92	0.046	0.184	0.510	0.694	0.0017	0.131	0.035	0.182	0.306	0.672	0.204	0.022	39.8	2.93
27	24	0.559	0.103	0.046	0.180	0.708	0.889	0.004	0.199	0.030	0.177	0.393	0.772	0.316	0.117	43.9	13.1
27	23	0.748	0.118	0.046	0.176	0.913	1.089	0.007	0.299	0.027	0.173	0.499	0.847	0.414	0.242	45.4	22.2
27	22	0.939	0.139	0.046	0.172	1.124	1.296	0.012	0.436	0.024	0.168	0.657	0.996	0.467	0.299	41.6	23.1
27	21	1.131	0.165	0.046	0.168	1.342	1.509	0.017	0.611	0.021	0.163	0.861	1.191	0.481	0.318	35.8	21.1
27	20	1.324	0.197	0.046	0.164	1.567	1.731	0.024	0.830	0.018	0.158	1.115	1.44	0.452	0.294	28.8	17.0

TABLE 3.

$B=0.6 Wb/m^2$

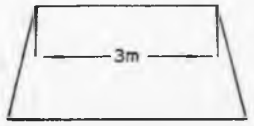

R_m zft	R_m Right	Power Transfer (MW)	Power Dissipation L.H.Duct (MW)	Hydraulic Loss in L.H.Duct (MW)	Wall Loss L.H.Duct (MW)	Total Input Power (MW)		Power Dissipation in electrode (MW)	Power Dissipation in R.H.Duct (MW)	Hydraulic Loss in R.H.Duct (MW)	Wall Loss in R.H.Duct (MW)	Total Power Loss(MW)		Useful Power Output(kW)		Efficiency %	
						t=0	t=0.005m					t = 0	t=0.005m	t = 0	t=0.005m	t = 0	t=0.005
27	26	0.740	0.342	0.046	0.750	1.129	1.879	0.002	0.370	0.039	0.747	0.900	2.397	0.328	–	29.2	–
27	25	1.486	0.368	0.046	0.735	1.900	2.635	0.007	0.522	0.035	0.728	0.978	2.441	2.922	0.194	48.4	7.36
27	24	2.237	0.411	0.046	0.719	2.605	3.414	0.016	0.793	0.030	0.709	1.297	2.809	1.398	0.605	51.8	17.7
27	23	2.992	0.473	0.046	0.704	3.512	4.215	0.029	1.195	0.027	0.690	1.770	3.164	1.741	1.051	49.6	25.1
27	22	3.755	0.555	0.046	0.688	4.356	5.043	0.046	1.741	0.024	0.671	2.412	3.771	1.944	1.273	44.6	25.2
27	21	4.523	0.659	0.046	0.671	5.227	5.898	0.069	2.443	0.021	0.651	3.238	4.560	1.989	1.338	38.0	22.7
27	20	5.294	0.788	0.046	0.655	6.128	6.916	0.097	3.316	0.018	0.631	4.265	5.550	1.863	1.365	30.4	19.7

TABLE 4.

B = 0·3Wb/m²

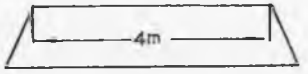

R_m Left	R_m Right	Power Transfer (MW)	Power Dissipation L.H.Duct (MW)	Hydraulic Loss in L.H.Duct (MW)	Wall Loss L.H.Duct (MW)	Total Input Power (MW)		Power Dissipation in electrode (MW)	Power Dissipation in R.H.Duct (MW)	Hydraulic Loss in R.H.Duct (MW)	Wall Loss in R.H.Duct (MW)	Total Power Loss(MW)		Useful Power Output(kW)		Efficiency %	
						t=0	t=0·005m					t = 0	t=0·005m	t = 0	t=0·005m	t = 0	t=0·005
27	26	0.331	0.005	0.058	0.208	0.484	0.702	0.0002	0.104	0.040	0.302	0.302	0.552	0.117	–	24.1	–
27	25	0.663	0.107	0.058	0.301	0.828	1.130	0.003	0.152	0.044	0.208	0.369	0.060	0.459	0.161	55.0	14.2
27	24	0.997	0.138	0.058	0.205	1.183	1.478	0.008	0.250	0.038	0.200	1.401	1.066	0.701	0.411	50.4	27.8
27	23	1.332	0.157	0.158	0.207	1.540	1.835	0.014	0.389	0.034	0.282	1.552	1.221	0.806	0.614	52.0	33.5
27	22	1.669	0.107	0.058	0.280	1.924	2.204	0.023	0.574	0.030	0.273	0.881	1.435	1.043	0.770	54.2	34.9
27	21	2.006	0.247	0.058	0.273	2.311	2.585	0.034	0.811	0.026	0.264	1.196	1.713	1.136	0.871	49.1	33.7
27	20	2.344	0.309	0.058	0.266	2.711	2.977	0.047	1.104	0.022	0.255	1.540	2.061	1.171	0.916	43.2	30.8

TABLE 5.

$B = 0{\cdot}6 Wb/m^2$

P_m Left	P_m Right	Power Transfer (MW)	Power Dissipation L.H.Duct (MW)	Hydraulic Loss in L.H.Duct (MW)	Wall Loss L.H. Duct (MW)	Total Input Power (MW)		Power Dissipation in electrode (MW)	Power Dissipation in R.H.Duct (MW)	Hydraulic Loss in R.H.Duct (MW)	Wall Loss in R.H.Duct (MW)	Total Power Loss (MW)		Useful Power Output (MW)		Efficiency %	
						t=0	t=0·005m					t=0	t=0·005m	t=0	t=0·005m	t=0	t=0·0
27	26	1.323	0.380	0.058	1.233	1.761	2.093	0.003	0.415	0.040	1.207	0.905	3.385	0.856	–	48.6	–
27	25	2.652	0.420	0.058	1.206	3.140	4.345	0.013	0.625	0.044	1.104	1.169	3.569	1.970	2.766	62.7	43.8
27	24	3.989	0.512	0.058	1.178	4.558	5.736	0.031	0.999	0.038	1.160	1.638	3.976	2.920	1.760	64.0	30.7
27	23	5.328	0.630	0.058	1.150	6.016	7.167	0.056	1.551	0.034	1.126	2.320	4.686	3.687	2.561	59.8	35.8
27	22	6.675	0.788	0.058	1.122	7.521	8.643	0.091	2.294	0.030	1.093	3.260	5.474	4.261	3.169	56.6	36.7
27	21	8.025	0.988	0.058	1.093	9.071	10.164	0.134	3.241	0.026	1.057	4.449	6.600	4.622	3.564	47.6	35.1
27	20	9.377	1.236	0.058	1.063	10.671	11.734	0.189	4.415	0.022	1.021	5.731	7.816	4.940	3.918	46.3	33.4

TABLE 6.

Figure 48

Showing the efficiency of flow couplers, having ducts whose dimensions are 0·4m. in a direction perpendicular to the field and 0·2m. in a direction parallel to the field, plotted against the magnetic Reynolds number of the right hand duct. In each case the magnetic Reynolds number in the left hand duct is 27. The continuous line is for ducts with insulating walls the dotted line is for ducts with stainless steel walls 0·005m. thick.

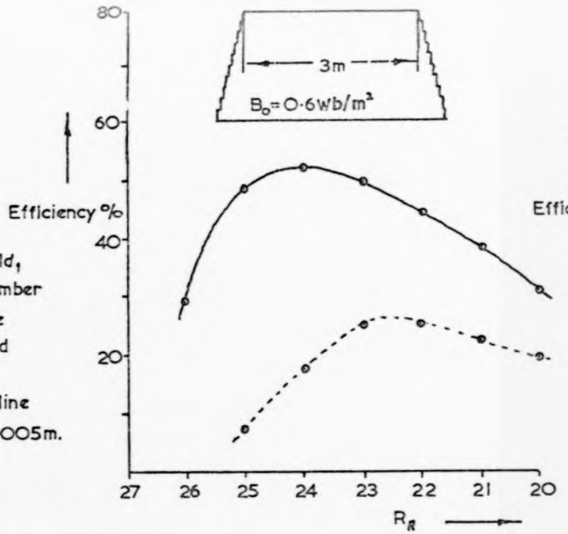

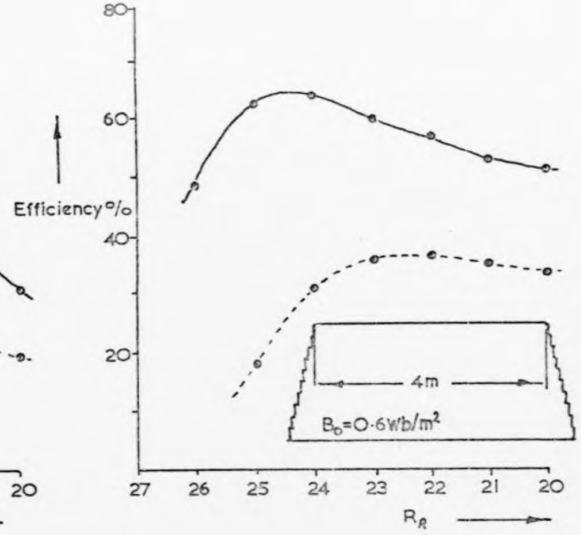

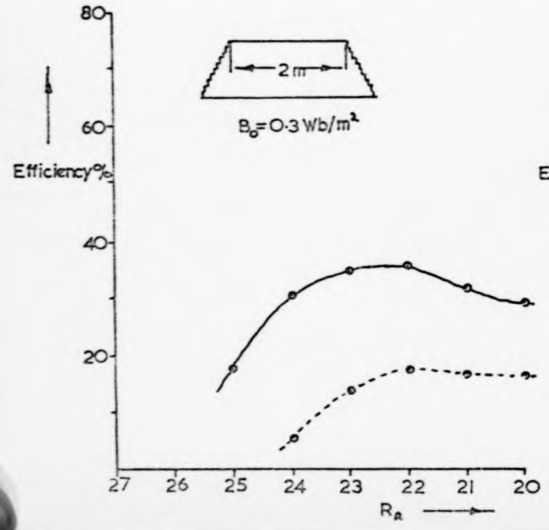

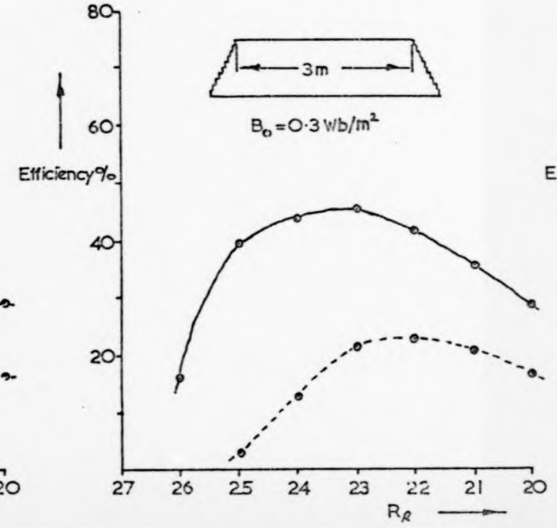

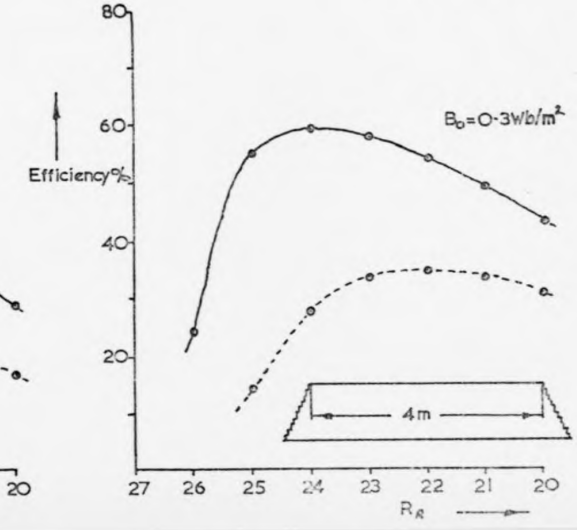

Figure 49

Showing how the power output of a flow coupler depends upon the magnetic Reynolds number of the right hand duct. The magnetic Reynolds number in the left hand duct is 27.

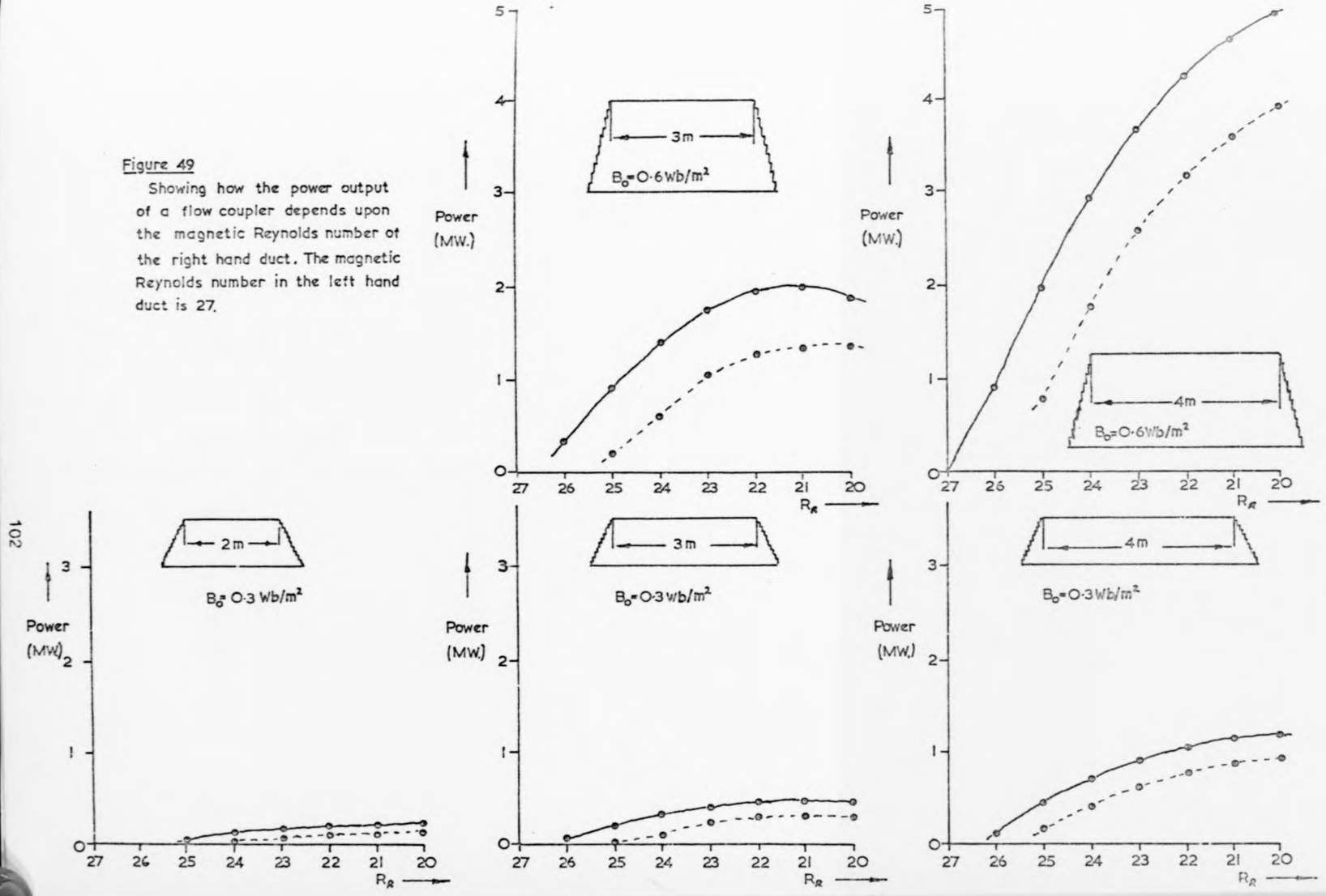

electrode dissipation, when the velocity in the left hand channel is kept constant such that $R_L = 27$ whilst the velocity in the right hand channel is varied from $R_R = 26$ to $R_R = 20$. They also show the percentage efficiency and the useful power available in the pump channel. We have performed these calculations for flow couplers which we considered to have perfectly insulating walls and for flow couplers with stainless steel walls 5mm thick. These results are presented graphically in figs. 48 and 49.

When the velocity of the fluid in the two channels is the same no power can be transferred from one channel to the other. If the liquid in the pump channel is slowed power is transferred from the generator to the pump. As the difference in the fluid velocity of the two channels is increased the efficiency of the system at first increase and then, as the ohmic dissipation in the ducts becomes greater, it decreases again. Changing the field from $0.3 wb/m^2$ to $0.6 wb/m^2$ slightly increases the maximum efficiency; from 46% to 52% for the 3 metre case. Figures 48 and 49 show the calculated performance of flow couplers in which the liquids move as solid bodies through the field region. The continuous curves refer to the performance of flow couplers which have insulating walls perpendicular to the field direction whilst the dotted curves are for flow couplers with 5mm thick stainless steel walls in a direction perpendicular to the field. It can be seen that the addition of conducting duct walls greatly reduces the efficiency. A real liquid flowing through a duct would have a low velocity boundary layer adjacent to the wall, whose presence would further reduce the efficiency of a flow coupler. It is evident that the performance would depend upon the distribution of the velocity within the duct. Unfortunately little is known about the nature of the velocity profiles which occur when real liquids flow through magnetic fields when the magnetic Reynolds number is large.

Chapter 8

Conclusions and Suggested Further Work.

In this thesis we have considered flow couplers of a similar type to that suggested by Davidson and Thatcher[2] in which the two ducts have equal cross sectional areas and lie in the gap of a magnet. We have not considered other possible arrangements of the ducts within a magnetic field.

We have shown that a two dimensional solution of the equation $\nabla^2 B_t = \frac{R_m}{a} \frac{\partial B_t}{\partial z}$ where B_t is the transverse magnetic field, R_m is the magnetic Reynolds number and a is a scale length, produces results which agree quite well with the fields we observed in a moving conductor in which the only currents were the induced eddy currents. We have observed experimentally that, in compensated devices with segmented electrodes, the magnetic field is unaffected by the magnitude of the current through the external circuit and is the same field that would exist if there was no contact between the moving metal and the external circuit. We also observed that, when two conductors passed side by side through the same magnet gap each having a different velocity, the field in one conductor was little affected by the motion of the other. To calculate the efficiency of a flow coupler we have assumed, on the basis of this experimental evidence, that the field in each channel is the same field which would occur if each stream moved individually as a solid body through the magnet gap. Although we have performed, in Chapter 4, a first order analysis of the velocity perturbation which occurs as a liquid flows through a transverse magnetic field, the duct flow of a liquid when the magnetic Reynolds number is high is imperfectly understood. This subject together with the study of turbulence at high magnetic Reynolds number might provide interesting, if difficult, fields for further study. We have indicated that the presence of low velocity boundary layers adjacent to the walls of the duct could adversely affect the performance of a flowcoupler.

The flow coupler suggested by Davidson and Thatcher was designed to have a throughput of 20,000 gals/min of liquid sodium in each duct, and to produce a pressure difference across the device of 120 lb/in^2. This would require a useful power output from the pump channel of 1.25 MW. Using a trapezoidal field profile and a peak field of $0.3 Wb/m^2$ we find that even a device whose electrodes extended for a distance of 4m in the flow direction would not give a sufficiently large power output. Doubling the applied magnetic field to $0.6 W/m^2$ greatly increases the power output and also increases the efficiency. Thus we expect a device with electrodes 4m long and a magnetic field of $0.6 W/m^2$, which drops to zero in a distance of 0.5 m at the ends of the device, to have an output of 3.6 MW and an efficiency of about 60% if it has insulating walls. With stainless steel walls 5 mm thick we expect a power output of 2.6 MW and an efficiency of about 35%.

It has been suggested that the mechanical pumps which are at present situated inside the reactor vessels of fast breeder reactors could be replaced by flow couplers. Flow couplers would have the advantages of needing no maintenance, they would not require to have rotating shafts penetrating the reactor vessel and in addition they would be nearly silent. It now appears that in order to do this it is necessary to have duct walls which are either constructed from some electrically insulating material or are made from very thin stainless steel. In addition one needs a higher magnetic field then the suggested value of $0.3 W/m^2$. Although the theory presented in this thesis has overestimated rather than underestimated the eddy current losses in a generator and in a pump, we conclude that flow couplers will only become competitive with mechanical pumps if suitable wall materials can be found, if the magnetic field can be significantly increased and if it can be shown that the performance is not badly affected by the slowly moving sodium in the boundary layers adjacent to the duct walls.

References

1) Pulley, O.O. British Patent No. 745,460 Improvements in or relating to Electromagnetic Liquid Metal Pumping Systems and,
Blake, L.R. British Patent No. 905,940 Improvements in or relating to Electromagnetic Liquid Metal Pumping Systems.

2) Davidson, D.F. Private correspondence.

3) Shercliff, J.A. "The Theory of Electromagnetic Flow-measurement" (C.U.P. 1962) Pages 79-80 and 37-38.

4) Wells, W.M. Experiments and Calculations on the Feasibility of Pumping Liquid Lithium in a Thermo-nuclear Blanket. Lawrence Radiation Laboratory Report No. UCRL 50544.

5) Yu.M. Mikhailov. Liquid - Metal Magnetohydrodynamic Generators at Large Magnetic Reynolds Numbers. Magnitnaya Gidrodinamika Vol. 1 No. 4 pp 113-119, 1965.

6) Watt,D.A. O'Connor R.J. and Holland E. Tests on an Experimental D.C. Pump for Liquid Metals. A.E.R.E. Report R/R 2274, 1957
and
Watt,D.A. Analysis of an Experimental D.C. Pump Theory of Design, A.E.R.E. Report R/R 2275, 1957.

7) Boucher,R.A. and Ames D.B. End Effect Losses in D.C. M.H.D. generators. Journal of Applied Physics, May 1969, Vol. 32. No. 5.

8) Shercliff,J.A. "The Theory of Electromagnetic Flow-measurement" (C.U.P.) pp 81.

9) Shercliff,J.A. "The Theory of Electromagnetic Flow-measurement" (C.U.P.) pp 37-38.

10) Meshii,T. and Ford J.A. Calibration of Electromagnetic Flowmeters in the Enrico Fermi Atomic Power Plant. Nuclear Applications and Technology Vol. 7 July 1969.

11) Shercliff,J.A. "The Theory of Electromagnetic Flow-measurement" (C.U.P. 1962) pp 71-74.

12) Nikuradse,J. Forschungs - Arb. Ing. - Wesen, Heft 356 (1932).

13) Kay,J.M. "An Introduction to Fluid Dynamics and Heat Transfer"

Appendix A.

A program for calculating the induced magnetic field and the power losses which occur when a moving conductor passes through a region of space in which there is a fringed transverse magnetic field.

We have shown in Equations (10), (11) and (12) of Chapter 3 that the induced field which occurs when a conductor moves through a transverse applied magnetic field which drops abruptly to zero at $z = \pm \ell$ may be found from the equations:-

$$B_i = \sum A_n e^{\alpha_1 z} \cos \frac{n\pi x}{2a} \qquad \text{when } z < -\ell, \quad \text{region I},$$

$$B_i = \sum (B_n e^{\alpha_1 z} + C_n e^{\alpha_2 z}) \cos \frac{n\pi x}{2a} \qquad \text{when } -\ell < z < +\ell, \quad \text{region II},$$

$$\text{and} \quad B_i = \sum D_n e^{\alpha_2 z} \cos \frac{n\pi x}{2a} \qquad \text{when } z > +\ell, \quad \text{region III}.$$

An, Bn, Cn and Dn are constants which are given in Equations (19), (20), (21) and (22), $\alpha_1 = \frac{1}{2a}\left(R_m + \left(R_m^2 + n^2\pi^2\right)^{1/2}\right)$

and $\alpha_2 = \frac{1}{2a}\left(R_m - \left(R_m^2 + n^2\pi^2\right)^{1/2}\right)$.

We consider a fringed magnetic field, that is one which does not drop abruptly to zero at $z = \pm \ell$, to be composed of a number, in this case 25, of abrupt fields superimposed upon each other. We define the amplitude of each element together with half of the distance over which it extends in the z-direction. The program calculates the induced magnetic field caused by each element of field at 209 values of the z-co-ordinate. Each z-position is separated from its neighbours by a distance DZ. We consider an initial field profile which is not symmetrical about Z = 0 as being composed of many elements of field where the centre of each element has been shifted by a distance ND.DZ from some arbitarily chosen centre of the field profile.

In this program we establish four arrays A, B, C and D so that An, Bn,

Cn and Dn can be calculated and stored for 100 values of n. A further array BI is established so that the induced field at 210 different z-positions and eleven x-positions may be recorded.

We read from cards the half height of the metal, a in our theory but E in this program, and the magnetic Reynolds number R. Then for each of the 25 elements of field we read the half length of the field TL, the magnitude of the element BO and an integer ND. The outer DO LOOP (DO 12 NA = 1, 25) selects segments of the initial field one at a time. An, Bn, Cn and Dn are calculated and stored (cards 20-46). z is set at a value determined by I, x is then set at a value determined by N. z is then tested to see whether this value of z is in region I, II or III and the appropriate part of the program is the selected. The appropriate series is then evaluated to calculate the induced magnetic field. The university computer is unable to handle numbers greater than e^{176}. In this program every exponent is tested and if it is found to be greater than e^{176} it is replaced by the largest number available to our computor, likewise if $e^{x} < e^{-176}$ the exponent is replaced by zero.

Between cards 127 and 134 the array BS is added to the array BI to calculate the induced field caused by all 25 segments.

The total induced magnetic field is printed so that each z co-ordinate is followed by eleven numbers, the first of which is the induced field at x = o and the last of which is the induced field at the edge of the metal.

The power dissipation within the metal may be found by evaluating the integral $\frac{P}{2} = \int_{-\infty}^{+\infty}\int_{0}^{t}\int_{0}^{a} \frac{j^2}{\sigma}\, dx\,dy\,dz$. If we assume that the magnetic field is solely in the y-direction then we find from curl $\underline{B} = \mu \underline{j}$ that $j_x = -\frac{1}{\mu}\frac{\partial B_i}{\partial z}$ and $j_z = \frac{1}{\mu}\frac{\partial B_i}{\partial x}$ so that $j^2 = \frac{1}{\mu^2}\left[\left(\frac{\partial B_i}{\partial z}\right)^2 + \left(\frac{\partial B_i}{\partial x}\right)^2\right]$.

The power dissipation is found by considering a small element of the bar of volume (DX. DZ. t), where DX is the distance between neighbouring

x co-ordinates, DZ is the distance between neighbouring z co-ordinates and t is the thickness of the bar in the y-direction. The mean values of $\frac{\partial B_i}{\partial x}$ and $\frac{\partial B_i}{\partial z}$ within this element are found from the induced field B_i and hence the power dissipated in this small volume is calculated.

The total power dissipated in one half of the metal is found by summing the power dissipated in the small elements of the bar (cards 142-162).

At high magnetic Reynolds numbers induced magnetic fields are produced well outside the applied field region and it is then necessary to modify this program so that it calculates the induced magnetic field at a greater number of z-co-ordinates. We include this program because with it we produced the theoretical results presented in Chapter 3. More efficient programs for computing the induced magnetic field formed the basis for the program presented in Appendix B.

```
&FORTRAN                                                        TIME =  0000  01

&LIST                                                           TIME =  0000  07
   1*       DIMENSION A(25,20),B(25,20),C(25,20),D(25,20),BI(210,11),BS(21
   2*      10,11),PA(210),BO(25),TL(25),ND(25)
   3*       READ(2,55)E,
   4*       READ(7,54)(T(I),I=1,25)
   5*       READ(7,54)(BO(I),I=1,25)
   6*       READ(7,54)(TL(I),I=1,25)
   7* C     TL=HALF LENGTH OF UNIFORM FIELD
   8* C     E=HALF WIDTH OF METAL
   9* C     R=RADIUS OF
  10* C     BO=UNIFORM FIELD
  11*       PIE=3.14159
  12*       DO 17 I=1,210
  13*       DO 16 N=1,11
  14*       BI(I,N)=0
  15*    16 CONTINUE
  16*    17 CONTINUE
  17*       DO 12 MA=1,25
  18*       WRITE(6,62)
  19* C     MA DETERMINES WHICH OF 25 LUMPS OF FIELD IS CONSIDERED.
  20*       DO 7 I=1,19,2
  21* C     GENERATE AN,BN,CN,DN ETC.
  22*       A1=(1/(2*E))*(R+SQRT((R*R)+(I*I*PIE*PIE)))
  23*       A2=(1/(2*E))*(R-SQRT((R*R)+(I*I*PIE*PIE)))
  24*       F=(1/R)*SQRT((R*R)+(I*I*PIE*PIE))
  25*       G=(-4/(I*PIE))*((-1)**((I+1)/2))
  26*       P=R/E
  27*       T1=TL(MA)*A1
  28*       T2=TL(MA)*A2
  29*       IF(T1-176)35,35,36
  30*    35 EX1=EXP(-T1)
  31*       EX2=EXP(T1)
  32*       GO TO 39
  33*    36 EX1=0
  34*       EX2=EXP(176)
  35*    39 IF(T2-176)38,37,37
  36*    37 EX3=EXP(T2)
  37*       EX4=EXP(-T2)
  38*       GO TO 64
  39*    38 EX3=0
  40*       EX4=EXP(176)
  41*    64 CONTINUE
  42*       A(MA,I)=(BO(MA)*G*P/F)*(EX1-EX2)
  43*       B(MA,I)=(BO(MA)*G*P/F)*EX1
  44*       C(MA,I)=-(BO(MA)*G*P/F)*EX3


  45*       D(MA,I)=(BO(MA)*G*P/F)*(EX4-EX3)
  46*    7 CONTINUE
  47* C     SET Z
  48*       DO 1 I=1,210
  49*       DZ=0.005
  50*       M=I-61
  51*       Z=M*DZ
  52* C     SET X
  53*       DO 2 N=1,11
  54*       Q=N-1
  55*       X=Q/50.
  56*       BS(I,N)=0
  57* C     TEST TO SEE IF THIS Z IS IN REGION 1,2, OR 3
  58*       IF(TL(MA)+Z)3,3,4
  59* C     REGION 1
  60*    3  DO 8 K=1,19,2
  61*       A1=(1/(2*E))*(R+SQRT((R*R)+(K*K*PIE*PIE)))
  62*       T1=A1*Z
  63*       M=(T1-176)*(T1+176)
  64*       IF(M)40,40,41
  65*    40 EX1=EXP(T1)
  66*       GO TO 48
  67*    41 IF(Z)76,75,66
  68*    76 EX1=0
  69*       GO TO 48
  70*    75 EX1=1
  71*       GO TO 48
  72*    66 EX1=EXP(-176)
  73*    48 H=(A(MA,K)*EX1)*COS(K*PIE*X/(2*E))
  74*       BS(I,N)=BS(I,N)+H
  75*     8 CONTINUE
  76*       GO TO 11
  77* C     TEST TO SEE IF THIS Z IS IN REGION 1,2, OR 3
  78*    4  IF(Z-TL(MA))5,5,6
  79* C     REGION 2
  80*    5  DO 9 J=1,19,2
  81*       A1=(1/(2*E))*(R+SQRT((R*R)+(J*J*PIE*PIE)))
  82*       A2=(1/(2*E))*(R-SQRT((R*R)+(J*J*PIE*PIE)))
  83*       T1=A1*Z
  84*       T2=A2*Z
  85*       M=(T1-176)*(T1+176)
  86*       IF(M)42,42,43
  87*    42 EX1=EXP(T1)
  88*       GO TO 49
  89*    43 IF(Z)67,68,69
  90*    67 EX1=0
  91*       GO TO 49
  92*    68 EX1=1
  93*       GO TO 49
  94*    69 EX1=EXP(176)
  95*    49 M=(T2+176)*(T2-176)
  96*       IF(M)44,44,45
  97*    44 EX2=EXP(T2)
  98*       GO TO 57
  99*    45 IF(Z)72,71,72
```

A2

```
      2 IF(Z)5,5,6
      5 WRITE(2,19,Z
        A1=(1/(2*E))*(R+SQRT((R**2)+(L**2)+(2*R*L*COS(J*PIE*PIE))
        A2=(1/(2*E))*(R-SQRT((R**2)+(L**2)+(2*R*L*COS(J*PIE*PIE))
        T1=A1**2
        T2=A2**2
        M=(T1-176)*(T1-176)
        IF(M-2)42,42,43
     42 EX1=1
        GO TO 45
     43 IF(Z)44,44,68,69
     44 EX1=0
        GO TO 49
     45 EX1=EXP(-176)
     49 M=(T2-176)*(T2-176)
        IF(M-44)44,44,45
     44 EX2=EXP(-T2)
        GO TO 47
     45 EX2=EXP(-71,72
     70 EX2=EXP(-176)
        GO TO 47
     71 EX2=1
        GO TO 47
     72 EX2=0
C
     47 H=((P(I,J)*EX1)+(Q(I,J)*EX2))*COS(J*PIE*X/(2*E))
        ES(I,N)=ES(I,N)+H
      9 CONTINUE
        GO TO 11
        RETURN
      6 DO 10 I=1,19,2
        A2=(1/(2*E))*(R-SQRT((R*R)+(L*L*PIE*PIE)))
        T2=A2*2
        M=(T2-176)*(T2-176)
        IF(M-6,47
46      EX2=EXP(-T2)
        GO TO 55
47      IF(Z)57,74,75
73      EX2=EXP(-176)
        GO TO 58
74      EX2=1
        GO TO 58
75      EX2=0
58      H=((P(I,J)*EX1)+(Q(I,J)*EX2))*COS(J*PIE*X/(2*E))
        PS(I,N)=PS(I,N)+H
10      CONTINUE
11      CONTINUE
C       NEXT PART ADDS INDUCED FIELDS IN APPROPRIATE MANNER.
        IA=I-1
        IF(IA)20,21,21
20      GO TO 2
21      IF(IA-23)22,22,23
C
23      DO 16 I=1,210
        XM=I
22      PI(I,N)=PS(I,N)+BS(IA,N)
        WRITE(2,51)XM
        WRITE(2,50)(PI(NR,N),NR=2,11)
2       CONTINUE
1       CONTINUE
12      CONTINUE
16      CONTINUE
C       POWER CALCULATION
        DX=0.02
        E=0.5
        T=0.02
        UMU=.0000012568
        SIGMA=58400000.0
        V=DT*DX*T
        DO 33 M=1,209
        DO 34 N=3,10
        NC=N-1
        DBY1=(PI(NC+1,N)-PI(NC,N))/DX
        DBX2=(PI(NC,N+1)-PI(NC,N))/DX
        DBY2=(PI(NC-1,N)-PI(NC,N))/DX
        DBZ1=(PI(NC,N+1)-PI(NC,N))/DZ
        DBZ2=(PI(NC,N-1)-PI(NC,N))/DZ
        DBZM=((DBZ1+DBZ2)/2
        P=((DBXM)**2+(DBZM)**2)*(V/SIGMA)/(UMU*UMU)
34      CONTINUE
33      CONTINUE
        WRITE(2,56)P
50      FORMAT(5F10.5,3X))
51      FORMAT(3X,9HPOSITION ,I3)
52      FORMAT(F10.5)
53      FORMAT(2F10.5))
54      FORMAT(8(F10.5))
55      FORMAT(2F14)
56      FORMAT(3X,1HPOWER IN WATTS IS ,F10.5)
60      FORMAT(3X,1H )
61      FORMAT(3X,1H )
62      FORMAT(3X,1H )
63      FORMAT(3X,1H )
        STOP
        END
```

Appendix B

A program to calculate the power dissipation in the sodium, the wall loss, the power transferred from one channel to the other and the electrode dissipation in a flow coupler.

In Chapter 7 we have shown that in a flow coupler which consists of two interconnected ducts of equal cross sectional area lying in the gap of magnet, the wall loss, the power transferred from one channel to the other and the electrode dissipation depend upon the potentials at the top and bottom edges of the duct where the electrodes make contact with the moving metal. We have also shown that the power loss in the moving metal depends upon both the currents which circulate between the two ducts and the eddy currents within the ducts.

In this program we once again consider a fringed magnetic field, that is one which does not drop abruptly to zero at the ends of the device, as being a number, in this case 10, of abrupt fields superimposed upon each other. Each element of field has the same magnitude B0 but extends over a different distance in the z-direction, that is it extends from z = -TL to z = +TL. In this way we have built up an initial field profile which is symmetrical about z=o. We have shown in Chapter 3 that the induced field which occurs when a conductor moves through a transverse magnetic field which drops abruptly to zero at $z=\pm \ell$ may be found from the equations

$$B_i = \sum_{n=1,3,5\ldots} A_n e^{\alpha_n z} \cos \frac{n\pi x}{2a} \qquad \text{when } z < -\ell, \text{ which is region I,}$$

$$B_i = \sum_{n=1,3,5\ldots} \left(B_n e^{\alpha_n z} + C_n e^{-\alpha_n z}\right) \cos \frac{n\pi x}{2a} \qquad \text{when } -\ell < z < +\ell, \text{ which is region II,}$$

and

$$B_i = \sum_{n=1,3,5\ldots} D_n e^{-\alpha_n z} \cos \frac{n\pi x}{2a} \qquad \text{when } z > +\ell, \text{ which is region III.}$$

An, Bn, Cn and Dn are constants which are given in Equations (19), (20), (21) and (22),

We have since shown that this equation is still applicable even when large currents are allowed to flow through the duct and through some external circuit provided that the external circuit is arranged so that the currents flowing through it do not produce a field with components in the y-direction.

At the start of the program we read the input data from cards. These cards we explained at the top of the computor program. If this is the first field calculation that the computor has performed, R in the program is set equal to RL, the magnetic Reynolds number is the left hand channel. If it is the second calculation R is set equal to RR, the magnetic Reynolds number in the right hand channel. An outer DO LOOP (DO 12 NA = 1,10) selects segments of the initial field one at a time. z is set at a value determined by I, x is set a value determined by N. The program now tests z to see whether it falls into region I, II or III. The appropriate part of the program is selected and a series is evaluated to find the induced field at this point. The induced fields due to each of the 10 segments are then added together to form the total induced magnetic field (cards 108-111). We have now calculated the magnetic field for chosen values of magnetic Reynolds numbers at 151 different z-positions and 11 different x-positions in both the left and right hand channels of the flow coupler. This information is stored in the two arrays BIL and BIR. BIL is the induced field in the left hand channel, BIR is the induced field in the right hand channel.

We calculate the electric potential at x = a in the left hand duct (UAL) and the electric potential at x = a in the right hand duct (UAR) at a chosen value of z. We use this information to compute the current which flows through a small element of the electrode. We then calculate the power transferred to the next channel through this element and the power dissipated in the element. We also calculate the power dissipated in a piece of duct wall of length DZ in the z-direction and of length 2a in the

x-direction. We next calculate the power loss in a small element of the sodium metal using the fact that the current density in the sodium is due partly to the current which circulates between the two ducts and partly to the eddy currents. We find from curl $\underline{B} = \mu \underline{j}$ that the x and z components of the eddy current density are given by $-\frac{1}{\mu}\frac{\partial \hat{b}}{\partial z}$ and $\frac{1}{\mu}\frac{\partial \hat{b}}{\partial x}$ respectively. We find these components by evaluating the gradient of the induced magnetic field (cards 187-200).

By repeating this process many times at many different z-positions and adding the contributions from each small element we eventually calculate half of the power transferred from one duct to the other (PT), the power dissipated in ONE electrode (PE), the power dissipated in one half of the left and right hand ducts (PL and PR), and the power dissipated in the duct walls (PLW and PRW). Where it is appropriate these figures have been multiplied by two before they are printed at the end of the program.

```
21:39 MAY 24,'73
!JOB RTURNER
!FORTRANH LS,GO
    EXTENDED FIV-H, VERSION D00
      1                 DIMENSION BIL(150,11),BIR(150,11),U1(20),
      2                1U2(10),TL(10),BS(151,11)
      3           C E IS HALF HEIGHT OF DUCT IN A DIRECTION PERP. TO THE FIELD.
      4           C     DP IS THE THICKNESS OF THE DUCT IN THE FIELD DIRECTION
      5           C SIGMA IS THE CONDUCTIVITY OF THE METAL IN THE DUCT.
      6                 READ(105,100)E,DP,SIGMA
      7           C EL IS THE HALF LENGTH OF THE ELECTRODES IN THE Z DIRECTION.
      8           C DT IS THE MEAN LENGTH OF ELECTRODE BETWEEN THE TWO DUCTS.
      9           C DW IS THE THICKNESS OF THE ELECTRODES.
     10           C SIGMAE IS THE CONDUCTIVITY OF THE ELECTRODES.
     11                 READ(105,101)EL,DT,DW,SIGMAE
     12           C W IS THE TOTAL THICKNESS OF THE SIDE WALLS OF ONE DUCT.
     13           C SIGMAW IS THE CONDUCTIVITY OF THE DUCT WALLS.
     14                 READ(105,103)W,SIGMAW
     15           C DZ IS THE INCREMENTAL CHANGE IN Z.
     16           C DX IS THE INCREMENTAL CHANGE IN X.
     17           C NP SETS THE FIRST Z POSITION AT WHICH THE FIELD IS CALCULATED.
     18                 READ(105,102)DZ,DX,NP
     19                 READ(105,54)(TL(I),I=1,10)
     20           C B0 IS THE SIZE OF EACH INCREMENT OF FIELD.
     21                 READ(105,51)B0
     22                 WRITE(108,50)B0
     23                 WRITE(108,50)E
     24                 WRITE(108,50)TL(1)
     25              72 READ(105,53)RL,RR
     26                 IF(RL)70,71,71
     27              71 CONTINUE
     28                 WRITE(108,59)RL,RR
     29           C     TL=HALF LENGTH OF UNIFORM FIELD
     30           C     E=HALF WIDTH OF METAL
     31           C     R=REYNOLDS NO
     32           C     B0=INITIAL FIELD
     33                 UM=0.0000012568
     34                 PIE=3.14159
     35                 II=0
     36              14 IF(II)13,13,19
     37              13 R=RL
                        GO TO 24
     39              19 R=RR
     40              24 CONTINUE
     41                 DO 17 I=1,151
     42                 DO 18 N=1,11
     43                 IF(II)25,25,26
     44              25 BIL(I,N)=0
     45                 GO TO 18
     46              26 BIR(I,N)=0
     47              18 CONTINUE
     48              17 CONTINUE
     49                 DO 12 NA=1,10
     50                 WRITE(108,62)
     51           C     NA DETERMINES WHICH OF 25 LUMPS OF FIELD IS CONSIDERED.
     52           C     SET Z
     53                 DO 1 I=1,151
     54                 M=I-NP
     55                 Z=M*DZ
     56           C     SET X
     57                 DO 2 N=1,11
     58                 Q=N-1
     59                 X=DX*Q
     60                 BS(I,N)=0
     61           C     TEST TO SEE IF THIS Z IS IN REGION 1,2, OR 3
     62                 IF(TL(NA)+Z)3,3,4
     63           C     REGION 1
     64              3  DO 8 K=1,11,2
     65                 F=(1/E)*SQRT((R*R)+(K*K*PIE*PIE))
     66                 G=(-4/(K*PIE))*((-1)**((K+1)/2))
     67                 P=R/E
     68                 A=B0*G*P/F
     69                 A1=(1/(2*E))*(R+SQRT((R*R)+(K*K*PIE*PIE)))
     70                 EX1=EXP(A1*(Z-TL(NA)))
     71                 EX2=EXP(A1*(Z+TL(NA)))
     72                 H=A*(EX1-EX2)*COS(K*PIE*X/(2*E))
     73                 BS(I,N)=BS(I,N)+H
     74              8  CONTINUE
     75                 GO TO 11
     76           C     TEST TO SEE IF THIS Z IS IN REGION 1,2, OR 3
     77              4  IF(Z-TL(NA))5,5,6
     78           C     REGION 2
     79              5  DO 9 J=1,11,2
     80                 F=(1/E)*SQRT((R*R)+(J*J*PIE*PIE))
     81                 G=(-4/(J*PIE))*((-1)**((J+1)/2))
     82                 P=R/E
     83                 A=B0*G*P/F
     84                 A1=(1/(2*E))*(R+SQRT((R*R)+(J*J*PIE*PIE)))
     85                 A2=(1/(2*E))*(R-SQRT((R*R)+(J*J*PIE*PIE)))
     86                 T1=A1*(Z-TL(NA))
     87                 T2=A2*(Z+TL(NA))
     88              42 EX1=EXP(T1)
     89              67 EX2=EXP(T2)
     90                 H=A*(EX1-EX2)*COS(J*PIE*X/(2*E))
     91                 BS(I,N)=BS(I,N)+H
     92              9  CONTINUE
     93                 GO TO 11
     94           C     REGION 3
     95              6  DO 10 L=1,11,2
     96                 F=(1/L)*SQRT((R*R)+(L*L*PIE*PIE))
     97                 G=(-4/(L*PIE))*((-1)**((L+1)/2))
     98                 P=R/E
     99                 A=B0*G*P/F
    100                 A2=(1/(2*E))*(R-SQRT((R*R)+(L*L*PIE*PIE)))
    101                 EX1=EXP(A2*(Z-TL(NA)))
    102                 EX2=EXP(A2*(Z+TL(NA)))
    103                 H=A*(EX1-EX2)*COS(L*PIE*X/(2*E))
    104                 BS(I,N)=BS(I,N)+H
    105              10 CONTINUE
    106              11 CONTINUE
```

```
      7 EX2=EXP(T2)
        F=A*(EX1-EX2)*COS(J*PIE*X/(2*E))
        BS(I,N)=BS(I,N)+F
      9 CONTINUE
        GO TO 11
C       REGION 3
      6 DO 10 L=1,11,2
        F=(1/L)*SQRT((R*R)+(L*L*PIE*PIE))
        G=(-4/(L*PIE))*((-1)**((L+1)/2))
        P=R/E
        A=BB*G*P/F
        A2=(1/(2*E))*(R-SQRT((R*R)+(L*L*PIE*PIE)))
        EX1=EXP(A2*(Z-TL(NA)))
        EX2=EXP(A2*(Z+TL(NA)))
        F=A*(EX1-EX2)*COS(L*PIE*X/(2*E))
        BS(I,N)=BS(I,N)+F
     10 CONTINUE
     11 CONTINUE
C       NEXT PART ADDS INDUCED FIELDS IN APPROPRIATE MANNER.
     22 IF(II)27,27,28

     27 BIL(I,N)=BIL(I,N)+BS(I,N)
        GO TO 2
     28 BIR(I,N)=BIR(I,N)+BS(I,N)
      2 CONTINUE
      1 CONTINUE
     12 CONTINUE
        IF(II-1)29,30,30
     29 II=2
        GO TO 14
     30 CONTINUE
C       POWER CALCULATION
        PL=0
        PR=0
        PT=0
        PLW=0
        PRW=0
        PE=0
        V=DZ*DX*DP
        RE=DT/(SIGMAE*2*EL*DW)
        RD=E/(SIGMA*2*EL*DP)
        RA=BB*10
     31 CONTINUE
        Z=((1-NA)*DZ)+(DZ/2)
        DO 33 NB=1,150
        IF((EL-Z)+(Z-EL))83,83,84
     84 RB=0
        RP=0
        GO TO 85
     83 DO 80 K=1,10
        U1(K)=0
        U2(K)=0
        DO 81 I=1,21,2
        X1=SQRT((RL*RL)+(I*I*PIE*PIE))
        A1=(RL+X1)/(2*E)
        A2=(RL-X1)/(2*E)
        X2=SQRT((RR*RR)+(I*I*PIE*PIE))
        B1=(RR+X2)/(2*E)
        B2=(RR-X2)/(2*E)
        AA=B1*(Z-TL(K))
     86 AA=EXP(AA)
     88 BB=B2*(Z+TL(K))
     89 BB=EXP(BB)
     91 CC=A1*(Z-TL(K))
     92 CC=EXP(CC)
     94 DD=A2*(Z+TL(K))
     95 DD=EXP(DD)
        B1=(8/(I*I*PIE*PIE))*((B2*AA)-(B1*BB))/(B1-B2)
        B2=(8/(I*I*PIE*PIE))*((A2*CC)-(A1*DD))/(A1-A2)
        U1(K)=U1(K)+B1
        U2(K)=U2(K)+B2
     81 CONTINUE
     80 CONTINUE
        UU=0
        UV=0
        DO 82 L=1,10

        UU=UU+U1(L)
        UV=UV+U2(L)
     82 CONTINUE
        UAL=-((RD*RR*BA*UU)/((RE+2*RD)*UM*SIGMA*10))
       1-(((RE+RD)*RL*BA*UV)/((RE+2*RD)*UM*SIGMA*10))
       2-((((RR*RD)+RL*(RE+RD))*BA)/(UM*SIGMA*(RE+2*RD)))
        UAR=-((RD*RL*BA*UV)/((RE+2*RD)*UM*SIGMA*10))
       1-(((RE+RD)*RR*BA*UU)/((RE+2*RD)*UM*SIGMA*10))
       2-((((RL*RD)+RR*(RE+RD))*BA)/((RE+2*RD)*UM*SIGMA))
        CURD=SIGMAE*(UAL-UAR)/DT
        RQ=CURD
        PT=PT+(RQ*UAL*DZ*DW)
        RE=RE+(((UAL-UAR)**2)*DZ/(2*EL*RE))
```

A2

4.

5.

```
      DO 82 L=1,10
      UU=UU+U1(L)
      UV=UV+U2(L)
   82 CONTINUE
      UAL=-((RD*RR*BA*UU)/((RE+2*RD)*UM*SIGMA*10))
     1-(((RE+RD)*RL*BA*UV)/((RL+2*RC)*LM*SIGMA*10))
     2-((((RE+RD)+RL*(RE+RD))*BA)/(UM*SIGMA*(RE+2*RD)))
      UAR=-((RD*RL*BA*UV)/((RE+2*RD)*UM*SIGMA*10))
     1-(((RE+RD)*RR*BA*UU)/((RE+2*RD)*LM*SIGMA*10))
     2-((((RL*RD)+RR*(RE+RD))*BA)/((RE+2*RD)*UM*SIGMA))
      CURD=SIGMAE*(UAL-UAR)/DT
      FQ=CURD
      PT=PT+(PQ*UAL*DZ*DW)
      PE=PE+(((UAL-UAR)**2)*DZ/(2*EL*RE))
      PLW=PLW+ (UAL*UAL*SIGMAW*W**2*DZ/E)
      PRW=PRW+ (UAR*UAR*SIGMAW*W**2*DZ/E)
      WRITE(108,15)PQ
   85 CONTINUE
      PQ=(N*PI)*DW/DP
      PP=-UN*CURD*DW/DF
      DO 34 N=1,10
      N1=N+1
      NC=NA+1
      DBLX1=(BIL(NB,N1)-BIL(NB,N))/DX
      DBLX2=(BIL(NC,N1)-BIL(NC,N))/DX
      DBLXM=(DBLX1+DBLX2)/2
      DBLZ1=(BIL(NC,N)-BIL(NB,N))/DZ
      DBLZ2=(BIL(NC,N1)-BIL(NB,N1))/DZ
      DBLZM=(DBLZ1+DBLZ2)/2
      DBLZM=PQ-DBLZM
      PL=PL+(((DBLXM*DBLXM)+(DBLZM*DBLZM))*(V/SIGMA))/(UM*UM))
      DBRX1=(BIR(NB,N1)-BIR(NB,N))/DX
      DBRX2=(BIR(NC,N1)-BIR(NC,N))/DX
      DBRXM=(DBRX1+DBRX2)/2
      DBRZ1=(BIR(NC,N)-BIR(NB,N))/DZ
      DBRZ2=(BIR(NC,N1)-BIR(NB,N1))/DZ
      DBRZM=(DBRZ1+DBRZ2)/2
      DBRZM=PP-DBRZM
      PR=PR+(((DBRXM*DBRXM)+(DBRZM*DBRZM))*(V/SIGMA))/(UM*UM))
   34 CONTINUE
      Z=Z+DZ
   33 CONTINUE
      PL=2*PL
      PR=2*PR
      PT=2*PT
      PE=2*PE
      WRITE(108,56)PL,PR
      WRITE(108,55)PLW,PRW
      WRITE(108,60)PE
      WRITE(108,61)PT
      GO TO 72
   70 CONTINUE
   15 FORMAT(3X,26HAPPLIED CURRENT DENSITY IS,E13.7)
   50 FORMAT(3X,F10.3)
   53 FORMAT(2(F10.5))
   51 FORMAT(F10.5)
  102 FORMAT(F10.5,F10.5,I4)
  103 FORMAT(F10.5,F10.2)
  101 FORMAT(3(F10.5),F10.2)
  100 FORMAT(F10.5,F10.5,F10.2)
   54 FORMAT( 8(F10.5))
   55 FORMAT(3X,16HPOWER IN LHW IS ,E13.6,12HWATTS,IN RHW,E13.6,6HWATTS.
     1)
   56 FORMAT(3X,20HPOWER DIS IN LHC IS ,E13.6,13HWATTS,IN RHC ,E13.6,6H
     1WATTS )
   59 FORMAT(3X,6HRL IS ,F10.5,6HRR IS ,F10.5)
   60 FORMAT(3X,26HPOWER DIS IN ELECTRODE IS ,E13.6,6HWATTS.)
   61 FORMAT(3X,18HPOWER TRANSFER IS ,E13.6,6HWATTS.)
   62 FORMAT(3X,1HR)
   63 FORMAT(3X,1HS)
      STOP
```

A3